

Energy & Environmental Science

Accepted Manuscript



This is an *Accepted Manuscript*, which has been through the Royal Society of Chemistry peer review process and has been accepted for publication.

Accepted Manuscripts are published online shortly after acceptance, before technical editing, formatting and proof reading. Using this free service, authors can make their results available to the community, in citable form, before we publish the edited article. We will replace this *Accepted Manuscript* with the edited and formatted *Advance Article* as soon as it is available.

You can find more information about *Accepted Manuscripts* in the [Information for Authors](#).

Please note that technical editing may introduce minor changes to the text and/or graphics, which may alter content. The journal's standard [Terms & Conditions](#) and the [Ethical guidelines](#) still apply. In no event shall the Royal Society of Chemistry be held responsible for any errors or omissions in this *Accepted Manuscript* or any consequences arising from the use of any information it contains.

**A review of developments in pilot-plant testing and
modelling of calcium looping process for CO₂ capture from
power generation systems**

Dawid P. Hanak, Edward J. Anthony, Vasilije Manovic*

*Combustion and CCS Centre, Cranfield University,
Bedford, Bedfordshire, MK43 0AL, UK*

Corresponding author: Edward J. Anthony*

Combustion and CCS Centre

Cranfield University

Bedford, Bedfordshire, MK43 0AL, UK

b.j.anthony@cranfield.ac.uk

A review of developments in pilot-plant testing and modelling of calcium looping process for CO₂ capture from power generation systems

Dawid P. Hanak, Edward J. Anthony, Vasilije Manovic*

Combustion and CCS Centre, Cranfield University, Bedford, Bedfordshire, MK43 0AL, UK

**b.j.anthony@cranfield.ac.uk*

Abstract

A nearly complete decarbonisation of the power sector is essential to meet the European Union target for greenhouse gas emissions reduction. Carbon capture and storage technologies have been identified as a key measure in reducing the carbon-intensity of the power sector. However, no cost-effective technology has yet been developed on a commercial scale, which is mostly due to high capital cost. Moreover, the mature technologies, such as amine scrubbing or oxy-combustion technologies, impose a high projected efficiency penalty (8–12.5% points) upon integration to the power plant. The calcium looping process, which is currently being tested experimentally in bench- and pilot-scale plants worldwide, is regarded as an promising alternative to the chemical solvent scrubbing approach, as it leads to the projected efficiency penalty of 6–8% points. The calcium looping concept has been developing rapidly due to the introduction of new test facilities, new correlations for process modelling, and process configurations for improved performance. The first part of this review provides an overview of the bench- and pilot- plant test facilities available worldwide. The focus is put on summarising the characteristics and operating conditions of the test facilities, as well as extracting the key experimental findings. Additionally, the experimental data suitable for validation or verification of the process models are presented. In the second part, the approaches to the carbonator and the calciner reactor modelling are

summarised and classified in five model complexity levels. Moreover, the models limitations are assessed and the needs for modelling baselines for further process analyses are identified. Finally, in the third part the approaches for the integration of the calcium looping to the power generation systems and for the improvement of the process performance are identified and evaluated. This review indicates that the calcium looping integration resulted in the projected efficiency penalty of 2.6–7.9% points for the coal-fired power plants and 9.1–11.4% points for the combined-cycle power plants. Also, it was found that calcium looping process can be used to develop a novel high-efficiency (46.7%_{LHV}) coal-fired power generation systems, making this technology even more promising compared to the other CO₂ capture technologies.

Keywords: Calcium looping process, process modelling, pilot plants, process integration, experimental testing, efficiency penalty

1	Table of contents	
2	<u>1 INTRODUCTION</u>	6
3	<u>2 CALCIUM LOOPING PROCESS FOR CO₂ CAPTURE</u>	9
4	<u>2.1 Process description</u>	9
5	<u>2.2 Calcium looping as a novel CO₂ capture technology</u>	12
6	<u>3 REVIEW OF CALCIUM LOOPING BENCH- AND PILOT-SCALE</u>	
7	<u>TESTING</u>	17
8	<u>3.1 Industrial Technology Research Institute</u>	19
9	<u>3.1.1 Experimental facility description</u>	19
10	<u>3.1.2 Test campaign using 1 kW_{th} bench-scale unit</u>	20
11	<u>3.1.3 Test campaign using 3 kW_{th} bench-scale unit</u>	21
12	<u>3.1.4 Data for process modelling</u>	22
13	<u>3.2 Consejo Superior de Investigaciones Científicas</u>	23
14	<u>3.2.1 Experimental facility description</u>	23
15	<u>3.2.2 Test campaign using 30 kW_{th} bench-scale unit</u>	25
16	<u>3.2.3 Test campaign using 1.7 MW_{th} pilot plant</u>	26
17	<u>3.2.4 Data for process modelling</u>	28
18	<u>3.3 Institute of Energy Systems and Technology at Darmstadt University</u>	
19	<u>of Technology</u>	28
20	<u>3.3.1 Experimental facility description</u>	28
21	<u>3.3.2 Test campaign</u>	29
22	<u>3.3.3 Data for process modelling</u>	31
23	<u>3.4 Institute of Combustion and Power Plant Technology at University of</u>	
24	<u>Stuttgart</u>	31
25	<u>3.4.1 Experimental facility description</u>	31
26	<u>3.4.2 Test campaign using a 10 kW_{th} DFB unit</u>	33
27	<u>3.4.3 Test campaign using the 200 kW_{th} DFB facility</u>	34
28	<u>3.4.4 Data for process modelling</u>	35
29	<u>3.5 Ohio State University</u>	35
30	<u>3.5.1 Experimental facility description</u>	35
31	<u>3.5.2 Test campaign</u>	36
32	<u>3.5.3 Data for process modelling</u>	37
33	<u>3.6 CANMET Energy Technology Centre</u>	37
34	<u>3.6.1 Experimental facility description</u>	37
35	<u>3.6.2 Test campaign using a 75 kW_{th} pilot plant</u>	39
36	<u>3.6.3 Data for process modelling</u>	40
37	<u>3.7 Cranfield University</u>	40
38	<u>3.7.1 Experimental facility description</u>	40
39	<u>3.7.2 Test campaign</u>	41
40	<u>3.7.3 Data for process modelling</u>	42
41	<u>3.8 Tsinghua University</u>	42

42	<u>3.8.1 Experimental facility description</u>	42
43	<u>3.8.2 Test campaign</u>	43
44	<u>3.8.3 Data for process modelling</u>	43
45	<u>3.9 Vienna University of Technology</u>	44
46	<u>3.9.1 Experimental facility description</u>	44
47	<u>3.9.2 Test campaigns</u>	44
48	<u>3.9.3 Data for process modelling</u>	47
49	<u>3.10 Summary</u>	47
50	<u>4 MODELS FOR THE CALCIUM LOOPING PROCESSES</u>	48
51	<u>4.1 Modelling of the sorbent average conversion</u>	49
52	<u>4.1.1 Maximum average conversion of non-pretreated sorbent</u>	51
53	<u>4.1.2 Maximum average conversion of hydrated sorbent</u>	53
54	<u>4.2 Modelling of carbonation and calcination kinetic rates</u>	55
55	<u>4.2.1 Apparent kinetics model for carbonation</u>	55
56	<u>4.2.2 Carbonation kinetic model for highly cycled particles</u>	56
57	<u>4.2.3 Changing grain size carbonation and calcination models</u>	57
58	<u>4.3 Carbonator reactor modelling</u>	62
59	<u>4.3.1 Semi-predictive model with simple hydrodynamics</u>	62
60	<u>4.3.2 Semi-predictive model with two-zone K-L hydrodynamics</u>	65
61	<u>4.3.3 Semi-predictive model with three-zone K-L hydrodynamics</u>	70
62	<u>4.4 Calciner reactor modelling</u>	72
63	<u>4.4.1 Semi-predictive model with simple hydrodynamics</u>	72
64	<u>4.4.2 Semi-predictive model with two-zone K-L hydrodynamics</u>	73
65	<u>4.4.3 Predictive model with CFD hydrodynamics</u>	74
66	<u>4.5 Summary</u>	76
67	<u>5 INTEGRATION OF CALCIUM LOOPING TO POWER PLANTS</u>	80
68	<u>5.1 Conventional coal-fired power plants</u>	81
69	<u>5.1.1 Feasibility study for calcium looping for conventional power</u>	
70	<u>generation systems</u>	81
71	<u>5.1.2 Heat integration with the primary and secondary steam cycle</u>	82
72	<u>5.1.3 Alternative configurations for efficiency improvement</u>	90
73	<u>5.1.4 Comparison between the average conversion and semi-predictive</u>	
74	<u>calcium looping model</u>	98
75	<u>5.2 Combined cycle power plants</u>	99
76	<u>5.2.1 Feasibility of calcium looping process for natural gas-fired power</u>	
77	<u>plants</u>	99
78	<u>5.2.2 High-reliability and high-efficiency coal-gasification power</u>	
79	<u>generation systems</u>	102
80	<u>5.2.3 Zero-emissions coal-based power generation systems</u>	107
81	<u>5.3 Summary</u>	111
82	<u>5.3.1 Integration impact on the overall process performance</u>	111
83	<u>5.3.2 Modelling approaches, assumptions and limitations</u>	113

84	<u>6 THE FUTURE OF CALCIUM LOOPING IN POWER GENERATION</u>	
85	<u>SYSTEMS</u>	118
86	<u>LIST OF ABBREVIATIONS</u>	119
87	<u>NOMENCLATURE</u>	120
88	<u>REFERENCES</u>	122
89		
90		

91 1 INTRODUCTION

92 The European Union aims to reduce its greenhouse gas emissions relative to
93 1990 levels by 30% by 2020 [1], 40% by 2030 [2; 3], and 80 - 95% by 2050. To
94 meet the 2050 target, a nearly complete decarbonisation of the power sector is
95 required due to the high fossil fuel contribution in the energy mix [4] Power
96 generation is expected to account for more than one-third of the total
97 greenhouse gas emissions in 2010 [5]. For this reason, transformation of the
98 power generation sector is a key to limiting the average global temperature
99 increase [6].

100 One reason behind the high carbon intensity of the power generation sector is
101 the major share (42%) of coal-fired power plants (CFPP) in the global supply of
102 electricity [7], the current average net thermal efficiency of which amounts to
103 33%_{LHV} due to the high (75%) share of subcritical units in the global CFPP fleet
104 [6]. Moreover, due to the recent emergence of shale gas in North America,
105 American exports of coal have increased. As a result, the price of coal has
106 fallen significantly in Europe and electricity generation from coal has increased
107 at the expense of gas-based electricity generation [6]. If the current market
108 trend continues, coal will continue to be used for power generation as predicted
109 by the Energy Information Administration [8]. Hence, a complete
110 decarbonisation of the power sector may be even more challenging in the
111 future.

112 Carbon capture and storage (CCS) technologies are expected to play a crucial
113 role in greenhouse gas emissions reduction from the power generation sector
114 [9]. However, the first-of-a-kind large-scale CO₂ capture plant was only
115 commissioned in 2014 [10], although the technology required for CCS
116 deployment exists in other industries [6; 11]. This is because no cost-effective
117 technology for fossil fuel power plants has yet been fully demonstrated on a
118 commercial scale. A relatively high capital cost, due to the size of equipment
119 required to accommodate the flue gas volume, and the efficiency penalty
120 associated with a significant increase in the cost of electricity [12], make CCS
121 infeasible at the moment. Nevertheless, the IEA 2°C scenario predicts that 63%

122 of the CFPPs will be equipped with CCS installations by 2050 [6]. There are
123 several mature CO₂ capture technologies that are close to market
124 commercialisation in the power generation sector [13; 14].

125 The first full-scale capture project at Boundary Dam is based on a chemical
126 absorption post-combustion capture plant using amine solvent [10], with other
127 post-combustion plants and oxy-combustion CFPPs under construction or in the
128 planning stage [9]. Such technologies impose a significant projected efficiency
129 penalty reaching up to 12.5% points, identified through analysis of the overall
130 process performance using computational and modelling tools [15-18]. A
131 reduction in the process efficiency, in turn, affects fuel economy and thus the
132 cost of electricity. Moreover, these CO₂ capture technologies would require
133 additional effort, and therefore cost, to mitigate the environmental, health and
134 safety issues [14]. These are the main drivers for development of novel
135 technologies that would affect electricity generation to a lesser degree, and
136 would not be harmful to the environment or human health. A promising
137 alternative to both oxy-combustion and chemical solvent absorption is a second
138 generation CO₂ capture technology called calcium looping (CaL) that uses a
139 calcium-based solid sorbent.

140 Development of the CaL process has advanced at a rapid rate over the past
141 decade, especially since 2009. This is seen not only in the increased number of
142 test facilities, but also in the increase in the development of process models.
143 The CaL process has been widely investigated using thermodynamic and
144 mathematical modelling, computational fluid dynamic (CFD) modelling and
145 process modelling and integration into power generation systems. Analysis of
146 mature technologies using process simulation and modelling tools has revealed
147 that this approach allows a cost-effective investigation of concept feasibility and
148 applicability, as well as development and optimisation of different process
149 configurations. In addition, a whole process approach allows determination of
150 the impact that integration of the CO₂ capture plant imposes on the power plant.
151 However, a reliable assessment of the process performance requires the
152 process models to be validated with experimental data.

153 **Table 1: A summary of the review studies related to calcium looping process**

Source	Review scope
Stanmore and Gilot [19]	<ul style="list-style-type: none"> - Summary of the sintering, sulphation, particle fragmentation and attrition effect on the sorbent activity. - Detailed information on the correlations for mathematical modelling of carbonation, calcination, sulphation and sintering. - A brief overview of the models for prediction of the aerodynamics and trajectories of particles, as well as reaction rates in the circulating fluidised bed (CFB).
Harrison [20]	<ul style="list-style-type: none"> - Comparison of the standard steam-methane reforming process and the CaL process for H₂ production. Review of the thermodynamic analyses, sorbent durability and process configurations. - Review of the experimental studies on hydrogen production.
Florin and Harris [21]	<ul style="list-style-type: none"> - Review of process configurations for the enhanced hydrogen production from biomass gasification. - Summary of the sorbent regeneration measures. - A brief reference to the sorbent activity decay. - Review of the experimental trials on hydrogen production from carbonaceous fuels using calcium looping.
Blamey et al. [13]	<ul style="list-style-type: none"> - Detailed description of the carbonation, calcination, sintering and sorbent performance under repeated cycle operation. - Summary of sorbent deactivation and reactivation measures. - Review of the calcium looping process applications. - A brief summary of semi-empirical correlations allowing estimation of the sorbent conversion.
Dean et al. [14]	<ul style="list-style-type: none"> - Summary of the calcium looping cycle fundamentals, sorbent deactivation and sorbent performance. - Review of the calcium looping thermodynamic and economic performance, as well as its applicability in the cement industry and hydrogen production. - A brief reference to the sorbent activity decay. - Review of the pilot plant trials for calcium looping before 2011.
Anthony [22]	<ul style="list-style-type: none"> - Review of sorbents performance improvements and reactivation strategies for natural and synthetic sorbents. - Brief outline of calcium looping process applicability and experimental facilities.
Liu et al. [23]	<ul style="list-style-type: none"> - Review of sorbent performance enhancements. - Review of synthesis methods for sintering resistant sorbents.
Kierzkowska et al. [24]	<ul style="list-style-type: none"> - Summary of the carbonation reaction fundamentals. - Review of recent developments in synthesis of CaO-based sorbents.
Romano et al. [25]	<ul style="list-style-type: none"> - Outline of CaL process simulations and notes on further modelling activities.
Boot-Handford et al. [15]	<ul style="list-style-type: none"> - Summary of the process performance, sorbent deactivation and regeneration. - A brief update on CaL pilot-plant trials.

154 Although pilot plant facilities and modelling approaches have been reviewed
155 (Table 1), some critical aspects have not been analysed in detail. Moreover, the
156 field of CaL has been developing rapidly due to the introduction of new test
157 facilities, new correlations for process modelling, and CaL process
158 configurations for improved performance. The aim of this paper is to review the
159 available test facilities worldwide, the modelling approaches, and the integration
160 studies that will guide the future development of the CaL process. The focus of
161 the first part of this review will be on recent developments in CaL technology.
162 The second part reviews the available approaches for prediction of the CaL
163 process performance. Finally, the third part identifies and evaluates the
164 approaches for CaL integration into power generation systems.

165

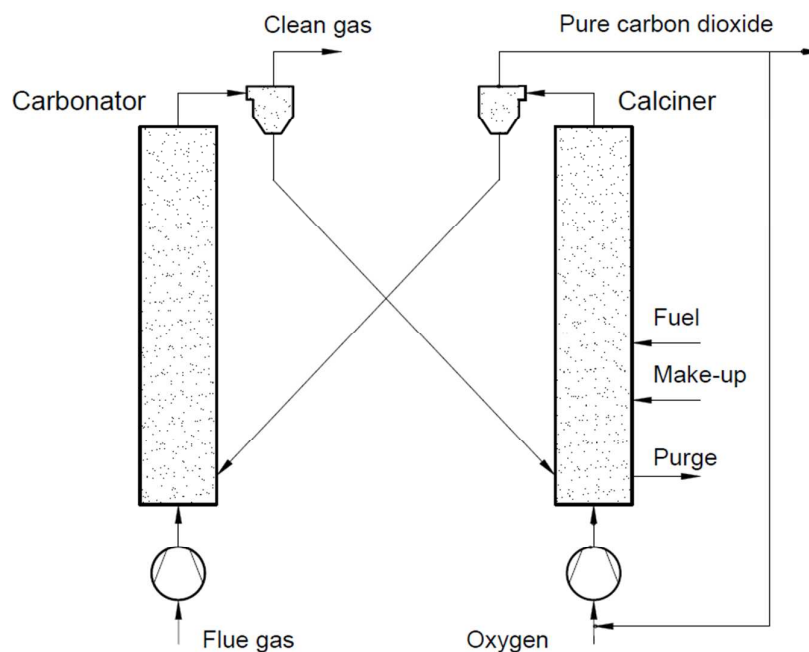
166 **2 CALCIUM LOOPING PROCESS FOR CO₂ CAPTURE**

167 **2.1 Process description**

168 Use of calcium-based sorbents for CO₂ absorption was patented in 1933 and
169 the research was primarily directed towards sorption-enhanced hydrogen
170 production [20; 26]. A configuration proposed by Hirama et al. [27] and Shimizu
171 et al. [28], which includes two interconnected CFBs operating under
172 atmospheric pressure (Figure 1), is the one most commonly referred to in the
173 literature as appropriate for power generation systems. Application of such a
174 configuration for the CaL process with appropriate design of the heat exchanger
175 network (HEN) has been shown to have a thermal efficiency comparable to
176 current combustion systems [29].

177 In the CaL process the flue gas from fuel combustion in air, which usually
178 contains between 4%_{vol} and 15%_{vol} CO₂ depending on the primary fuel used, is
179 fed to the carbonator. In contrast to amine scrubbing, there is no requirement
180 for flue gas precooling as absorption in the CaL process is conducted at a high
181 temperature to assure high capture efficiency. Under such conditions, CO₂
182 reacts chemically with CaO through an exothermic solid-gas reaction.

183 CO₂ is removed from the flue gas in the form of solid CaCO₃ at a reasonably
 184 fast rate [26; 28; 30; 31]. CO₂ removal efficiency decreases rapidly as the
 185 temperature increases and becomes zero at approximately 775°C as the
 186 equilibrium partial pressure of CO₂ exceeds the partial pressure in flue gas
 187 containing 15%_{vol} CO₂ above this temperature [32]. The optimal operating
 188 temperature of the carbonator ranges between 580°C and 700°C due to the
 189 trade-off between the reaction kinetics and the equilibrium driving forces [33;
 190 34].



191

192 **Figure 1: Conceptual scheme of CaL process system for CO₂ capture**

193 CaCO₃ is transferred to another fluidised-bed reactor, the so-called calciner, in
 194 which it is calcined and CO₂ is reclaimed [26]. Calcination is conducted at 850–
 195 950°C to achieve rapid reaction without excessive sintering [14; 28; 35]. It
 196 needs to be highlighted that at 900°C, the equilibrium CO₂ partial pressure is
 197 about 1 bar [36], and hence a pure CO₂ stream can be theoretically achieved in
 198 the calciner operated at that temperature under atmospheric conditions.
 199 However, the higher calciner temperature is favourable and required in the
 200 terms of reaction kinetics. On the other side, a practical conversion rate can be
 201 achieved at temperatures below 900°C if the gas atmosphere in calciner is

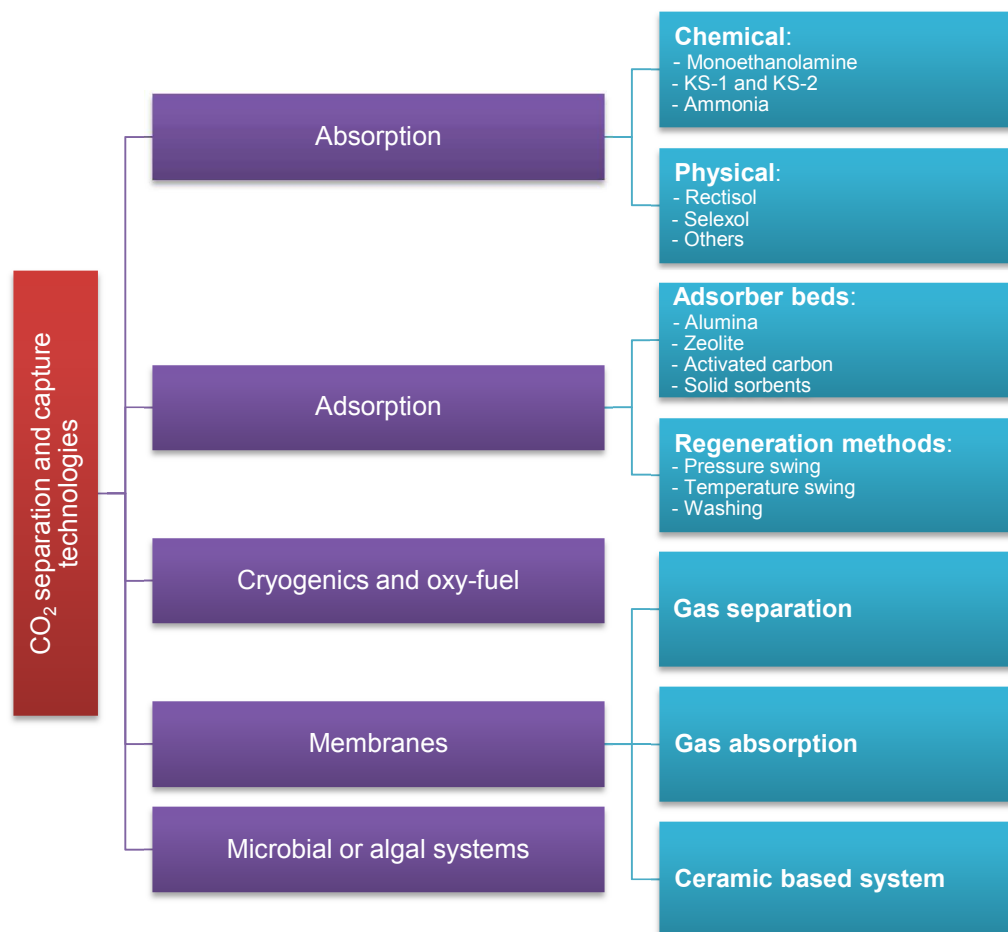
202 diluted by steam, which can be easily separated by condensation from the CO₂
203 steam. Furthermore, since the high-grade heat is available in the CaL process,
204 which can be recovered to produce additional amount of steam for the steam
205 cycle, the higher carbonator and the calciner temperatures are preferred in
206 order to allow reaching desired steam parameters. Therefore, selection of the
207 CaL operating temperatures can be seen as a design trilemma, in which the
208 CO₂ capture level restricted and process performance must be maximised,
209 while the unit size minimised. As calcination is endothermic, additional fuel in
210 the calciner is required. To produce a CO₂ stream of high purity, which can be
211 directly transported for safe storage or use after the purification and
212 compression stages, combustion takes place in an O₂/CO₂ environment [28; 37;
213 38]. Although this configuration has been demonstrated at the pilot-plant scale
214 [14], other configurations that use indirect heat sources may become available
215 in future [30; 39]. It is estimated that the calcination step consumes 35% to 50%
216 of the overall heat input to the system [40].

217 If it were not for sorbent sintering, attrition, and sulphation, the cyclic operation
218 of carbonation and calcination would be performed without sorbent purge and
219 make-up, and these processes would only be limited by thermodynamic
220 equilibrium and the chemical reaction and diffusion rates. Manovic and Anthony
221 [41] noted that the carbonator and the calciner should be operated within a
222 particular temperature range in which the minimum temperature is determined
223 by the desired reaction rate while the maximum temperature is related to the
224 desired CO₂ concentration. In general, the lower temperature limit is related to
225 the desired partial pressure of CO₂, hence purity of the CO₂ stream, while the
226 upper temperature is limited by the sorbent structural properties. Unfortunately,
227 the conversion of the sorbent decreases with the number of carbonation and
228 calcination cycles due to changes in particle structure [42], especially due to
229 enhanced sintering of CaO, which has been shown to be enhanced above
230 900°C [43]. Regardless of having a negative impact on the sorbent
231 performance, sulphur oxides would be efficiently captured due to the high Ca/S
232 ratio in the calciner and the carbonator [44], through indirect (1) and direct
233 sulphation (2) [45].



234 **2.2 Calcium looping as a novel CO₂ capture technology**

235 CO₂ capture technologies commonly referred to in literature are: absorption-
236 based separation using physical or chemical solvents; adsorption-based
237 separation using solid sorbents; membrane separation; cryogenic separation
238 techniques and oxy-fuel combustion; and biological systems using microbes or
239 algae (Figure 2) [46-49]. However, due to the relatively low concentration of
240 CO₂ in the flue gas (4-15%_{vol}), large volumes of flue gas needs to be processed,
241 and such technologies still have not been commercially deployed in the power
242 industry due to a considerable drop in the net thermal efficiency of the
243 integrated system, but also due to high equipment capital cost. As a result, the
244 cost of electricity in the CFPPs and natural gas-fired combined cycle power
245 plants retrofitted with CCS is expected to increase by 60-125% and 30-55%,
246 respectively [50-52]. Although this is the key reason why development of new
247 technologies needs to be pursued, there are also other issues which must be
248 considered, such as environmental impact and operational safety.



249

250 **Figure 2: Classification of the CO₂ separation and capture technologies (Adapted**
 251 **with permission from Rao and Rubin [53]. Copyright 2015 American Chemical**
 252 **Society.)**

253 Application of amines for CO₂ separation, such as monoethanolamine (MEA),
 254 has been first proposed for fuel gas or combustion gas by Bottoms in 1930 [54].
 255 This technology has been widely applied for sour gas sweetening and is used to
 256 remove CO₂ from natural gas or other industrial gases for ammonia and
 257 methanol production, as well as to produce CO₂ for enhanced oil recovery [53;
 258 55; 56]. Using MEA or different amine-based solvents, such as piperazine (PZ)
 259 or methyldiethanolamine (MDEA), is currently the most likely technology to be
 260 applied to reduce the environmental impact of fossil fuel power plants [13; 15;
 261 57]. Although several amine scrubbing processes have been operated in other
 262 industries [58; 59], the first full-scale demonstration plant using amine scrubbing

263 technology from the power sector, is Cansolv's integrated SO_2/CO_2 process,
264 fitted to Unit 3 of the Boundary Dam CFPP, was only commissioned in 2014
265 [10]. The following problems need to be resolved before amine scrubbing can
266 be widely deployed in power generation:

- 267 • Solvent regeneration uses steam from the power plant steam cycle
268 creating a projected efficiency penalty of 9.5–12.5% points when
269 reference MEA solvent is employed [16-18; 60]. Yet, recent studies
270 identify that the projected efficiency penalty can be reduced to 8.5%
271 points using amine-blends, such as MDEA/PZ [61], or to 7.0% points
272 using PZ solvent [61; 62].
- 273 • Amine solvents are prone to degradation due to reaction with O_2 and O_2 -
274 containing components in the flue gas, such as NO_x and SO_x , resulting in
275 heat stable salts [63].
- 276 • Solvent concentration is limited to 30% (MEA) to prevent plant equipment
277 corrosion [64].
- 278 • Inappropriate handling and disposal of degradation products may cause
279 environmental and health issues [14; 64-66].

280 Using ammonia for CO_2 capture, which imposes a lower efficiency penalty, is
281 proposed as an alternative to amine scrubbing [67]. Development of ammonia-
282 based CO_2 capture processes reached the pilot plant stage in a relatively short
283 period of time. However, some projects were cancelled due to cost and
284 schedule overruns [68-70]. The main advantages of ammonia over amine-
285 based solvents are:

- 286 • It is commercially available at a lower price than MEA.
- 287 • It has higher CO_2 absorption capacity compared to an MEA solution of
288 the same concentration.
- 289 • There is lower heat of reaction resulting in lower heat requirement for
290 solvent regeneration. This is reflected in a projected efficiency penalty of

291 4.1 to 7% points [71-73] although this has not been substantiated
292 experimentally [59].

- 293 • There is no solvent degradation on contact with the flue gas components.
- 294 • The stripper can be operated at elevated pressure, hence temperature,
295 leading to reduced compression work.
- 296 • Ammonia is not as corrosive as amines and can be used as a
297 multicomponent (CO₂, SO₂, NO_x, HCl and HF) capture solvent [74-76].

298 Unfortunately, although substitution of amines with ammonia may bring some
299 reduction in the energy intensity of the capture process, it does not improve the
300 process safety as ammonia is both a toxic substance and highly flammable.
301 Moreover, a major drawback of ammonia is its high volatility leading to
302 ammonia slip during the CO₂ absorption process [63]. To comply with
303 environmental requirements, the ammonia slip can be controlled either by
304 adding an additional ammonia water wash or by operating the absorber below
305 20°C. Unfortunately, in both cases the resulting capital and operating costs
306 increase and thus, as was expected [59; 74; 77], only a slight reduction of the
307 average cost of CO₂ avoided from \$61/t-CO₂ to \$53/t-CO₂ was reported [78].

308 Another technology that is relatively close to market commercialisation is oxy-
309 fuel combustion, in which the fuel is combusted in an O₂-rich atmosphere.
310 Although there are neither commercial nor full-scale demonstration plants
311 operating at the moment [59], some projects are in the planning stage [9]7.
312 However, a recent suspension of funding at an advanced stage of the
313 FutureGen project [79; 80] shows that completion of such projects is highly
314 dependent upon financial incentives and political climate. The primary
315 advantage of oxy-combustion technology is that it produces a nearly pure CO₂
316 stream after the flue gas has been through SO_x and NO_x emission control
317 systems and ash separation units. This CO₂ then only needs to be conditioned
318 and dehydrated prior to compression and transport. The main challenges of this
319 technology, which are likely to slow its wide implementation, are:

- 320 • The net efficiency of the oxy-fuel power plant is reduced by 8–12% points
321 [15] because of the cryogenic air separation unit (ASU) for O₂ production
322 [13].
- 323 • High safety standards are required to prevent oxygen leakage [13].
- 324 • The combustion temperature must be controlled to avoid hot spots in the
325 combustion zone that would enhance NO_x production in the boiler [15].
- 326 • Air leakage into the boiler must be minimised to maintain desired purity
327 of the CO₂ stream and to minimise the power requirement of the CO₂
328 compression and purification unit [81; 82].

329 If the direct combustion of fuel is considered as a means for satisfying the heat
330 requirement in the calciner, the CaL process can be seen as a merging of the
331 post-combustion CO₂ capture and the oxy-combustion technologies, where only
332 some portion of fuel is burned in an O₂-rich environment. Currently, CaL
333 concepts are being tested experimentally at bench- and pilot-scale plants
334 worldwide. The main advantages of the CaL system over the solvent-based
335 CO₂ capture technologies are:

- 336 • Heat can be recovered and used to generate an additional amount of
337 high-pressure steam through the exothermic carbonation of lime at 650–
338 700°C and utilisation of heat available in the process streams [83].
- 339 • The predicted efficiency penalty is 7% to 8% points [84], with the CO₂
340 capture stage accounting for 2% to 3%, which is mainly due to the
341 oxygen requirement [39]. This is comparable to the efficiency penalty of a
342 flue gas desulphurisation unit (FGD) (0.5–4%) [85].
- 343 • The technology uses fluidised bed reactors, which have been
344 commercially proven for coal combustion systems.
- 345 • Compared to oxy-fuel power plant, 30–50% less O₂ is required for oxy-
346 combustion of fuel in the calciner, leading to smaller ASU size [28; 39].
- 347 • Natural limestone or dolomite, the source for CaO, is globally available
348 and inexpensive [31] and CaO is characterised by high CO₂ absorption
349 capacity.

- 350 • The average cost of CO₂ avoided is estimated to be \$29–50/t-CO₂ which
351 is more than 50% less than for amine scrubbing [78; 86-89].
352 • Compared to solvents, CaCO₃ and CaO are much less hazardous to the
353 operators' health and the environment [14].

354 Reduction in the sorbent CO₂ carrying activity on cycling operation as a result of
355 sintering, attrition and sulphation appears to be the major challenge of this
356 technology. Although this results in a considerable amount of spent sorbent to
357 be replaced, some part of the sorbent can be reused for cement production,
358 increasing the profitability of both the power and cement industries [14].

359

360 **3 REVIEW OF CALCIUM LOOPING BENCH- AND PILOT-** 361 **SCALE TESTING**

362 Insight into system behaviour under various operating conditions is required to
363 optimise process parameters and to assess feasibility, before commercial-scale
364 installations are designed and built. Although the CaL process has only been
365 considered for CO₂ capture from fossil-fuel power systems since 1999, a
366 number of test facilities have already been built (Table 2), with rapid progress
367 after 2009. The review by Dean et al. [14] devoted to the CaL process has
368 described bench-scale tests using the 10 kW_{th} unit at IFK (University of
369 Stuttgart), 30 kW_{th} unit at the INCAR-CSIC, 75 kW_{th} unit at CANMET Energy
370 and 120 kW_{th} unit at the Ohio State University. However, this review mostly
371 focused on the attrition and material performance during the bench-scale tests.
372 Moreover, the developments in the pilot-plant testing by 2010 and 2013 have
373 been outlined by Anthony [22] and Boot-Handford et al. [15], respectively. This
374 section focuses on the progress in CaL process testing at a bench- and pilot-
375 scale from 2010, with the aim of gathering the valuable design and operational
376 data for development and validation of process models,.

377 Table 2: Review of design and operating conditions of bench- and pilot-scale calcium looping facilities

Research institute	Size (kW _{th})	Carbonator				Calciner				Inlet CO ₂ content (% _{vol})	Max. CO ₂ capture level (%)	CO ₂ purity (% _{vol})
		Type*	Diameter (m)	Height (m)	Temperature (°C)	Type*	Diameter (m)	Height (m)	Temperature (°C)			
Industrial Technology	1	BFB	0.1	2.5	600–700	MB	0.05	0.9	800–900	12.5	99	N/A
Research Institute	3	BFB	0.1	2.5	600–700	RK	0.27	5	500–1000	12.5	99	N/A
	1900	BFB	3.3	4.2	650	RK	0.9	5	500–1000	12.1–14.5	N/A	N/A
Consejo Superior de Investigaciones Científicas	30	CFB	0.1	6.5	568–722	CFB	0.1	6	800–1000	15–16	90	27
	1700	CFB	0.65	15	600–715	CFB	0.75	15	820–950	12.5	90	85
Darmstadt University of Technology	1000	CFB	0.59	8.66	650–670	CFB	0.4	11.35	<1000	12–12.6	92	N/A
IFK at University of Stuttgart	10	BFB	0.114	3.5	630–700	CFB	0.071	12.4	850–900	15	97	20–55
	200	CFB	0.023	10	650	CFB	0.021	10	875–930	15	N/A	N/A
	200	CFB	0.033	6	600–680	CFB	0.021	10	875–930	15–16	93	N/A
Ohio State University	120	EB	N/A	N/A	450–650	RK	N/A	N/A	850–1300	3–25	>90	N/A
Vienna University of Technology	100	BFB	0.28**	2	650	CFB	0.08**	5	850	N/A	N/A	N/A
CANMET Energy	75	BFB/MB	0,1	2–5	580–720	CFB	0,1	4,5–5	850–950	8	97	N/A
Cranfield University	25	EB	0.1	4.3	600–650	BFB	0.165	1.2	900–950	15	80	N/A
Tsinghua University	10	BFB	0.149	1	630	BFB	0.117	1	850	15	95	22.5

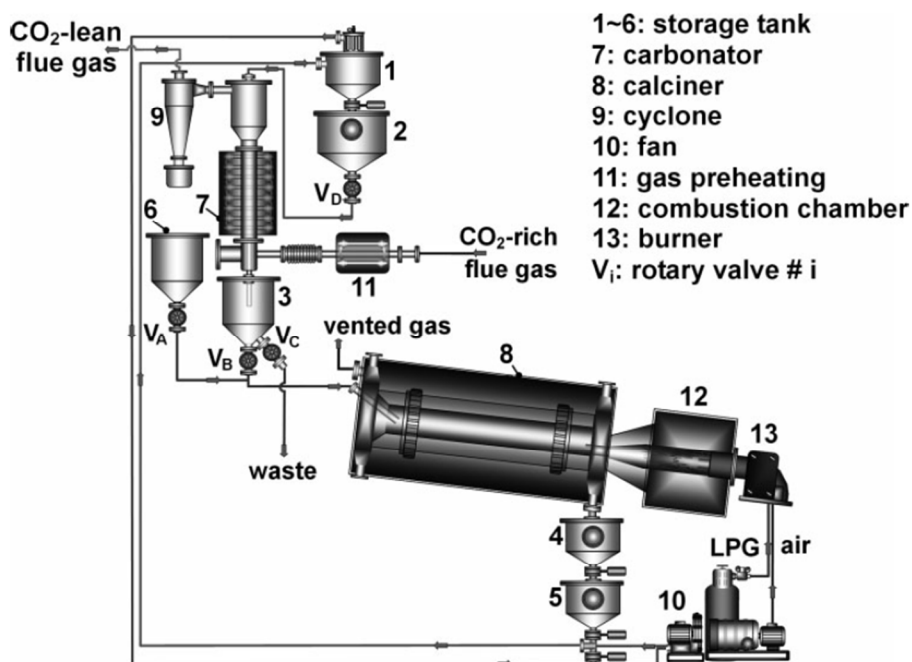
*BFB - Bubbling Fluidized Bed; CFB - Circulating Fluidised Bed; MB - Moving Bed; EB - Entrained Bed; RK - Rotary Kiln. ** Equivalent diameter based on cross-section area.

378 3.1 Industrial Technology Research Institute

379 3.1.1 Experimental facility description

380 3.1.1.1 Bench-scale unit

381 The Industrial Technology Research Institute (ITRI) in Taiwan has developed a 1 kW_{th}
 382 bench-scale unit, which can be operated in either batch or continuous mode. The unit
 383 comprises a bubbling fluidised bed (BFB) carbonator (gas velocity of 0.2–0.4 m/s), with
 384 a gas distributor located at the entrance, and a moving bed (MB) calciner. The solids
 385 are transported between the carbonator and the calciner through a 1 inch solid
 386 circulation pipe of 0.5 m length [90].



387
 388 **Figure 3: 3 kW_{th} bench-scale unit at ITRI (Reprinted with permission from Chang et al.**
 389 **[91]. Copyright 2015 Wiley.)**

390 The unit was modified by substituting the MB calciner with an air-fired rotary kiln
 391 calciner (RK) (Figure 3). This increased the capacity to 3 kW_{th}. The calciner was
 392 designed to have a length-to-diameter ratio of 18.5 and an inclination angle of 5°, based
 393 on operating experience in the cement industry. Such design corresponds to a

394 residence time of approximately 30 min at a speed of 1 rpm. Furthermore, liquefied
395 petroleum gas is directly fired in the calciner using the 58 kW_{th} burner. The gas enters
396 the BFB carbonator through the perforated plate distributor composed of 96 holes of 1.5
397 mm in diameter. Although the carbonation reaction is exothermic, the carbonator was
398 heated using an external heating system to balance the heat losses to the environment
399 [91].

400 **3.1.1.2 Pilot-scale facility**

401 Design of the 1.9 MW_{th} pilot plant, which removes a tonne of CO₂ per hour from the
402 Hualien cement plant flue gas containing 20–25% of CO₂ [92], was based on experience
403 with the 3 kW_{th} unit. The perforated plate gas distributor was selected due to higher
404 attainable velocities, based on cold model tests. The design consists of a double-
405 layered perforated plate with 6 mm holes and an open-area ratio of 1.56%. As a means
406 of temperature control 36 2 m water-cooled double steel jackets were suspended at the
407 top of the carbonator. The system is designed to operate with an average conversion of
408 20–40% and CO₂ capture levels of 80–95%. Heat for calcination is provided through
409 direct oxy-combustion of diesel in the RK calciner which requires flue gas recirculation
410 for temperature control. A key benefit of this configuration is more uniform temperature
411 distribution in the calciner and thus, increased usable length for calcination.

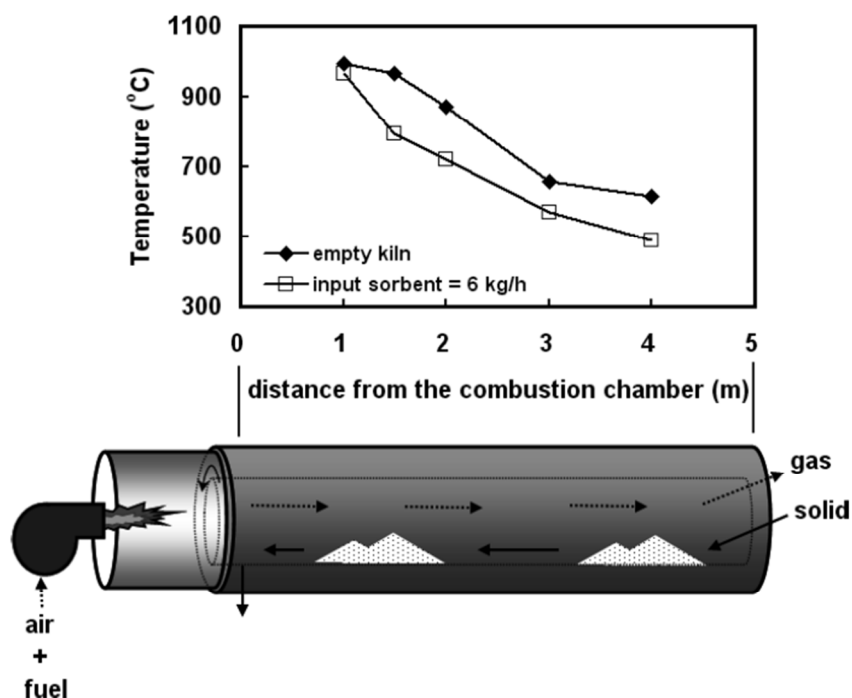
412 **3.1.2 Test campaign using 1 kW_{th} bench-scale unit**

413 Tests were performed to assess CO₂ capture efficiency using a fluidising medium in the
414 carbonator composed of 85%_{vol} air and 15%_{vol} CO₂. Prior to performing the
415 experiments, the industrial grade limestone was calcined at a temperature of 850°C
416 [90].

417 During 57 h of continuous operation 0.1 kg/h of fresh limestone was supplied to the
418 calciner. The experiment revealed that the CO₂ capture level in the carbonator was
419 maintained at above 99% over the entire time. Although preliminary results indicated the
420 practicability of such a configuration, the MB carbonator was difficult to operate [91].

421 3.1.3 Test campaign using 3 kW_{th} bench-scale unit

422 As in the previous case, the flue gas entering the carbonator contained approximately
 423 15%_{vol} CO₂, representative of values found in CFPPs. The flue gas was first preheated
 424 to 230°C and then fed from the feed tank to the carbonator at a controlled rate of
 425 47 dm³/min. To account for the sorbent deactivation, fresh limestone was fed to the
 426 calciner, while some of the solids circulating in the system, which comprises both
 427 inactive and active sorbent, was purged from the system.



428
 429 **Figure 4: Temperature distribution in the rotary kiln calciner in the first test (Reprinted**
 430 **with permission from Chang et al. [91]. Copyright 2015 Wiley.)**

431 The first test performed using the modified 3 kW_{th} unit was a batch test to evaluate
 432 operation of the RK calciner. It demonstrated that if the calciner is fed with fresh
 433 limestone at the rate of 6 kg/h, the useable length for the calcination reaction is
 434 approximately 1.5 m, corresponding to a sorbent residence time of 9 minutes. This
 435 arises because a temperature of 1000°C was observed 1 m from the combustion
 436 chamber and thus excessive sintering would occur in this region (Figure 4). On the

437 other hand, a temperature of 721°C was observed 2 m from the combustion chamber
438 causing operating conditions downstream of the calciner to be unsuitable for the
439 endothermic calcination reaction. Nevertheless, the calcination efficiency was found to
440 be higher than 96%, while the carbonation conversion was 63.7%, proving low sorbent
441 sintering rates [91].

442 The 3 kW_{th} pilot plant was then used to run a 100-h campaign, the main objective of
443 which was to keep the CO₂ capture level above 85%. This campaign showed that
444 selection of the appropriate fresh sorbent make-up rate and spent sorbent purge rate is
445 not only critical for reaching the desired CO₂ capture level, but also for ensuring stable
446 and efficient operation of the system; if the make-up rate was lower than the purge rate,
447 the total solid inventory in the system was reduced and excessive degradation of the
448 sorbent activity was observed. On the other hand, increasing the solid inventory through
449 an increased make-up rate improved the CO₂ capture level to above 99%. However, this
450 would increase the operating cost of the process as it would require more heat input to
451 the calciner. It needs to be highlighted that such a high level of inventory in the calciner
452 had not been expected at the design stage, and thus, its efficiency dropped to 39%
453 because insufficient heat was supplied through liquid petroleum gas combustion to
454 sustain the endothermic calcination reaction.

455 When the inventory in the carbonator, which was operated at approximately 650°C,
456 fluctuated around the desired value the CO₂ capture level varied between 80% and
457 100%. The average residence time of solids in the carbonator was 2 h, with an average
458 conversion of solids in the carbonator of 30% and a calcination efficiency of 75%. This
459 campaign also revealed that particle attrition is an important phenomenon in the CaL
460 system as the mean particle size decreased from 248 μm to 188 μm over this period
461 [91].

462 **3.1.4 Data for process modelling**

463 An unconventional process configuration developed at the ITRI, which includes the RK
464 calciner, is beneficial in investigating integration opportunities between the power and

465 cement industries. Since the equipment sizes and the key operating conditions have
466 been disclosed [90; 91], the data available should be sufficient to, at least, verify the
467 model behaviour in terms of solids inventory or operating temperatures under varying
468 operating conditions. Moreover, a simple verification could be performed for the calciner
469 and calciner performance. It will be of benefit to benchmark the model with the
470 performance of the 1.9 MW_{th} pilot plant, provided that detailed experimental data
471 become available.

472 **3.2 Consejo Superior de Investigaciones Científicas**

473 **3.2.1 Experimental facility description**

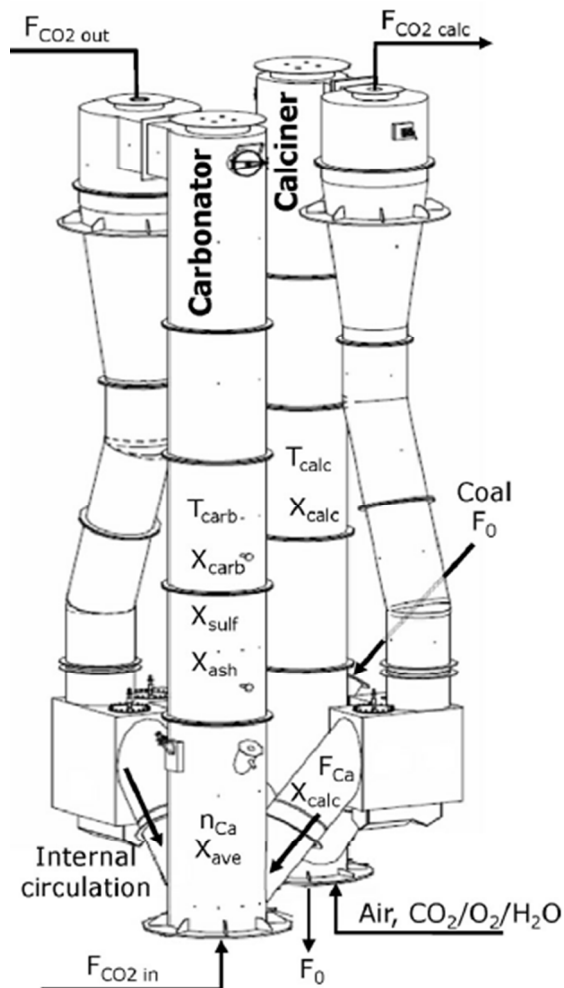
474 **3.2.1.1 Bench-scale unit**

475 The Instituto Nacional del Carbón - Consejo Superior de Investigaciones Científicas
476 (INCAR-CSIC) has developed a 30 kW_{th} unit which consists of two interconnected CFB
477 reactors. The carbonator is 6 m high and 0.1 m in internal diameter. It is fluidised using
478 a synthetic flue gas containing 3–25%_{vol} of CO₂ and is operated at 568–722°C [93]. The
479 heating system in the carbonator is only used during system start-up. Coal is
480 combusted in 2–6% excess air to maintain the desired temperature in the calciner [93].
481 The calciner is 6.5 m high and the same internal diameter and is operated at 800–
482 900°C. Each reactor is equipped with a high-efficiency cyclone, from which the solids
483 are directed through a vertical standpipe to the BFB loop seal [94].

484 **3.2.1.2 Pilot-scale facility**

485 By combining the experience gained through running the 30 kW_{th} unit and the industrial
486 experience for large-scale CFB combustors, INCAR-CSIC in agreement with ENDESA,
487 Foster Wheeler and HUNOSA, with substantial R&D support from University of Stuttgart
488 (IFK), Lappeenranta University, Imperial College and the University of Ottawa and
489 CanmetENERGY, developed a 1.7 MW_{th} pilot plant designed to process approximately
490 1% of the flue gas produced in the 50 MW_{el} La Pereda CFPP in Asturias, Spain (Table
491 4). This project, called CaOling, was part-funded by the European Union 7th Framework
492 Programme. The pilot plant comprises two interconnected CFB reactors 15 m in height

493 with an internal diameter of 0.75 m in the calciner and 0.65 m in the carbonator (Figure
 494 5) operating with gas velocities of 3–5 m/s which are similar to those encountered in
 495 industrial CFBs [95].



496

497 **Figure 5: Design of the 1.7 MW_{th} pilot plant at INCAR-CSIC (Adapted with permission**
 498 **from Arias et al. [96]. Copyright 2015 Elsevier.)**

499 The typical operating temperatures for the carbonator and calciner are 600–715°C and
 500 820–950°C, respectively. The temperature in the carbonator can be controlled through
 501 removable bayonet tubes. The calciner is directly fired with coal, either in an oxy-
 502 combustion or air-combustion environment. Fresh limestone is continuously fed to the
 503 calciner to maintain the desired average conversion of sorbent of 0.1–0.7 (Table 3). In

504 both CFB reactors the solids leaving the risers are separated from the gas stream in the
 505 high-efficiency cyclones, and then directed to the double BFB loop seals by gravity. This
 506 design allows control of the solid looping rates between, and thus the solid inventories
 507 in, the CFB reactors [96].

508 **Table 3: Operating conditions of the 1.7 MW_{th} pilot plant at INCAR-CSIC [95; 96]**

Input from power plant	Value	Pilot plant operating conditions	Value
Flue gas flow rate (kg/h)	680–2300	Maximum coal flow (kg/h)	325
CO ₂ concentration (% _{vol})	12.6	Maximum fresh sorbent flow (kg/h)	300
O ₂ concentration (% _{vol})	5.5	O ₂ flow to calciner (kg/h)	300–600
H ₂ O concentration (% _{vol})	7.0	CO ₂ flow to calciner (kg/h)	700–2250
SO ₂ concentration (% _{vol})	0.07	Air flow to calciner (kg/h)	600–2500
N ₂ concentration* (% _{vol})	74.83	Inventory in carbonator (kg/m ²)	100–1000

*nitrogen concentration calculated to balance the remaining constituents.

509 3.2.2 Test campaign using 30 kW_{th} bench-scale unit

510 The preliminary experiments conducted by Alonso et al. [94] revealed operating issues
 511 with the unit. A main concern was insufficiently high separation efficiency of the
 512 cyclones (92–97%) that led to loss of solids inventory. This resulted in unstable
 513 operation of the system as the solid looping rates and the solids inventory could only be
 514 kept constant for a short time. Nevertheless, this study showed that the carbonator was
 515 operated in nearly isothermal conditions ($\pm 20^\circ\text{C}$) and that the actual CO₂ capture levels
 516 were close to equilibrium values at a particular carbonator temperature, provided that
 517 the amount of solid bed inventory and the solid looping rate were satisfactory.

518 On extension of the risers' heights and reconstruction of the high-efficiency cyclones,
 519 the system stability was improved. The modified system operated with CO₂ capture
 520 levels of 70–90%, which were close to the equilibrium value at 650°C, depending on the
 521 gas velocity (2.0–2.1 m/s) and the solids circulation rates (0.8–2.3 kg/m²s). However, for
 522 the highly cycled particles, which can attain an average conversion close to the residual

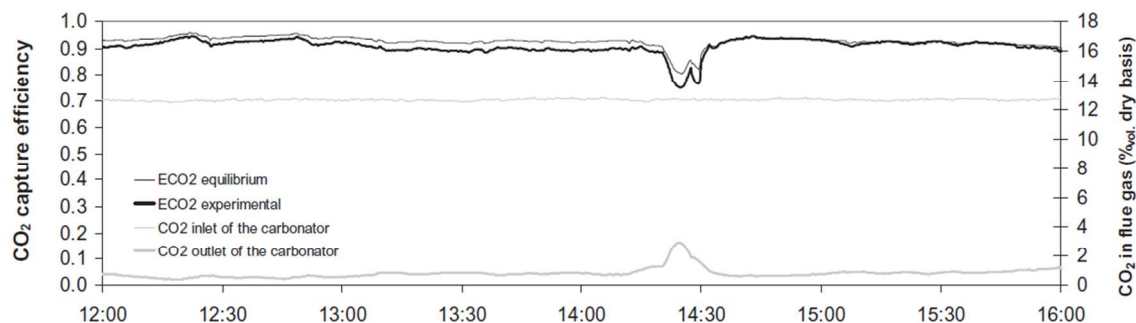
523 conversion of 0.07–0.12, the CO₂ capture level dropped to 65–75% for a solids
524 circulation rate of 1.0–1.8 kg/m²s [94].

525 In tests carried out by Rodríguez et al. [93], the 30 kW_{th} unit was used to treat flue gas
526 containing 20%_{vol} CO₂. Initially 20 kg of limestone was loaded into the system that was
527 operated at 800–850°C for the calciner and 630–700°C for the carbonator, with gas
528 velocities of 3 m/s. The analysis revealed that the purity of the CO₂ stream released
529 from the calciner was approximately 27%_{vol} and the concentration of CO₂ in the clean
530 gas was approximately 7%_{vol}. This corresponded to an actual CO₂ capture level of
531 approximately 70%, which was lower than the equilibrium CO₂ capture level within this
532 temperature range. It was found that under realistic operating conditions an actual CO₂
533 capture level of 70–90% was achievable for bed inventories of 400 kg/m² for solid
534 looping rates of 0.5–2.2 kg/m²s.

535 **3.2.3 Test campaign using 1.7 MW_{th} pilot plant**

536 Arias et al. [96] reports that the 1.7 MW_{th} pilot plant was operated for more than 1800 h,
537 with 380 h in CO₂ capture mode with a CO₂ capture level of 40–95%. Stable operation
538 under oxy-combustion in the calciner (excess O₂ of more than 5%_{vol}) has been
539 maintained for 170 h.

540 Representative results from the experimental trials were reported for the first time by
541 Sánchez-Biezma et al. [97] (Figure 6). These results confirm the findings from previous
542 studies that if the process is operated with proper solid inventory and sorbent activity,
543 the actual CO₂ capture in the carbonator is close to the equilibrium value at given
544 temperature (above 90% at 660°C). Moreover, a SO₂ capture level of more than 95%
545 was achieved.



546

547 **Figure 6: Representative steady state results captured during testing of the 1.7 MW_{th} pilot**
548 **plant at INCAR-CSIC (Reprinted with permission from Sánchez-Biezma et al. [97].**
549 **Copyright 2015 Elsevier.)**

550 As no fresh limestone was added to the system, the conversion of the CaO to CaCO₃
551 decreased towards the residual value of 0.1. Also, there were several issues with
552 maintaining proper solid inventories when the oxy-firing mode was tested. Although CO₂
553 purity in the gas leaving the calciner reached 85% when the calciner temperature was
554 950°C, low solid inventory and sorbent activity caused the CO₂ capture level to drop
555 below the equilibrium level, to around 75%. Nevertheless, the authors claim that high
556 CO₂ capture levels can be achieved even if highly deactivated sorbent is used with high
557 sulphate conversions, provided the system is operated with the proper solid inventory.

558 Arias et al. [96] reported and thoroughly investigated the steady state operation of the
559 1.7 MW_{th} pilot plant at INCAR-CSIC. In the initial phase of the experimental trials, a CO₂
560 capture level of less than 40% was reached due to the high content of non-calcined
561 limestone in the solid inventory because the calciner was operated below 920°C.
562 Moreover, the conversion dropped to 0.067 after more than 5 h of continuous operation
563 without fresh limestone make-up. The same conclusion was drawn as in the study by
564 Sánchez-Biezma et al. [97] that a CO₂ capture level of more than 80% can be reached,
565 even when the sorbent has reached its residual conversion and there is a high SO₂
566 capture level (95%), provided enough solid inventory is available. These results confirm
567 trends determined using the 30 kW_{th} unit and prove that the solid inventory and the
568 sorbent conversion are the most relevant operating parameters in the carbonator
569 reactor.

570 3.2.4 Data for process modelling

571 Information available in the literature, which includes detailed descriptions of the bench-
572 and the pilot-scale facilities, provides essential input into model development. Most of
573 the operating conditions, such as temperatures, solid looping rates, oxygen
574 consumption rates and CO₂ contents in off-gases from the calciner and the carbonator
575 have been disclosed. This allows for a local validation of model predictions. Moreover,
576 global performance of the carbonator and the calciner can be validated.

577 Tests conducted using both facilities revealed that the carbonator operates at nearly
578 isothermal conditions, which allows the assumption of isothermal conditions in
579 modelling the FB reactors. Moreover, the actual CO₂ capture level was found to be
580 close to that determined by equilibrium at a given temperature. Such assumption is,
581 however, only valid for relatively active sorbent, as the experimental trials showed a
582 reduction in CO₂ capture level for highly cycled particles.

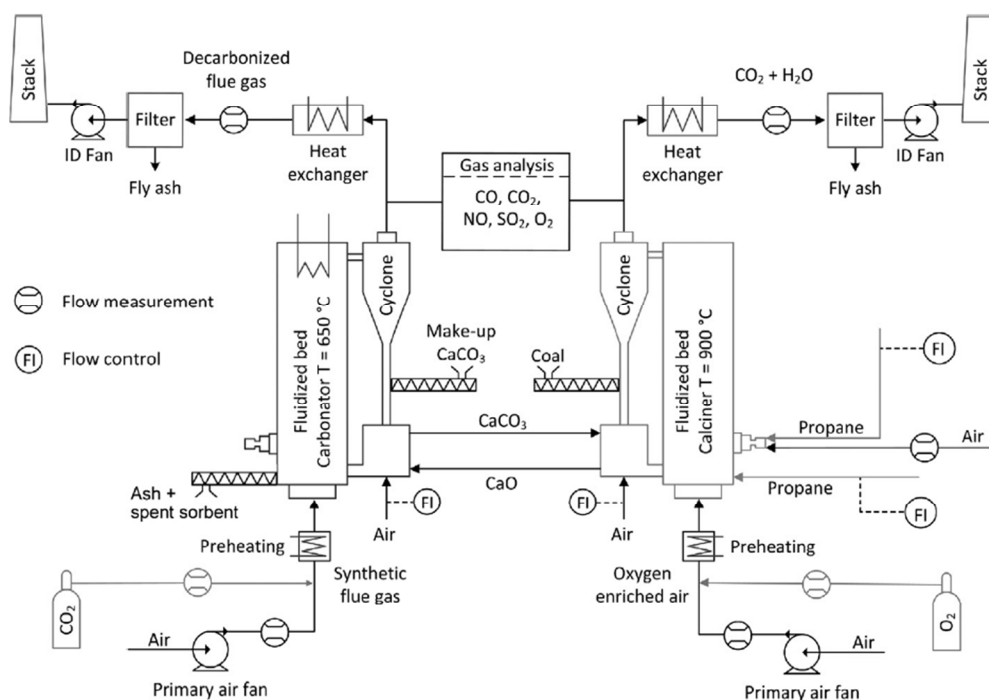
583 3.3 Institute of Energy Systems and Technology at Darmstadt 584 University of Technology

585 3.3.1 Experimental facility description

586 The 1 MW_{th} pilot plant erected and commissioned at Darmstadt University of
587 Technology comprises two interconnected CFB reactors that are refractory lined to
588 minimise heat loss (Figure 7). The carbonator, which is 8.66 m high and 0.59 m in
589 internal diameter, is equipped with internal cooling tubes to control the temperature.
590 Moreover, in contrast to other pilot plants, fresh limestone is fed to the carbonator,
591 where it is heated to 650°C utilising the exothermal carbonation reaction. Such
592 configuration is claimed to reduce fuel and O₂ consumption in the calciner [98]. In
593 addition, synthetic flue gas, which can be heated up to 350°C using auxiliary electric
594 heaters, is used as a fluidising medium in the carbonator. O₂-enriched air preheated up
595 to 450°C is used to fluidise the calciner that is 11.35 m high and 0.4 m in internal
596 diameter. To maintain the calcination reaction, the pilot plant is designed to combust

597 either gaseous fuel, using a gas burner or a bed lance, or solid fuel, which is introduced
598 by a gravimetric dosing system.

599 Unlike other pilot plants, the so *residence time* lids between the loop seals of the CFBs are
600 transferred by screw conveyors. These can be equipped with heat transfer jackets,
601 allowing for accurate solids circulation rate and is capable of flexible operation under
602 various loads. However, in a commercial-scale unit, large volumes of solids will be
603 transferred between the reactors and the solid loads will vary due to changes in the
604 power plant load, making the screw conveyors mechanically inefficient [99]. The flue
605 gas and the CO₂ stream are subsequently cooled down in the heat exchangers, and
606 then cleaned from fly ash in the fabric filters.



607
608 **Figure 7: Process flow diagram of the 1 MW_{th} pilot plant at Darmstadt University of**
609 **Technology (Reprinted with permission from Ströhle et al. [98]. Copyright 2015 Elsevier.)**

610 3.3.2 Test campaign

611 The first tests using the 1 MW_{th} pilot plant were conducted in July 2011. Since then, the
612 facility has been operated for around 400 h to analyse CO₂ capture using the CaL

613 process. In the first campaign, lasting 72 h, a continuous separation of CO₂ from the
614 1300 Nm³/h synthetic gas comprising 10–12%_{vol} CO₂ was analysed [98]. Throughout
615 the campaign, the make-up flow was maintained at 70–150 kg/h and the solid looping
616 rate between 1500 and 3000 kg/h. The study revealed that lower CO₂ capture levels are
617 obtained if CaO, which has been calcined at 1000°C before the test, is fed to the
618 carbonator rather than fresh limestone. This is because a large fraction of older sorbent
619 was present in the bed and caused a drop in the fraction of active sorbent. An increase
620 in CO₂ capture level was observed when fresh limestone was fed to the carbonator.
621 Despite the poor performance of the calciner cyclone and the low CO₂ concentration in
622 the CO₂ stream caused by limited firing power in the calciner, the total CO₂ capture level
623 was greater than 90%.

624 After increasing the power of the burners and the lances and improving the cyclone
625 performance, a second test campaign using propane firing in the calciner was carried
626 out. These changes led to a significant reduction in the make-up rate. Moreover, the
627 fluidisation air was enriched with 50% O₂ to maintain a desirable gas velocity in the
628 calciner and to ensure nearly complete combustion of propane. Again, the carbonator
629 was operated at 660°C and was fed with synthetic flue gas containing 12%_{vol} CO₂. To
630 maintain a desired average CO₂ capture level in the carbonator, the solid looping rate
631 was kept at 2000 kg/h, which corresponded to an average Ca:C molar ratio of 11.6. The
632 maximum CO₂ capture level in the carbonator was found to be 85%, increasing to 92%
633 when oxy-combustion of propane in the calciner is considered.

634 In the third campaign, the calciner was fired with pulverised coal and the fluidisation air
635 enriched by 45–50% O₂. The temperature in the carbonator reached 670°C. The same
636 amount of synthetic flue gas was used as in the second campaign. To reach the same
637 CO₂ capture level in the carbonator (85%), the solid looping ratio needed to be
638 increased to approximately 2800 kg/h (Ca:C = 17.2). The CO₂ concentration in the
639 clean gas was close to the equilibrium CO₂ concentration at that operating temperature.
640 Therefore, the reaction was limited by chemical equilibrium leading to stable operating

641 conditions. The CO₂ capture level dropped to approximately 60% when the temperature
642 in the carbonator dropped to 610°C [98].

643 **3.3.3 Data for process modelling**

644 The description of the facility by Ströhle et al. [98] provides the information on
645 equipment dimensions required for detailed process modelling. The data gathered from
646 the three campaigns allow validation of the performance of a model overall and in
647 respect of the carbonator CO₂ capture level. Some information on local parameters,
648 such as fluidising air temperature, CO₂ flow rate at the inlet to the carbonator and the
649 solid looping rates is available and would increase the quality of model validation. In
650 addition, an operating range for some parameters, such as the fresh sorbent make-up
651 rate and solid looping rate, was disclosed and would allow validation of a model at
652 different operating points.

653 **3.4 Institute of Combustion and Power Plant Technology at University** 654 **of Stuttgart**

655 **3.4.1 Experimental facility description**

656 **3.4.1.1 10 kW_{th} bench-scale dual fluidised bed unit**

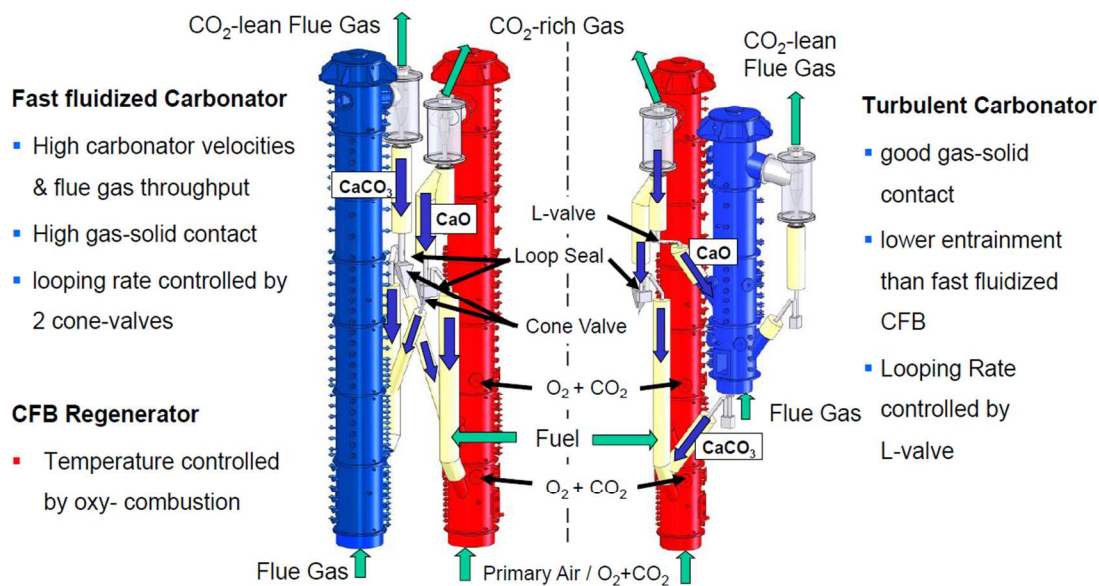
657 The Institute of Combustion and Power Plant Technology (Institut für Feuerungs-und
658 Kraftwerkstechnik, IFK) at the University of Stuttgart has developed a CaL bench-scale
659 unit based on a 10 kW_{th} dual fluidised bed (DFB) that can be operated in continuous
660 mode [100]. The practicability and stability of the DFB system was first analysed using a
661 down-scaled cold model [101; 102].

662 In the 10 kW_{th} IFK unit, the CFB (gas velocity of 4-6 m/s) and the BFB (gas velocity less
663 than 1.2 m/s) can each be operated either as the carbonator or calciner. A benefit of
664 operating the BFB as the carbonator and the CFB as the calciner is ease in process
665 control. The novel configuration of this DFB system results in control of the calcium
666 circulation rate between the beds by varying the cone valve opening and the BFB
667 absolute pressure. Due to heat losses to the environment, the CFB, the BFB and the

668 solid circulation system are electrically heated [103]. The temperature in the calciner
 669 can be raised by direct natural gas combustion in O₂-enriched air (40%_{vol} O₂), if the
 670 electric heating system capacity is insufficient [100].

671 3.4.1.2 200 kW_{th} pilot-scale dual fluidised bed facility

672 To investigate the long-term performance of the process under real combustion
 673 conditions, a 200 kW_{th} pilot plant was built at the IFK. The pilot plant design includes a
 674 CFB calciner operating in a fast-fluidisation regime and a reconfigurable CFB
 675 carbonator that can operate either under a turbulent or fast-fluidised fluidisation regime
 676 (Figure 8) [104; 105]. A design involving two symmetric CFBs, which operate in a fast-
 677 fluidised regime, required redesign of the solid circulation system and implementation of
 678 two cone valves for controlling the looping ratios in both CFBs independently [105].
 679 Conversely, for the configuration with the carbonator operating in the turbulent regime,
 680 the solid circulation rate is controlled through the L-valve which is directly fed from the
 681 CFB calciner [104].



682

683 **Figure 8: Comparison of 200 kW_{th} DFB pilot plant configurations at IFK [106]**

684 The fast-fluidised CFB calciner, 10 m in height and 0.021 m in internal diameter, is
 685 equipped with a staged oxidant supply for oxy-combustion of solid fuel (coal, wood

686 pellets, wood chips). Although the firing system is designed to handle up to 70%_{vol} O₂ to
687 meet the energy demand in the calciner, flue gas recirculation is implemented to
688 achieve realistic operating conditions. In the turbulent fluidised bed carbonator (6 m in
689 height and 0.033 m in internal diameter), the heat is removed using the FB heat
690 exchanger. It is also designed to operate under lower fluidisation velocities and with
691 lower residence time than the CFB carbonator [104]. The fast-fluidised CFB carbonator,
692 10 m high and 0.023 m in internal diameter [102], is fluidised with the flue gas, and the
693 heat released due to the exothermal reaction is removed via a water-cooled heat
694 exchanger in the dense bed region and bayonet cooler in the lean bed region. The
695 facility has a 400 kW_{th} gas burner to generate hot gas and heat up the system during
696 start-up. To minimise the heat loss in the system, the reactors are lined with insulating
697 concrete and refractory material resistant to abrasion [105].

698 **3.4.2 Test campaign using a 10 kW_{th} DFB unit**

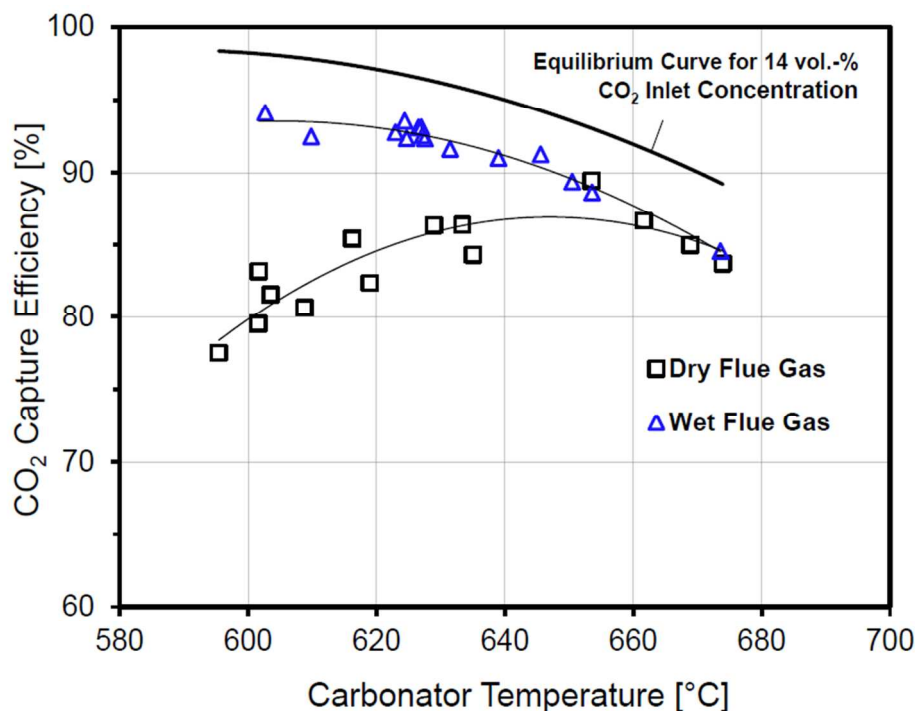
699 The tests were conducted using German limestone from Swabian Alb that was used to
700 clean synthetic flue gas having 15%_{vol} CO₂ to simulate CFPP conditions. It was
701 relatively straightforward to achieve steady state operation with a minor make-up of
702 fresh sorbent to account for attrition losses. When the carbonator was operated at
703 660°C, the achievable CO₂ capture level exceeded 90%. The maximum level of 97%
704 was observed in the periods when fresh sorbent was added to the carbonator, causing
705 its temperature to drop to around 625°C.

706 The effect of the carbonator operating temperature and the CO₂ capture level was then
707 analysed and compared with the equilibrium data. The CO₂ capture level was reported
708 to be close to that determined by chemical equilibrium at the given temperature, which
709 was assured by maintaining a Ca:C ratio higher than 14 [103]. A recent study by Varela
710 et al. [107] identified that the CO₂ capture level of 90% is achievable at Ca:C ratio of 8,
711 provided that steam is present in the carbonator and the calciner. Such behaviour is
712 explained by likely enhancement of sorbent morphology in the presence of steam,
713 favouring sorption and desorption of CO₂. Moreover, the increase of the CO₂

714 concentration in the calciner, which can be associated with CO₂ recycle to lower O₂
 715 concentration in the fluidising gas, was found to significantly affect the reactor efficiency.

716 3.4.3 Test campaign using the 200 kW_{th} DFB facility

717 Dieter et al. [104] reported that more than 600 h of successful operation has been
 718 recorded and the facility was found to be hydrodynamically stable. The tests performed
 719 mainly aimed at reaching steady state conditions under variable temperature with
 720 synthetic flue gas containing 14%_{vol} CO₂.



721
 722 **Figure 9: Effect of the carbonator temperature on the CO₂ capture level data from the 200**
 723 **kW_{th} DFB at IFK [106]**

724 Although O₂ concentrations reached 50%_{vol} during wood pellet combustion, no hot spots
 725 were observed and the temperature profile in the calciner was uniform (875–930°C).
 726 This indicates the key benefit of staged oxidant supply. However, the desired
 727 temperature of 650°C was observed only in the dense region of the turbulent FB
 728 carbonator, while the temperature was reduced in the upper region. Nevertheless, the
 729 CO₂ capture level was maintained above 90% indicating that most of the reaction takes

730 place in the dense region. Fluctuations in the carbonator temperature (620–650°C) have
731 a minor effect on the carbonator efficiency. Furthermore, higher CO₂ capture levels are
732 obtained if wet flue gas, such as from the desulphurisation unit, is fed to the carbonator.
733 These results were found to closely follow the trend determined by the equilibrium
734 calculations revealing good gas-solid contact in the carbonator (Figure 9). This means
735 that lower looping ratios would be required to reach the desired CO₂ capture level,
736 leading to energy saving in the regenerator [104].

737 **3.4.4 Data for process modelling**

738 The literature provides a detailed description of the equipment sizes and configurations,
739 allowing for development of a model. Nevertheless, the limited information available on
740 the equipment operating conditions and efficiencies and the lack of detailed stream data
741 will restrict model validation, especially in terms of the conversion rates and the solid
742 looping rates. However, the results from both campaigns clearly indicate that the
743 carbonator performance can be reasonably well represented using equilibrium models,
744 provided an appropriate solid inventory, sorbent conversion and looping rate of
745 Ca:C>14 are assumed.

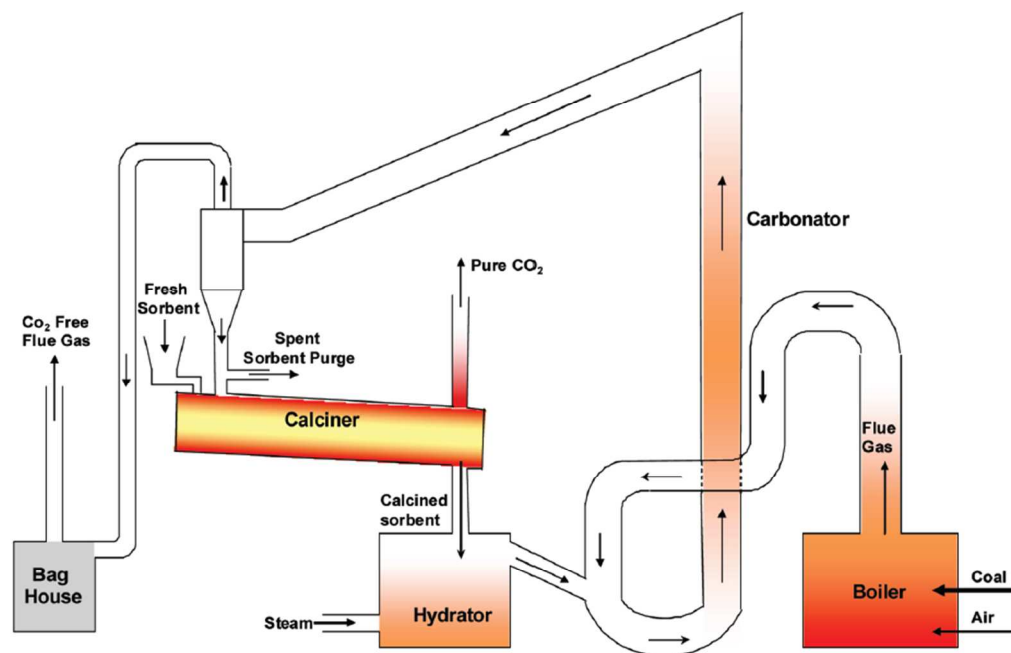
746 **3.5 Ohio State University**

747 **3.5.1 Experimental facility description**

748 The researchers at Ohio State University have pioneered the concept of simultaneous
749 CO₂ and SO₂ capture using the Carbonation-Calcination Reaction process (CCR). The
750 process was proposed as a merger of the Ohio State Carbonation Ash Reactivation
751 (OSCAR) process [108-110] and the Calcium-based Reaction Separation for CO₂
752 (CaRS-CO₂) process [111], two processes developed and patented by Ohio State
753 University.

754 In the 120 kW_{th} sub-pilot plant (Figure 10) the CaO or Ca(OH)₂ can be fed to the
755 carbonator, which is the entrained bed (EB) reactor operated at 450–650°C to allow for
756 CO₂ and SO₂ capture. Sorbent regeneration is conducted in the electrically-heated RK

757 calciner. Calcined sorbent is then hydrated using steam to improve the sorbent
 758 conversion over multiple cycles [112]. Some of the deactivated sorbent (2–10%) is
 759 purged and the fresh sorbent is fed directly to the calciner.



760

761 **Figure 10: Process flow diagram of the Ohio State University sub-pilot plant (Reprinted**
 762 **with permission from Wang et al. [112]. Copyright 2015 American Chemical Society.)**

763 3.5.2 Test campaign

764 The CCR sub-pilot plant was used to purify flue gas produced in air-combustion of coal
 765 and natural gas in the stoker and containing 12.5%_{vol} CO₂ and 1450 ppm_v of SO₂. Prior
 766 to being fed to the carbonator the flue gas was maintained at 650°C using natural gas.

767 In the once-through test, Wang et al. [112] showed that the presence of fly ash in the
 768 carbonator does not affect the CO₂ and SO₂ capture levels. In addition, the amount of
 769 fly ash entering the carbonator needs to be considered when deciding on the purge
 770 fraction to maintain the proper amount of active sorbent in the system.

771 The study clearly indicated that application of Ca(OH)₂ with the mass median diameter
 772 (D₅₀) of 3 μm results in CO₂ capture levels between 40 and 100% for Ca:C ratios

773 between 0.5 and 1.7. This performance was superior to traditional lime, as CO₂ capture
774 levels of 9% were found for ground lime ($D_{50} = 600 \mu\text{m}$) and pulverised ground lime (D_{50}
775 $= 18 \mu\text{m}$) at the same Ca:C ratio. Nevertheless, as pointed out by Dean et al. [14],
776 separation and fluidisation of such small particles from the gas stream in industrial-scale
777 reactors would be extremely challenging and, therefore, the process feasibility and
778 practicability is somewhat questionable.

779 **3.5.3 Data for process modelling**

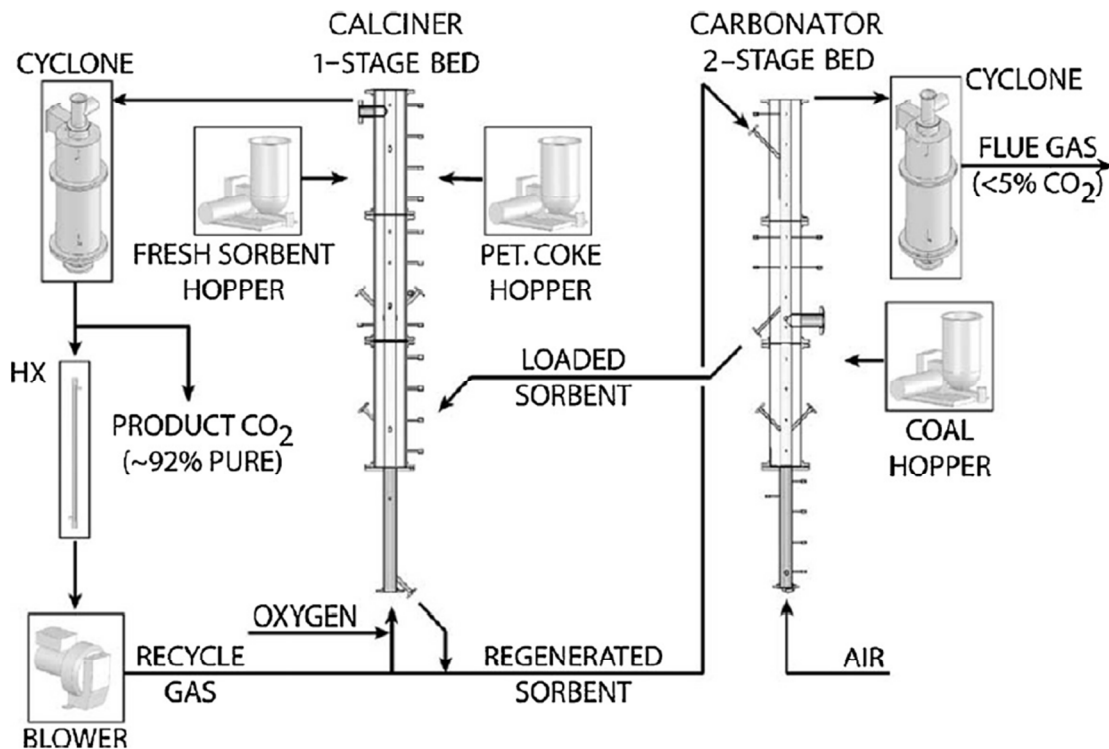
780 Information on design characteristics of the CCR process available in the papers and
781 patents is limited and does not reveal the equipment sizes. This would not allow for
782 detailed model development. Nevertheless, simplified models, which consider only
783 thermodynamic performance, could be developed.

784 The results of the test campaign are detailed enough to validate the global performance
785 of a model. Unfortunately, no detailed information is provided on the local data, such as
786 the solid looping rates or limestone make-up.

787 **3.6 CANMET Energy Technology Centre**

788 **3.6.1 Experimental facility description**

789 CanmetENERGY has developed a 75 kW_{th} pilot-scale DFB system which operates in
790 semi-continuous mode to demonstrate the process feasibility. The system was first
791 designed and analysed using process simulation by Hughes et al. [29]. The pilot plant
792 comprises a CFB calciner and a carbonator operated under either moving or bubbling
793 bed conditions (Figure 11).



794

795 **Figure 11: Schematic of the 75 kW_{th} pilot plant developed at CANMET Energy (Reprinted**
 796 **with permission from Hughes et al. [29]. Copyright 2015 Elsevier.)**

797 Depending on the application the calciner is 4.5–5 m in height and 0.1 m in internal
 798 diameter and can be operated under air, O₂-enriched air or oxy-firing with flue gas
 799 recycle. The carbonator was divided into two stages to distinguish the
 800 combustion/sulphation and carbonation processes. Therefore, depending on the test
 801 performed it is 2–5 m in height and 0.1 m in internal diameter. Such configuration allows
 802 air or a mixture of air and superheated steam to fluidise both stages. To minimise the
 803 heat losses in the system, the reactors are lined with refractory and insulation materials.
 804 Moreover, each reactor is equipped with three 4.5–5 kW_{el} electric heaters that are used
 805 during start-up and sometimes to control the reactor temperature [33; 113]. The
 806 CANMET Energy pilot plant has a novel solid transport system for sorbent looping that
 807 includes a 45° “T” that collects solids from the calciner-pierced distributor. The solids
 808 rate through the conveying line to the carbonator is controlled using a solenoid valve.
 809 The calcined sorbent enters the carbonator through the L-valve. Similarly, the 45° “T”

810 line allows the carbonated sorbent to be directed to the calciner or to the second stage
811 of the carbonator for SO₂ capture.

812 3.6.2 Test campaign using a 75 kW_{th} pilot plant

813 The 75 kW_{th} pilot plant has been operated under continuous mode for more than 50
814 hours (Table 4). During the tests, the carbonator was fed with a synthesised mixture of
815 air and CO₂, to achieve CO₂ concentrations of 15–16%_{vol}. The fluidising air was
816 preheated to 250°C prior to being fed to the carbonator. The calciner was operated
817 under three heating modes: electric heating, biomass combustion in air, and oxy-
818 combustion of biomass and bituminous coal with flue gas recycle.

819 **Table 4: Operating conditions of the 75 kW_{th} CanmetENERGY pilot plant**

Parameter	Minimum	Maximum
CFB Calciner		
Initial sorbent inventory (kg)	4.5	5.0
Sorbent make-up batch (kg)	0.3	0.5
Biomass consumption rate (kg/h)	4.0	7.6
Coal consumption rate (kg/h)	2.6	5.8
Air flow rate (air-firing mode) (kg/h)	8.0	14.4
O ₂ flow rate (oxy-firing mode) (kg/h)	5.2	7.7
Moving or bubbling FB carbonator		
Air flow rate (slpm)	40	100
CO ₂ flow rate (slpm)	7.5	19.0
CO ₂ concentration at inlet (% _{vol})	15.0	16.5
Air flow for solid conveying (slpm)	35	55

820 The tests performed by Lu et al. [33] confirmed that the CaL system can operate with a
821 CO₂ capture level of 97% within the first several cycles. As the superficial gas velocity
822 was increased, the CO₂ capture level decreased, which can be associated with lower
823 residence time of gas in the carbonator. A considerable drop in the CO₂ capture level to
824 approximately 72% was observed after 25 cycles. This confirms the impact of sorbent

825 deactivation on process performance and implies the need for fresh sorbent make-up.
826 The highest CO₂ capture level (98%) was reached within the temperature window of
827 580–600°C for fresh sorbent and approximately 700°C after 20 cycles. When the
828 temperature dropped below 500°C, the reaction rate slowed significantly. This was
829 reflected in the off-gas CO₂ concentration of approximately 9–10%_{vol} CO₂, hence in a
830 drop of CO₂ capture level.

831 Finally, testing oxy-combustion of fuel in the calciner has proven this approach to be
832 appropriate for providing heat for sorbent regeneration. There were no hot spots in the
833 calciner, in spite of the high O₂ concentration in the primary gas of 40–50%_{vol} balanced
834 with the recycled flue gas. The maximum concentration of CO₂ was 85%_{vol}.

835 **3.6.3 Data for process modelling**

836 Information available in papers by Lu et al. [33] and Symonds et al. [113] include
837 detailed descriptions of the process configuration and equipment dimensions which can
838 be used to set up a model. Analysis of the CO₂ capture level under various operating
839 conditions allows validation of the global performance of a model. Again, their study
840 confirmed that the actual CO₂ capture levels could be close to the equilibrium values in
841 practice. Their study also revealed that the carbonator temperature can be used as a
842 means to maintain the desired CO₂ capture level, even with highly cycled sorbent.
843 Although no information on the solid looping ratios and rates was provided, several
844 operating limits were included in the paper by Lu et al. [33] that can form a basis for
845 local validation of a model.

846 **3.7 Cranfield University**

847 **3.7.1 Experimental facility description**

848 A 25 kW_{th} bench-scale CaL rig developed at Cranfield University consists of an EB
849 carbonator, 4.3 m high and 0.1 m in internal diameter, and a BFB calciner, 1.2 m high
850 and 0.165 m in internal diameter. The desired operating temperature in the carbonator

851 (600°C) and the calciner (900 - 950°C) is maintained using electric heating elements
852 [114].

853 **Table 5: Optimal gas composition in 25 kW_{th} Cranfield University pilot plant [114]**

Fluidising gas	Carbonator	Calciner
CO ₂ volumetric flow rate (L/min)	-	40
O ₂ volumetric flow rate (L/min)	-	16
Air volumetric flow rate (L/min)	150	-
CH ₄ volumetric flow rate (L/min)	22.5	11

854 The calciner is directly heated through oxy-combustion of natural gas. The resulting flue
855 gas is used as the fluidising medium. The flue gas generated in the air-combustion of
856 natural gas, which contains 8%_{vol} CO₂, is used as the fluidising medium in the
857 carbonator. The optimal operating gas input rates are presented in Table 5. Solid input
858 to the calciner is achieved using a screw feeder with a maximum feeding rate of 1.6
859 kg/h. This proves the practical applicability of the screw conveyors for solid fuel and
860 sorbent handling in the CaL units, as explained in Section 3.3.1. The solid looping rates
861 are controlled via two fluidised loop seals, at the top and bottom of the calciner [115].
862 The unit has two cyclones at the top of the carbonator to ensure that the sorbent lost
863 with the flue gas is kept to a minimum [114].

864 3.7.2 Test campaign

865 A primary objective of the test campaign was maximisation of CO₂ capture level through
866 modification of the process configuration and the operating conditions. CO₂ capture
867 levels of 50% and 70% were reached with carbonator temperature windows of 650–
868 700°C and 600–650°C, respectively. This improvement in efficiency at lower
869 temperatures is attributed to its effects on chemical equilibrium, as reducing the
870 temperature reduces the equilibrium CO₂ content and in turn increases the equilibrium
871 CO₂ capture level.

872 Moreover, in batch runs the optimum CO₂ capture level, which was close to 90%,
873 occurred for particle sizes between 125–250 μm. This was in agreement with results
874 from another study carried out in the same group by Kavosh [116]. This behaviour was
875 explained by an increase in the surface-to-volume ratio as the particle size was
876 reduced. However, it was found that below 125 μm, the CO₂ capture level dropped
877 below 50%. It appears likely that such small particles were Geldart's group C, and thus
878 were difficult to fluidise leading to bed agglomeration [117].

879 The maximum CO₂ capture level of 80% in the carbonator was reached after rig
880 modifications resulting from the cold model, temperature and particle size distribution
881 optimisation, and implementation of air shakers and heating elements to the loop seals
882 to enhance solids transfer and temperature [115].

883 **3.7.3 Data for process modelling**

884 The 25 kW_{th} unit has been described in detail in the analysed sources. As the
885 description includes information on the equipment characteristics and operating
886 conditions, it can be used for model development. The reliability of the CO₂ capture
887 level prediction can be validated for various carbonator temperatures and particle size
888 distributions. Unfortunately, the local level validation will be limited to flue gas and fuel
889 oxy-firing in the calciner as no data on the solid circulating rates and solid inventory
890 were disclosed.

891 **3.8 Tsinghua University**

892 **3.8.1 Experimental facility description**

893 The DFB system developed at Tsinghua University consists of two interconnected
894 BFBs. The internal diameters of the carbonator and the calciner are 0.149 m and 0.117
895 m, respectively, and the height of each bed is 1 m. In this system, solids are transferred
896 between the beds through the cyclones and the downcomers. In addition, solid injection
897 nozzles are used to transport solids from the bed to the riser in each BFB. To
898 compensate for the heat losses and to maintain the desired temperature in the

899 carbonator and the calciner, each reactor was equipped with four 2.5 kW_{th} electric
900 heaters. Additional electric heaters are used for heating the flue gas, the risers, the
901 cyclones and the downcomers [118].

902 **3.8.2 Test campaign**

903 In the test campaign, dolomite ($D_{50} = 0.5$ mm) was used as a source of natural sorbent
904 to clean synthetic flue gas containing 12.1–14.5%_{vol} CO₂. The solid looping rate was
905 maintained at 30–36 kg/h which corresponded to an inventory height of 0.3 m in the two
906 BFBs. When the desired temperatures in the carbonator (630°C) and the calciner
907 (850°C) were achieved, the CO₂ fraction in the clean gas was 1.2%_{vol}, which
908 corresponds to a CO₂ capture level of 89.2% in the carbonator. When the operating
909 temperature of the carbonator was increased to 680°C, the CO₂ fraction increased to
910 10%_{vol} due to chemical equilibrium limitations.

911 In continuous CO₂ capture from synthetic flue gas, the calciner was operated at 810°C,
912 which led to maximum purity of 22.5%_{vol} CO₂. On the other hand, the carbonator was
913 operated at 640°C reducing the CO₂ fraction in the clean gas to 0.7%_{vol}, which
914 corresponds to a CO₂ capture level of 95%. Under such operating conditions the
915 average conversion in the carbonator reached 70.4%. Due to incomplete calcination,
916 the average conversion of particles leaving the carbonator was 16.2%. Finally, Feng et
917 al. [118] have noted that after 7 h of continuous operation, the mean size of the particles
918 was reduced to 0.16 mm and 0.42 mm in the calciner and the carbonator, respectively.

919 **3.8.3 Data for process modelling**

920 The bench-scale unit can serve as a basis for model development as its equipment
921 sizes and operating conditions are or can be determined from other data provided by
922 Fang et al. [118]. A model can be validated at a global level as data are available for the
923 carbonator CO₂ capture level under different operating conditions. Also, as the inlet gas
924 flow rates to BFBs, the solid looping rates, and the CO₂ fraction in the gas streams from
925 the carbonator and the calciner are available, local validation of the process streams
926 can be conducted.

927 **3.9 Vienna University of Technology**

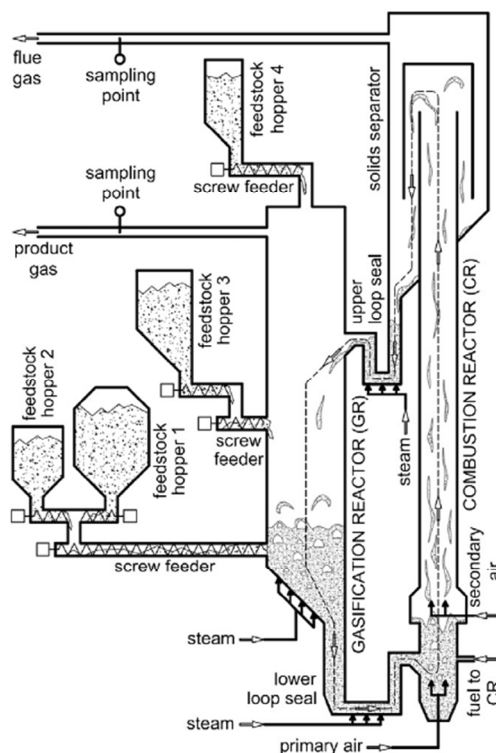
928 **3.9.1 Experimental facility description**

929 Researchers at the Vienna University of Technology have been testing a sorption-
930 enhanced reforming (SER) process for biomass gasification in the 100 kW_{th} DFBgasifier
931 facility (Figure 12), another possible application of the CaL process [119; 120]. Such
932 process has a potential of improving the performance and reliability of the integrated-
933 gasification combined cycle (IGCC) power plants. Other processes that utilise the
934 sorption-enhanced reactions, such as a sorption-enhanced steam methane reforming
935 (SE-SME), can yield high-purity H₂ (>95%_{vol}) [121; 122]. However, this process is more
936 likely to be applied to meet increasing demands for H₂ in industrial processes, such as
937 ammonia synthesis and fossil fuels processing [123], rather than for large-scale power
938 generation.

939 In conventional solid feedstock gasification process the BFB gasifier reactor operates at
940 850–900°C, while air-combustion of fuel in the CFB combustor takes place at 920°C.
941 For this system, olivine was a suitable bed material with satisfactory resistance to
942 attrition and moderate tar cracking activity [120]. The solids are transported between the
943 reactors via two loop seals which are fluidised with steam. The concept was then
944 successfully used for development of the biomass-fired 8 MW_{th} combined heat and
945 power plant in Guessing, Austria that delivers 1.8 MW_{el} of electricity and 4.5 MW_{el} of
946 heat to the local community [124].

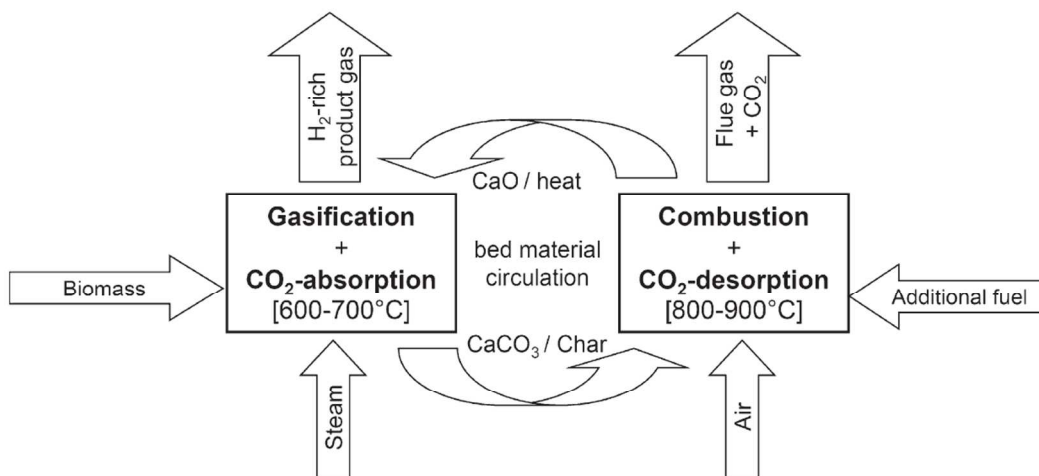
947 **3.9.2 Test campaigns**

948 The 100 kW_{th} unit has been modified to operate under SER process conditions with in-
949 situ CO₂ capture using limestone (Figure 13). To assure proper conditions for the
950 carbonation reaction, the BFB reactor temperature was reduced to approximately 700°C
951 [120] by reducing the solid looping rates between the reactors [125].



952

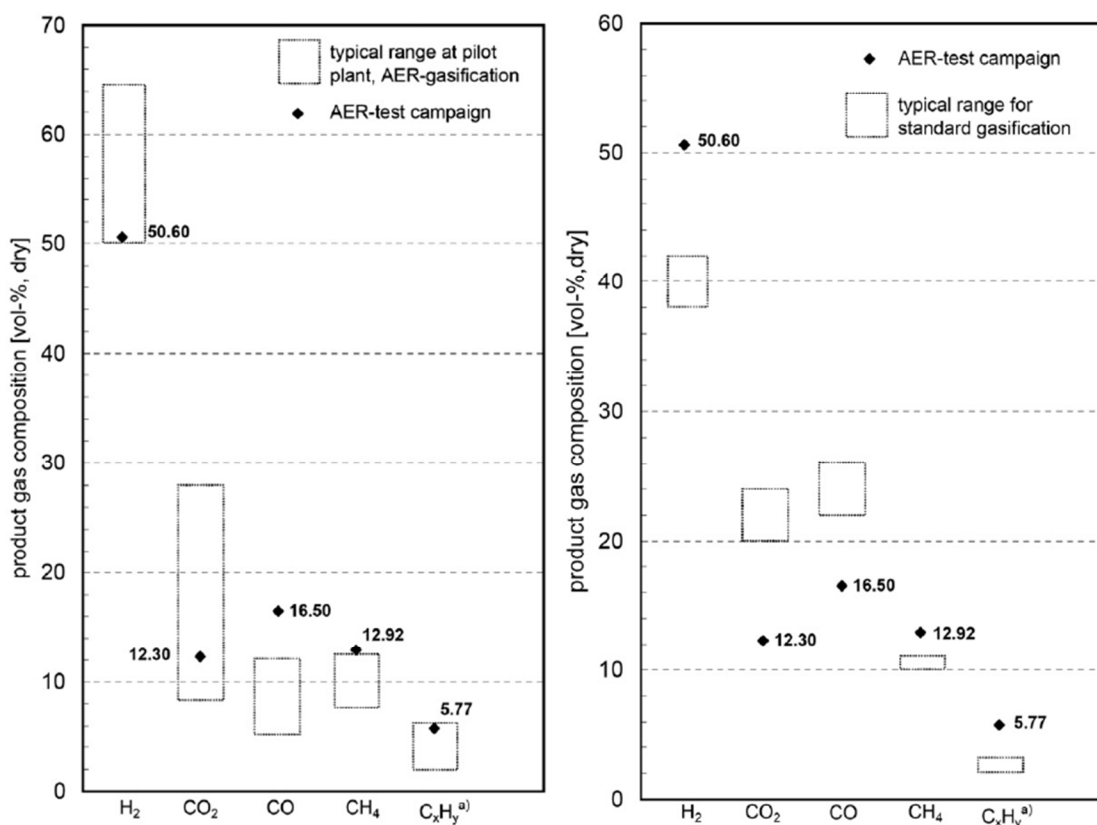
953 **Figure 12: Process flow diagram of the 100 kW_{th} bench-scale plant at Vienna University of**
 954 **Technology (Reprinted with permission from Kirnbauer et al. [126]. Copyright 2015**
 955 **Elsevier.)**



956

957 **Figure 13: Schematic representation of the sorption-enhanced reforming process with in-**
 958 **situ CO₂ capture using calcium looping process (Reprinted with permission from**
 959 **Koppatz et al. [125]. Copyright 2015 Elsevier.)**

960 The analysis by Pfeifer et al. [120] has revealed that compared to the conventional
 961 process, up to 70%_{vol} higher H₂ yields are achievable. This is largely the result of an
 962 equilibrium shift in the water-gas shift reaction caused by CO₂ removal from the gasifier.
 963 Moreover, a simultaneous reduction of the tar content from 4–8 g/Nm³ to 0.3–0.9 g/Nm³
 964 was observed.



965
 966 **Figure 14: Comparison of the syngas composition in conventional and SER gasification**
 967 **processes and the typical range at the pilot plant (Adapted with permission from Koppatz**
 968 **et al. [125]. Copyright 2015 Elsevier.)**

969 A first test campaign using the 8 MW_{el} Guessing CHP operating in SER mode was
 970 reported by Koppatz et al. [125]. A temperature difference was required between the
 971 BFB gasifier and the CFB combustors to allow for efficient carbonation-calcination
 972 reactions. Therefore, the gasification temperature was reduced from 850–900°C to 650–
 973 750°C, while the combustion temperature was reduced from 950°C to 850°C. This was
 974 achieved through low solid looping rates. Moreover, olivine was substituted with

975 limestone as the bed material. The content of H₂ and CH₄ in the syngas, hence its
976 quality, decreases with increase of the gasification temperature. This could be explained
977 by reduction of the driving force for the carbonation reaction, as the equilibrium partial
978 pressure of CO₂ increases with temperature. The quality of the syngas produced in SER
979 operating mode was higher than in the conventional process.

980 **3.9.3 Data for process modelling**

981 A detailed description of the experimental facility, which includes both the equipment
982 dimensions and operating conditions, gives an opportunity for comprehensive
983 equipment modelling. However, as the key objective of the test campaign was to
984 improve syngas quality, no information was provided on the CO₂ capture level.
985 Nevertheless, the available results allow validation of the syngas composition and
986 comparison with the one reached in the conventional process. Although this kind of
987 information does not provide a clear indicator of the CaL process performance in terms
988 of the CO₂ capture level, it can still be used to validate the process performance.

989 **3.10 Summary**

990 In most of the studies, the key parameter describing performance of the CaL process is
991 the CO₂ capture level. If a system is operated with appropriate solid inventory and
992 sorbent conversion, the actual CO₂ capture level is close to the value determined by
993 chemical equilibrium. This allows validation of the global performance of a model, which
994 could be either equilibrium- or kinetics-based. Furthermore, unconventional
995 configurations developed at ITRI and Ohio State University, which include the RK
996 calciner, would be beneficial for validating a model when the power and cement
997 integration is investigated.

998 The testing campaigns provide valuable insight in understanding process performance
999 under varying operating conditions. Some information on local parameters, such as
1000 fluidising air temperature, flue gas composition and flow rate, CO₂ concentration in the
1001 gases leaving the CaL system, solid inventories or looping rates were disclosed.
1002 However, no complete data were available for any of the reviewed experimental

1003 campaigns. Further tests and more detailed data are required to allow validation of a
1004 model at the local level, and thus increase the quality of its prediction.

1005

1006 **4 MODELS FOR THE CALCIUM LOOPING PROCESSES**

1007 Development of novel power generation technologies needs to employ a range of
1008 analysis tools to evaluate various technology aspects. Therefore, experimental trials
1009 using bench- and pilot-scale facilities should be supported with analyses utilising
1010 mathematical and computational models that can be treated as a complementary
1011 source of information on process performance. Moreover, such models allow analysing
1012 the process scaling-up, and thus, expected net efficiency penalties, as well as operating
1013 and capital costs. Since the models vary in complexity and hence in computational
1014 requirements they can be applied at different stages of concept development to
1015 optimise the operating parameters of a process, to evaluate its performance under
1016 different operating conditions, or even to reliably size the equipment in the most time-
1017 efficient manner.

1018 The current literature offers a selection of models for the key units, the carbonator and
1019 the calciner. They range from models based purely on thermodynamic equilibrium,
1020 usually defined by Gibbs' free energy minimisation [26; 32; 127-131], through models
1021 considering sorbent degradation using semi-empirical correlations derived to fit
1022 experimental results [11; 16; 34; 39; 42; 84; 86; 132-146], to semi-predictive [28; 30; 31;
1023 37; 93; 135; 147-149] and predictive models [150] that account for FB hydrodynamics
1024 and reaction kinetics. As the complexity of the models increases, the accuracy of their
1025 predictions increases as well. It needs to be stressed, however, that models of different
1026 complexity are suitable at different stages of process development; for example,
1027 thermodynamic or semi-empirical models would be more suitable for conceptual design
1028 studies, while predictive models would be appropriate at an advanced project stage,
1029 such as front-end engineering design. The CaL models available in the literature are
1030 reviewed in this section and their limitations are identified.

1031 **4.1 Modelling of the sorbent average conversion**

1032 The greatest challenge of using solid sorbents to capture CO₂ is the loss of their
1033 conversion with the number of carbonation/calcination cycles [145]. Thus far, the decay
1034 in sorbent maximum conversion, which is defined as the ratio of the actual and the
1035 theoretical mass of CaO that could have been converted to CaCO₃ for fully carbonated
1036 sorbent, has been represented using semi-empirical correlations. Since such
1037 representation includes fitting parameters, it would predict the activity decay well only
1038 for sorbent for which the values of fitting parameters were determined experimentally.

1039 Dean et al. [14] have noted that the primary cause for sorbent deactivation is sintering
1040 of CaO during calcination at temperatures higher than 900°C [151], and high CO₂ and
1041 steam partial pressures [43]. High affinity of sorbent to SO₂ and H₂S, which are often
1042 present in the flue gas generated in a power plant, especially in units without FGD
1043 plants, would further affect the process performance due to increase in the solid looping
1044 rate. Although the once-through test performed by Sun et al. [152] in presence of SO₂
1045 revealed no difference in the CO₂ capture in the chemically-controlled region of the
1046 carbonation, the calcination rate, and thus the sorbent conversion deteriorated as a
1047 result of CaSO₄ accumulation. Such observation was also made by Grasa et al. [153].
1048 The experimental trials showed that due to high Ca:S ratios in the system, the SO₂ and
1049 H₂S capture efficiencies could reach 100% [112]. As the regeneration process of
1050 sulphated sorbent is possible only at very high temperatures or in reducing conditions
1051 [154; 155], this would enhance sorbent sintering causing a further reduction in the
1052 activity. Moreover, attrition leading to excessive elutriation of sorbent and ash fouling
1053 could occur under such conditions [13; 14].

1054 Sorbent performance is usually represented as a drop in the maximum sorbent particle
1055 conversion with the number of carbonation/calcination cycles (N). Since 2002, many
1056 semi-empirical correlations were developed to characterise the drop in the sorbent
1057 performance, for which the fitting parameters are often determined from the
1058 thermogravimetric analysis (TGA) [28; 156-160]. Such correlations were developed for
1059 non-pretreated sorbents [42; 139-145], and thermally pretreated sorbents [34; 138] that

1060 experience self-reactivation [34; 161]. The most of the semi-empirical correlations have
 1061 been reviewed by Dean et al. [14], and only the most important ones, required to
 1062 understand the more complex models, are presented here.

1063 A first semi-empirical model for the maximum sorbent conversion was developed by
 1064 Abanades [145] based on the assumption that decay in the maximum carbonation
 1065 conversion in the chemically-controlled stage depends only on the number of
 1066 calcination/carbonation cycles.

$$X_N = k^{N+1} + X_r \quad (3)$$

1067 There was a high degree of correlation between the maximum sorbent conversion
 1068 predicted by the model and the experimental data (98.2%) [28; 156; 158-160] for a
 1069 deactivation constant (k) and a residual carbonation conversion (X_r) of 0.782 and 0.174,
 1070 respectively.

1071 A study by Grasa and Abanades [143] has confirmed that the sorbent conversion
 1072 decreases asymptotically to residual conversion that amounts to 0.075–0.08 and is
 1073 constant when the number of calcination/carbonation cycles is higher than 50. Based on
 1074 the proportionality between conversion and the surface area of highly cycled particles
 1075 through the product layer thickness ($X = S/S_0$), Grasa and Abanades [143] have
 1076 proposed a semi-empirical correlation for decay of the sorbent maximum conversion
 1077 which is formulated similarly to typical catalyst deactivation correlations.

$$X_N = \frac{1}{\frac{1}{1 - X_r} + kN} + X_r \quad (4)$$

1078 With a deactivation constant (k) of 0.52 and residual conversion (X_r) of 0.075, the
 1079 prediction of the semi-empirical model presented in Equation (4) was accurate for a
 1080 wide range of limestones, particle sizes and CO₂ partial pressures.

1081 Li and Cai [139] have adopted a five-parameter correlation, with a similar structure to
 1082 the one proposed by Abanades [145].

$$X_N = a_1 f_1^{N+1} + a_2 f_2^{N+1} + X_r \quad (5)$$

1083 Although, the constants in Equation (5) were determined for a particular sorbent, no
 1084 particular reference to their physical meaning was made. This semi-empirical model
 1085 was found to successfully predict the decay in conversion of different sorbents
 1086 (limestone, dolomite, $\text{CaO}/\text{Ca}_{12}\text{Al}_{14}\text{O}_{33}$), provided the fitting parameters were known.

1087 4.1.1 Maximum average conversion of non-pretreated sorbent

1088 The aforementioned semi-empirical models allow determination of the maximum
 1089 carbonation conversion of sorbent particles that have undergone a given number of
 1090 carbonation/calcination cycles. In real systems, however, the population of particles
 1091 would comprise particles that have undergone different numbers of carbonation and
 1092 calcination cycles. Based on the assumption that the solids are well mixed in the
 1093 reactor, Abanades [145] proposed calculating the maximum average conversion in the
 1094 carbonator as:

$$X_{ave,max} = \sum_{N=1}^{N=\infty} r_N X_N \quad (6)$$

1095 The mass fraction of the particles that has undergone N carbonation/calcination cycles
 1096 (r_N) is directly related to the solid looping rate (F_R) and fresh limestone makeup rate (F_0)
 1097 as shown in Equation (7).

$$r_N = \frac{F_0 F_R^{N-1}}{(F_0 + F_R)^N} \quad (7)$$

1098 Using the definition of the maximum carbonation conversion presented in Equation (3),
 1099 Abanades et al. [39] have indicated that for a fluidised bed calciner (perfectly stirred
 1100 reactor), the average conversion of sorbent entering the carbonator can be expressed
 1101 using Equation (8) as a function of the empirical parameters: solid looping rate and
 1102 fresh limestone make-up rate.

$$X_{ave,max} = \frac{k(1 - X_r)F_0}{F_0 + F_R(1 - X_r)} + X_r \quad (8)$$

1103 Assuming that all sulphur present in the fuel reacts with the active sorbent to form
 1104 CaSO₄, Equation (8) can be modified to account for sorbent deactivation caused by
 1105 CaSO₄ formation.

$$X_{ave,max} = \frac{k(1 - X_r)F_0}{F_0 + F_R(1 - X_r)} + X_r - \frac{F_{CO_2}}{F_0 r_{C/S} \gamma_{comb}} \quad (9)$$

1106 As Equation (3) does not account for the residual conversion of sorbent, Equation (4)
 1107 proposed by Grasa and Abanades [143] appears to be the most commonly applied in
 1108 the literature. However, Li and Cai [139] have claimed that it is difficult to determine an
 1109 explicit solution for an infinite sum in Equation (6) when the maximum conversion of the
 1110 sorbent is formulated similarly to Equation (4). Therefore, they have derived a
 1111 correlation for the average conversion by incorporating Equation (5) into Equation (6)
 1112 and calculating the limit of the infinite sum of the geometric series. For $f_2 = 0$ the
 1113 proposed correlation reduces to Equation (8) derived by Abanades et al. [39].

$$X_{ave,max} = \frac{a_1 f_1 F_0}{F_0 + F_R(1 - f_1)} + \frac{a_2 f_2 F_0}{F_0 + F_R(1 - f_2)} + X_r \quad (10)$$

1114 Rodríguez et al. [11] have considered the impact of the reactor performance indicators,
 1115 which define the extent of calcination (f_{calc}) or carbonation (f_{carb}) in each reactor, as well
 1116 as the impact of the uncalcined sorbent (r_0) on the maximum average conversion.

$$f_{calc} = \frac{X_{carb} - X_{calc}}{X_{carb}} \quad (11)$$

$$f_{carb} = \frac{X_{carb} - X_{calc}}{X_{ave,max} - X_{calc}} \quad (12)$$

$$r_0 = \frac{F_0(1 - f_{calc})}{F_0 + F_R f_{calc}} \quad (13)$$

1117 Having incorporated Equations (11) - (13) into Equation (6), and utilising the maximum
 1118 conversion model proposed by Li and Cai [139], Rodríguez et al. [11] derived a semi-
 1119 empirical correlation for maximum average conversion.

$$X_{ave,max} = (F_0 + F_R r_0) f_{calc} \left[\frac{a_1 f_1^2}{F_0 + F_R f_{carb} f_{calc} (1 - f_1)} + \frac{a_2 f_2^2}{F_0 + F_R f_{carb} f_{calc} (1 - f_2)} + \frac{X_r}{F_0} \right] \quad (14)$$

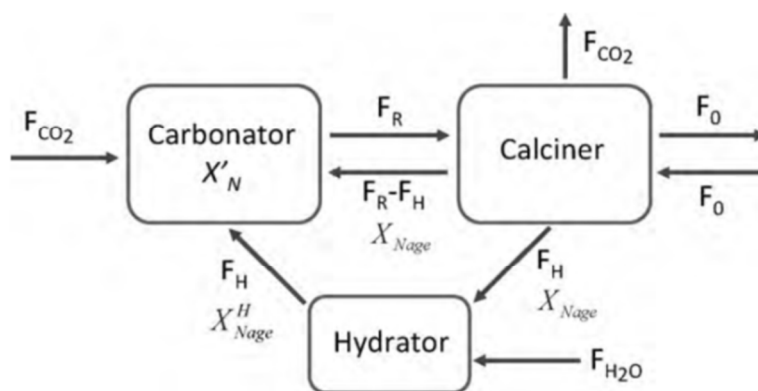
1120 Equation (14) reduces to an equation similar to the one derived by Li and Cai [139] for
 1121 $f_{calc} = 1$ and $f_{carb} = 1$, with the only difference being the squared f_1 and f_2 fitting
 1122 parameters. However, it allows estimation of the maximum average sorbent conversion
 1123 that can be reached in the carbonator. Mantripragada and Rubin [162] stated that the
 1124 actual conversion depends on the carbonation and calcination degree; hence the actual
 1125 conversion in the carbonator and the calciner, which can be seen as equivalent to rich-
 1126 and lean-loading in the solvent scrubbing technologies, are corrected based on the
 1127 carbonator and the calciner performance, using the following expressions:

$$X_{carb} = \frac{f_{carb}}{1 - (1 - f_{carb})(1 - f_{calc})} X_{ave,max} \quad (15)$$

$$X_{calc} = (1 - f_{calc}) X_{carb} \quad (16)$$

1128 4.1.2 Maximum average conversion of hydrated sorbent

1129 Partial hydration is an option for sorbent reactivation that yields higher average sorbent
 1130 conversions compared to unhydrated sorbent [163-167]. Hence, the system can operate
 1131 at lower solid looping and make-up rates leading to a reduced heat requirement for the
 1132 calciner [40]. In this concept (Figure 15) some of the solids leaving the calciner (F_H) are
 1133 diverted to the hydrator, while the remaining ($F_R - F_H$) circulate to the carbonator as
 1134 usual. Therefore, the average conversion models reviewed in Section 4.1.1 are not
 1135 applicable.



1136
 1137 **Figure 15: Calcium looping process with sorbent reactivation through hydration**
 1138 **(Reprinted with permission from Arias et al. [137]. Copyright 2015 Elsevier.)**

1139 Arias et al. [137] have proposed a conversion model that can be used to predict the
 1140 performance of a CaL plant with a hydrator operating in a continuous mode. As such a
 1141 configuration does not produce any change in the number of carbonation/calcination
 1142 cycles that each particle has undergone, the fraction of particles that has undergone N
 1143 carbonation/calcination cycles can be still estimated using Equation (7). Moreover, since
 1144 different fractions of sorbent having different maximum conversions are fed to the
 1145 carbonator, the maximum conversion for a given calcination/carbonation cycle number
 1146 N can be represented as:

$$X'_N = X_{N_{age}} \frac{F_R - F_H}{F_R} + X_{N_{age}}^H \frac{F_H}{F_R} \quad (17)$$

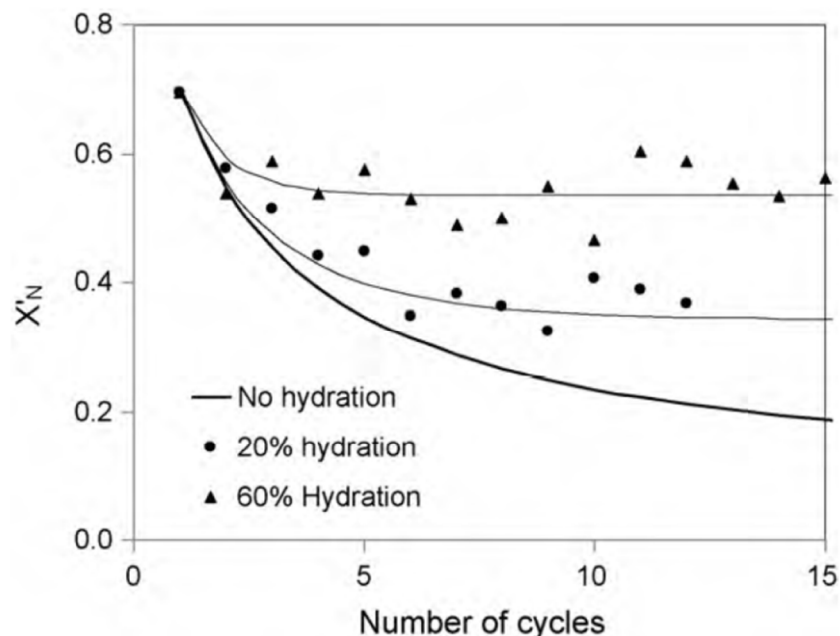
1147 To estimate the maximum conversion X'_N , the particle age N_{age} , with conversion
 1148 capacity in the previous cycle N-1, needs to be determined. For known value of X'_{N-1} ,
 1149 which was taken by Arias et al. [137] as approximately 0.7, the particle age before its
 1150 N^{th} calcination is estimated using Equation (4) in reverse.

$$N_{age-1} = \left(\frac{1}{k}\right) \left(\frac{1}{X'_{N-1} - X_r} - \frac{1}{1 - X_r}\right) \quad (18)$$

1151 The corresponding maximum conversions for the hydrated ($X_{N_{age}}^H$) or non-pretreated
 1152 ($X_{N_{age}}$) sorbent can then be estimated using Equation (4). The decay constant (k^H) and
 1153 the residual conversion (X_r^H) for the regenerated sorbent depend on the degree of
 1154 hydration, and were estimated to be 0.63 and 0.15, respectively for 20% hydration, and
 1155 1.39 and 0.36, respectively for 60% hydration based on experimental data from Grasa
 1156 et al. [166] (Figure 16).

1157 Stable maximum conversions were reached for a relatively small number of cycles. This
 1158 is a result of a balance between the increase in sorbent conversion due to hydration and
 1159 the loss in each carbonation/calcination cycle due to sintering [137]. Finally, the
 1160 maximum average conversion of the sorbent can be determined as:

$$X_{ave,max} = \sum_{N=1}^{N=\infty} r_N X'_N \quad (19)$$



1161
 1162 **Figure 16: Comparison of the experimental data in Grasa et al. [166] and the model**
 1163 **prediction with $F_H/F_R=1$ (Reprinted with permission from Arias et al. [137]. Copyright 2015**
 1164 **Elsevier.)**

1165 4.2 Modelling of carbonation and calcination kinetic rates

1166 4.2.1 Apparent kinetics model for carbonation

1167 Lee [168] has developed a kinetic model for CaO carbonation conversion that is
 1168 reportedly simple to implement during process design and modelling. In this model, the
 1169 CaO conversion rate is expressed as a function of the kinetic rate constant (k_r) and the
 1170 actual and maximum conversion.

$$1171 \frac{dX}{dt} = k_r \left(1 - \frac{X}{X_{max}}\right)^n \quad (20)$$

1172 When $n = 2$, the model prediction is close to the experimental data presented by Bhatia
 1173 and Perlmutter [169], as well as Gupta and Fan [170]. This was reflected in a lowest
 correlation coefficient of 95%.

1174 Equation (20) was formulated in such a way that it could be used to describe both
 1175 chemical- and diffusion-controlled regions of the carbonation reaction. Having estimated
 1176 the values for activation energies and pre-exponential factors using data from both
 1177 sources, Lee [168] identified that the type of limestone does not have a great impact on
 1178 the chemical-controlled regime parameters, while it does for the diffusion-controlled
 1179 ones (Table 6). This was explained by the strong impact of the CaO morphology on the
 1180 reaction rate in the diffusion-controlled region.

1181 **Table 6: Characteristic parameters for the rate constant k [168]**

Controlling mechanism	Bhatia and Perlmutter [169]		Gupta and Fan [170]	
	Activation energy (kJ/mol)	Pre-exponential factor (1/s)	Activation energy (kJ/mol)	Pre-exponential factor (1/s)
Chemical reaction	72.2	171.67	72.7	193.33
Mass transfer	189.3	$2.62 \cdot 10^8$	102.5	$3.88 \cdot 10^3$

1182 4.2.2 Carbonation kinetic model for highly cycled particles

1183 Grasa et al. [171] have proposed a model for sorbent conversion that utilises a rate
 1184 expression consistent with a grain model for the carbonation reaction. The expression is
 1185 similar to the one determined by Abanades et al. [136].

$$\frac{dX}{dt} = k_s S_N (1 - X)^{\frac{2}{3}} (C_{CO_2} - C_{CO_2,eq}) \quad (21)$$

1186 The model assumes that the active surface area of the particle that has undergone N
 1187 calcination/carbonation cycles decreases proportionally with the maximum conversion
 1188 of the particles at the end of the fast carbonation period. It also assumes that the
 1189 CaCO₃ layer thickness (h) reaches a maximum of 50 nm in this period.

$$S_N = \frac{V_{MCaCO_3} \rho_{CaO}}{M_{CaO} h} X_N \quad (22)$$

1190 Using Equation (4) to determine the maximum conversion at given cycle N, the active
 1191 surfaces were determined to be between 1×10^6 and 2×10^6 m^2/m^3 for highly cycled
 1192 particles, while the rate constant k_s was estimated to be 3.2×10^{-10} to 8.9×10^{-10} m^4/mol -
 1193 s. Similar values were yielded (3.1×10^{-10} to 8.7×10^{-10} m^4/mol -s) when the pore model
 1194 described in Equation (23) was applied with the pore structural parameter defined as Ψ_N
 1195 $= 4\pi L_N/S_N^2$.

$$\frac{dX}{dt} = k_s S_N (C_{CO_2} - C_{CO_2,eq}) (1 - X) \sqrt{1 - \Psi \ln(1 - X)} \quad (23)$$

1196 Moreover, Grasa et al. [171] have pointed out that the central value of the estimated
 1197 rate constant is remarkably close to the value of 6.05×10^{-10} m^4/mol -s estimated using
 1198 the pore model by Bhatia and Perlmutter [169].

1199 4.2.3 Changing grain size carbonation and calcination models

1200 Recently, Yu et al. [172] have developed a kinetic model to represent the carbonation
 1201 process through modification of the existing changing grain size model that was
 1202 previously used to represent the reaction between CaO and SO₂ [173]. This model
 1203 assumes that carbonation is an unsteady-state process with the CO₂ concentration
 1204 inside the particle represented in the radial coordinate system as the sum of the
 1205 diffusion and chemical reaction terms.

$$\frac{dC_{CO_2}}{dt} = r_{CO_2} + \frac{1}{R^2} \frac{\partial}{\partial R} \left(D_e R^2 \frac{\partial C_{CO_2}}{\partial R} \right) \quad (24)$$

1206 The first term in Equation (24) accounts for the reversible carbonation reaction for which
 1207 the reaction rate per unit volume of the particle includes both carbonation and
 1208 calcination reaction rates.

$$r_{CO_2} = - \left[k_{carb} S_0 \left(\frac{r_i}{r_0} \right)^2 V_R C_{CO_2} - k_{calc} S_0 \left(\frac{r_i}{r_0} \right)^2 \right] \quad (25)$$

1209 In the model, the carbonation rate constant is represented using Equation (26)
 1210 proposed by Sun et al. [174], while Equation (27) used for the calcination rate constant
 1211 is taken from Borgwardt [175].

$$k_{carb} = \begin{cases} 1.67 \cdot 10^{-4} \exp\left(-\frac{24000}{R_g T}\right) (P_{CO_2} - P_{CO_2,eq}) & \text{if } P_{CO_2} - P_{CO_2,eq} < 10 \text{ kPa} \\ 1.67 \cdot 10^{-3} \exp\left(-\frac{24000}{R_g T}\right) & \text{if } P_{CO_2} - P_{CO_2,eq} > 10 \text{ kPa} \end{cases} \quad (26)$$

$$k_{calc} = 3 \cdot 10^{-2} \exp\left(-\frac{205000}{R_g T}\right) \quad (27)$$

1212 The equilibrium partial pressure ($P_{CO_2,eq}$) was calculated as a function of the reactor
 1213 temperature [36], and the initial surface area of CaO was determined based on the
 1214 initial particle porosity (ε_0), initial grain radius (r_0) and molar volume of CaO and CaCO₃.

$$P_{CO_2,eq} = 10^{\left(7.079 - \frac{8808}{T}\right)} \quad (28)$$

$$S_0 = \frac{3(1 - \varepsilon_0) V_{m,CaO}}{r_0 V_{m,CaCO_3}} \quad (29)$$

1215 According to the changing grain size model, the change in the un-reacted radius of the
 1216 CaO grain is dependent on the carbonation and calcination rate constants.

$$\frac{dr_i}{dt} = -(k_{carb} V_R V_R C_{CO_2} - k_{calc} V_R) \quad (30)$$

1217 The local and average conversions of CaO were expressed as:

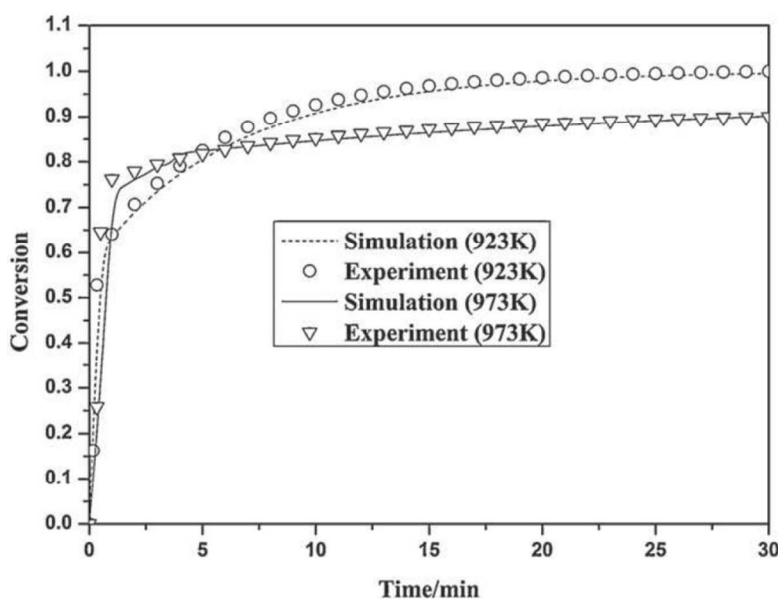
$$X = 1 - \left(\frac{r_i}{r_0}\right)^3 \quad (31)$$

$$X(t) = \frac{1}{\frac{4}{3}\pi R_0^3} \int_0^{R_0} 4\pi R^2 X dR \quad (32)$$

1218 The second term in Equation (24) accounts for the effective diffusivity of CO₂ through
 1219 the sorbent particle. It accounts for the product layer diffusivity (D_p), molecular diffusivity
 1220 of CO₂ in N₂ (D_{m,CO_2}), the Knudsen diffusivity (D_K) and the porosity changes inside the
 1221 particle during the reaction (ε).

$$D_e = \left[(1 - X) \left(\frac{1}{D_{m,CO_2}} + \frac{1}{D_K} \right)^{-1} + XD_p \right] \varepsilon^2 \quad (33)$$

1222 Yu et al. [172] have validated the model with the experimental result for the CGMG75
 1223 sorbent, which was composed of 75%_{wt} CaO and 25%_{wt} MgO, and 15%_{vol} CO₂ in the
 1224 synthetic flue gas. As shown in Figure 17, the model prediction accurately reproduces
 1225 the experimental data in both chemical-controlled and diffusion-controlled regions of the
 1226 carbonation process.

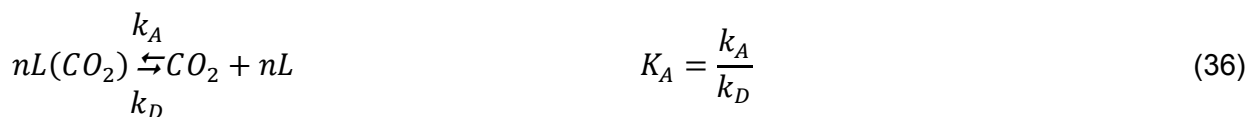
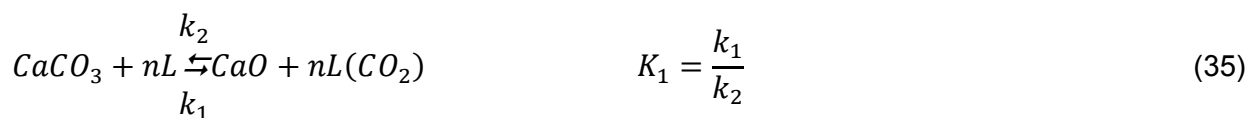


1227
 1228 **Figure 17: Validation of the Yu et al. [172] model with the experimental data (Reprinted**
 1229 **with permission from Yu et al. [172]. Copyright 2015 Elsevier.)**

1230 García-Labiano et al. [176] proposed incorporating the Langmuir-Hinshelwood
 1231 mechanism into the changing grain size model to describe the calcination process. The
 1232 model is based on the similar mass balance to the one presented in Equation (24), but
 1233 with the negative sign for the CO₂ source term, and accounts for both the diffusion and
 1234 the reaction of the gas in a differential volume of the particle.

$$\frac{\partial C_{CO_2}}{\partial t} = -r_{CO_2} + \frac{1}{R^2} \frac{\partial}{\partial R} \left(D_e R^2 \frac{\partial C_{CO_2}}{\partial R} \right) \quad (34)$$

1235 However, in contrast to the model by Yu et al. [172], the calcination reaction is
 1236 described using the two-stage Langmuir-Hinshelwood mechanism. In the first stage,
 1237 considering that one CO₂ molecule can be chemisorbed on n out of L active sites, the
 1238 CaCO₃ is decomposed to CaO and adsorbed CO₂. CO₂ is then desorbed from the
 1239 active site in the second step.



1240 The kinetic rate of calcination per unit of particle volume was then described as:

$$r_{\text{CO}_2} = k_{\text{calc}} S_e (1 - \theta) \left(1 - \frac{P_{\text{CO}_2}}{P_{\text{CO}_2, \text{eq}}} \right) \quad (37)$$

1241 The fraction of the active sites (θ) was found to be well represented by the Freundlich
 1242 isotherm, for which the adsorption constant was represented using the Arrhenius
 1243 expression.

$$\theta = c_0 \exp\left(-\frac{E}{R_g T}\right) P_{\text{CO}_2}^{\frac{1}{2}} \quad (38)$$

1244 According to the changing grain size model, the reaction surface is dependent on the
 1245 particle radius that, in turn, changes as the reaction proceeds.

$$S_e = S_0 \left(\frac{r_1}{r_0}\right)^2 \quad (39)$$

$$r_0 = \frac{3(1 - \varepsilon_0)}{S_0} \quad (40)$$

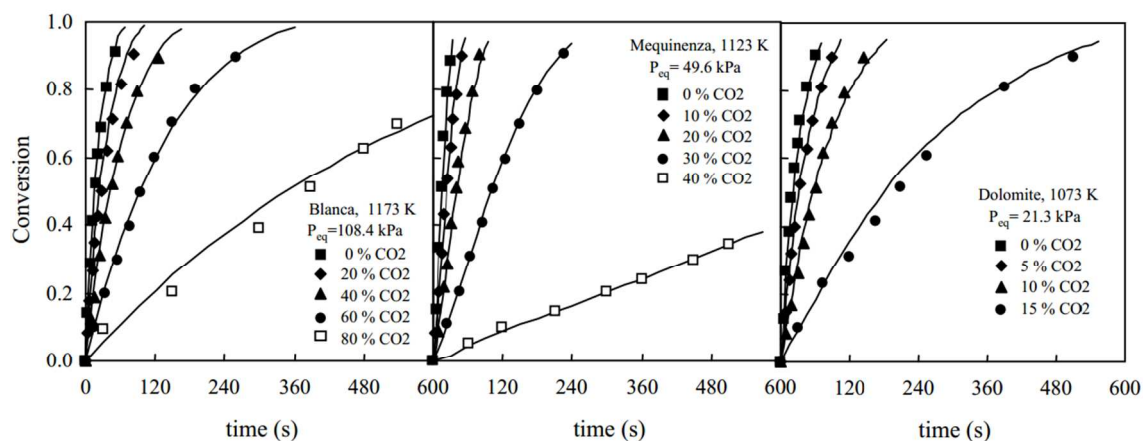
$$r_1 = k_{\text{calc}} V_{M, \text{CaCO}_3} \left(1 - \frac{P_{\text{CO}_2}}{P_{\text{CO}_2, \text{eq}}} \right) \quad (41)$$

1246 The effective diffusion was represented as a combination of the molecular and Knudsen
 1247 diffusions, as well as the particle porosity.

$$D_e = \left(\frac{1}{D_{m,CO_2}} + \frac{1}{D_K} \right)^{-1} \varepsilon^2 \quad (42)$$

$$\varepsilon = \varepsilon_0 - \frac{\rho_{CaCO_3} (V_{M,CaO} - V_{M,CaCO_3})}{M_{CaCO_3}} (1 - \varepsilon_0) X(R, t) \quad (43)$$

1248 The variation in the porosity inside the particle was determined from the initial porosity,
 1249 the stoichiometric volume ratio of solid product to reactant product, and the local
 1250 conversion of $CaCO_3$ given previously by Equation (31). The average conversion at a
 1251 given time is represented using the same form as in Equation (32).



1252
 1253 **Figure 18: Validation of the García-Labiano et al. [176] model with the experimental data**
 1254 **(Reprinted with permission from García-Labiano et al. [176]. Copyright 2015 Elsevier.)**

1255 García-Labiano et al. [176] have validated the prediction of the model at different CO_2
 1256 partial and equilibrium pressures using different limestone compositions and found good
 1257 agreement between the model prediction and the experimental data (Figure 18). The
 1258 changing grain size models, which were adapted to the carbonation and calcination
 1259 processes, were found to closely represent the particle conversion at given
 1260 temperature. Although these did not account for sorbent sulphation and ash
 1261 accumulation, such models would provide a valuable tool in calciner modelling, provided
 1262 they are coupled with reactor hydrodynamics.

1263 4.3 Carbonator reactor modelling

1264 4.3.1 Semi-predictive model with simple hydrodynamics

1265 Alonso et al. [30] have developed a model for the carbonator that combines simple
1266 hydrodynamics correlations with the average conversion of the sorbent and residence
1267 time distribution functions. They have introduced a definition of the active fraction (f_a) of
1268 the particles that is dependent only on the actual residence time (t^*) and the average
1269 residence time (τ) in the carbonator.

$$f_a = 1 - \exp\left(-\frac{t^*}{\tau}\right) \quad (44)$$

$$\tau = \frac{N_{Ca}}{F_R} = \frac{W_{CaO}}{M_{CaO}F_R} \quad (45)$$

1270 This definition of the active fraction of the particles in the carbonator, along with the
1271 definition for the average maximum conversion given by Equation (6), led to the
1272 following expression for the actual average sorbent conversion at the exit of the
1273 carbonator (46) and the CO₂ capture level in the carbonator (47).

$$X = X_{ave,max} \frac{\tau}{t^*} \left[1 - \exp\left(-\frac{t^*}{\tau}\right)\right] = X_{ave,max} \frac{f_a}{\ln\left[\frac{1}{1-f_a}\right]} \quad (46)$$

$$E_{carb} = \frac{F_R}{F_{CO_2}} X_{ave,max} \frac{f_a}{\ln\left[\frac{1}{1-f_a}\right]} \quad (47)$$

1274 Based on the carbon balance in the carbonator reactor, the same amount of CO₂
1275 disappears from the gas phase and reacts with CaO to form CaCO₃.

$$F_{CO_2} E_{carb} = F_R X = N_{Ca} f_a \frac{dX_{ave,max}}{dt} \quad (48)$$

1276 Only one value for the active fraction exists for a given operating point of the system
1277 that is characterised by the sorbent looping rate (F_R), fresh sorbent make-up rate (F_0),
1278 CO₂ rate to the carbonator (F_{CO_2}) and solids inventory (W_{CaO}). Therefore, the value for
1279 the active fraction at which the system is in balance is calculated iteratively.

1280 The average reaction rate expression shown in Equation (49) proposed by Alonso et al.
 1281 [30] does not consider the characteristic term for the grain models $(1-X)^{2/3}$. Although this
 1282 change makes it slightly different from the expressions proposed by Abanades et al.
 1283 [136] and Grasa et al. [171]., the authors claim that this will not have a significant effect
 1284 on prediction accuracy, as the conversion is low despite the relatively fresh sorbent and
 1285 thus this term would be close to unity.

$$\frac{dX_{ave,max}}{dt} = k_s S_{ave,max} (C_{CO_2} - C_{CO_2,eq}) \quad (49)$$

1286 Alonso et al. [30] assumed a conservative value for the carbonation rate constant of
 1287 4×10^{-10} m⁴/mol-s that falls within the lower part of the range 3.2×10^{-10} – 8.9×10^{-10}
 1288 m⁴/mol-s identified by Grasa et al. [171]. In contrast to the previous study by Abanades
 1289 et al. [136], the average surface available for the carbonation reaction is calculated as a
 1290 function of the average conversion, using an expression proposed by Grasa et al. [171].

$$S_{ave,max} = \frac{\frac{\rho_{CaO}}{M_{CaO}}}{h \frac{\rho_{CaCO_3}}{M_{CaCO_3}}} X_{ave,max} \quad (50)$$

1291 Finally, the CO₂ capture level in the carbonator can be estimated from the carbon
 1292 balance in the gas phase which can be formulated as a differential equation assuming a
 1293 plug flow of the gas phase and perfect mixing of the solids.

$$\begin{aligned} F_{CO_2} \frac{dE_{carb}}{dz} &= Af_a \frac{\rho_{CaO}}{M_{CaO}} r_{ave} \\ &= Af_a \frac{\rho_{CaO}}{M_{CaO}} k_s S_{ave,max} \rho_{M,g} \left[\frac{(f_{CO_2,0} - f_{CO_2,eq}) + (f_{CO_2,0} f_{CO_2,eq} - f_{CO_2,0}) E_{carb}}{1 - f_{CO_2,0} E_{carb}} \right] \end{aligned} \quad (51)$$

1294 Rodríguez et al. [93] and Charitos et al. [149] have developed a kinetic expression for
 1295 the carbonation process based on the experimental studies using the 30 kW_{th} unit at
 1296 INCAR-CSIC and the 10 kW_{th} unit at IFK. Their model is based on a CO₂ mass balance
 1297 for a system operating at steady state, which is similar to the one formulated by Alonso
 1298 et al. [30], and is related to the amount of CO₂ captured in the bed.

$$F_{CO_2} E_{carb} = \frac{W_{CaO}}{M_{CaO}} \frac{dX}{dt} \quad (52)$$

1299 Assuming that only a fraction of the CaO reacts with the CO₂ in the carbonator (X_{ave}),
1300 the first-order expression for the carbonation kinetic rate is:

$$\frac{dX}{dt} = \varphi_e k_{carb} X_{ave,max} (\overline{v_{CO_2}} - v_{CO_2,eq}) \quad (53)$$

1301 Rodríguez et al. [93] found that for two limestones investigated at the INCAR-CSIC unit
1302 the carbonation rate constant (k_{carb}) was 0.37 s⁻¹. The investigation revealed that the
1303 reaction rate constant depends on the test unit as it was equal to 0.26 s⁻¹ for the IFK unit
1304 and 0.33 s⁻¹ for the INCAR-CSIC unit. The authors claim that this is in agreement with
1305 previous publications [169; 177] reporting that temperature has little effect on
1306 carbonation rates. Moreover, the proposed model includes an effectivity factor (φ_e) that
1307 accounts for all physical resistances to the carbonation process and ideally it should be
1308 equal to unity for a stationary system. In reality, analysis of the experimental data
1309 revealed that the carbonator effectivity factor varies between 0.8 and 1.3. Such a high
1310 deviation from unity was probably a result of measurement uncertainty, as estimation of
1311 the solid circulation rates and average carbonation conversion is associated with an
1312 error reaching ±20% [93; 149].

1313 Finally, using the definition for the active fraction of sorbent (f_a) proposed by Alonso et
1314 al. [30], an expression for the CO₂ capture level, which links the average conversion of
1315 sorbent and the residence time distribution in the bed, was proposed.

$$E_{carb} = \varphi_e k_{carb} X_{ave,max} f_a \tau (\overline{v_{CO_2}} - v_{CO_2,eq}) \quad (54)$$

1316 In the carbonator models proposed by Alonso et al. [30], Rodríguez et al. [93] and
1317 Charitos et al. [149] only a simple hydrodynamic was considered, and the average
1318 sorbent conversion correlations in estimating the carbonator CO₂ capture level. In the
1319 model by Alonso et al. [30], the effect of the decay in sorbent conversion on the kinetic
1320 reaction rate is considered through estimation of the average surface area that is
1321 available for the carbonation reaction. Conversely, the model by Rodríguez et al. [93]

1322 and Charitos et al. [149] assumes a fixed value for the carbonation rate constant, which
 1323 was found to be similar for different limestones. Nevertheless, these models do not
 1324 consider either sorbent sulphation or ash accumulation. However, the average sorbent
 1325 conversion correlation used in each model can be easily adapted to account for sorbent
 1326 sulphation, leading to more accurate prediction of the solid looping rates, and thus the
 1327 heat requirement in the calciner.

1328 4.3.2 Semi-predictive model with two-zone K-L hydrodynamics

1329 Shimizu et al. [28] have carried out a study using a quartz fixed bed reactor with an
 1330 inner diameter of 20 mm, and identified that the change in CO₂ concentration did not
 1331 affect the kinetic constant ($k_r = 0.025 \text{ m}^3/\text{mol}\cdot\text{s}$) and the maximum conversion at which
 1332 the reaction rate approaches zero ($X_{\text{max}} = 0.3$). As the reaction was found to be first
 1333 order with respect to the CO₂ concentration, the following kinetic expression was
 1334 proposed:

$$\frac{dX}{dt} = k_r C_{\text{CO}_2} (X_{\text{max}} - X) = k_r C_{\text{CO}_2} X_{\text{max}} \exp(-k C_{\text{CO}_2} t) \quad (55)$$

1335 Assuming perfect mixing of solids and determining their average solid residence time in
 1336 the reactor, Shimizu et al. [28] determined the average reaction rate as:

$$\tau = \frac{AH_D(1 - \varepsilon_f)}{F_R} \quad (56)$$

$$\overline{\frac{dX}{dt}} = \int_0^{\infty} k_r C_{\text{CO}_2} X_{\text{max}} \exp(-k_r C_{\text{CO}_2} t) \frac{1}{\tau} \exp\left(-\frac{t}{\tau}\right) dt = \frac{k_r C_{\text{CO}_2} X_{\text{max}}}{k_r C_{\text{CO}_2} \tau + 1} \quad (57)$$

1337 To account for BFB reactor hydrodynamics in estimating the CO₂ capture level, a two-
 1338 zone model for an intermediate-sized particle by Kunii and Levenspiel (K-L) [178] was
 1339 employed. The model assumes that the fluidised bed consists of bubble and emulsion
 1340 regions in which the CO₂ concentration changes with height.

$$-\delta u_b^* \frac{dC_{\text{CO}_2,b}}{dz} = \delta K_{be} (C_{\text{CO}_2,b} - C_{\text{CO}_2,e}) + \frac{\gamma_b k_r C_{\text{CO}_2,b} X_{\text{max}} \rho_s}{M(k_r C_{\text{CO}_2,b} \tau + 1)} \quad (58)$$

$$-(1 - \delta)u_{mf} \frac{dC_{CO_2,e}}{dz} = -\delta K_{be}(C_{CO_2,b} - C_{CO_2,e}) + \frac{(1 - \delta)(1 - \varepsilon_{mf})k_r C_{CO_2,e} X_{max} \rho_s}{M(k_r C_{CO_2,\tau} + 1)} \quad (59)$$

1341 Equations (58) and (59) can be solved with the initial condition that $C_b = C_e = C_{in}$ at $z =$
 1342 0. The superficial gas velocity at the minimum fluidising conditions (u_{mf}) can be
 1343 expressed as:

$$u_{mf} = \frac{d_p^2(\rho_s - \rho_g)g\varepsilon_{mf}^3\Phi_s^2}{150\mu(1 - \varepsilon_{mf})} \quad (60)$$

1344 Assuming a bubble diameter (d_b), the bubble and emulsion interchange coefficient (K_{be})
 1345 is defined as:

$$K_{be} = 4.5 \left(\frac{u_{mf}}{d_b} \right) \quad (61)$$

1346 Furthermore, the velocity of the rising bubble gas (u_b^*) is determined from the bubble
 1347 rise velocity (u_b), the minimum fluidisation velocity (u_{mf}) and the superficial gas velocity
 1348 (u_0).

$$u_b^* = u_b + 3u_{mf} \quad (62)$$

$$u_b = u_0 - u_{mf} + 0.711(gd_b)^{0.5} \quad (63)$$

1349 The last parameter required to compute CO_2 concentrations is the volume of bubbles
 1350 per unit bed volume (δ) defined as:

$$\delta = \frac{u_0 - u_{mf}}{u_b + 2u_{mf}} \quad (64)$$

1351 Finally, the average CO_2 concentration at a given bed height is represented by
 1352 considering both the emulsion and the bubble zones:

$$C_{CO_2,ave,z} = \frac{\delta u_b^* C_{CO_2,b} + (1 - \delta)u_{mf} C_{CO_2,e}}{u_0} \quad (65)$$

1353 Using a similar approach to Shimizu et al. [28], Abanades et al. [136] have proposed a
 1354 carbonator model based on the two-zone K-L formulations for CO_2 mass balance in the
 1355 emulsion and the bubble phases. However, in their model the bubble fraction is

1356 estimated as proportional to the extremes for fine and large particles defined by Kunii
1357 and Levenspiel [179].

$$\delta = \frac{u_0 - u_{mf}}{u_b + \frac{5u_{mf} - u_b \varepsilon_{mf}}{4}} \quad (66)$$

1358 Furthermore, the velocity of the rising bubble gas was defined based on the gas
1359 balance in the bed cross-section as:

$$u_b^* = \frac{u_0 - (1 - \delta)u_{mf}}{\delta} \quad (67)$$

1360 Having assumed that there were no solids in the bubble phase ($\gamma_b = 0$), and that only an
1361 active fraction of CaO (f_a), defined as the difference between the maximum carbonation
1362 conversion (X_N) and the actual conversion of CaO to CaCO₃ (X), reacted in the fast
1363 reaction regime, the following K-L formulations for the CO₂ mass balance in the bubble
1364 and emulsion phases were derived:

$$-\delta u_b^* \frac{dC_{CO_2,b}}{dz} = \delta K_{be} (C_{CO_2,b} - C_{CO_2,e}) \quad (68)$$

$$-(1 - \delta)u_{mf} \frac{dC_{CO_2,e}}{dz} = -\delta K_{be} (C_{CO_2,b} - C_{CO_2,e}) + (1 - \delta)(1 - \varepsilon_{mf})f_a k_r C_{CO_2,e} \quad (69)$$

1365 Similarly to Shimizu et al. [28], Abanades et al. [136] have used Equation (61) to
1366 estimate the gas-interchange coefficient (K_{be}). Conversely, the overall reaction rate
1367 constant (k_r) was determined by considering both the kinetic- and diffusion-controlled
1368 regions of the carbonation reaction.

$$k_r = \frac{1}{\frac{d_p}{6k_g} + \frac{1}{K_{ri}}} \quad (70)$$

1369 The mass transfer coefficient (k_g) is estimated using the Turnbull and Davidson [180]
1370 correlation for the Sherwood number (Sh) that considers the effective CO₂ diffusivity in
1371 air, Reynolds number at minimum fluidisation conditions (Re_{mf}) and Schmidt number
1372 (Sc).

$$Sh = \frac{D_{CO_2}}{d_p k_g} = 2\varepsilon_{mf} + 0.95Re_{mf}^{0.5}Sc^{0.3} \quad (71)$$

1373 The carbonation rate is considered to be first order with respect to CO₂ and the mass
 1374 transfer of CO₂ toward the CaO particle. It is expressed using semi-empirical Equation
 1375 (72) similar to the one proposed by Bhatia and Perlmutter [169] with correction for
 1376 decreasing conversion of the sorbent with number of cycles, which is calculated using
 1377 Equation (4). In addition, the kinetic rate constant is a function of the conversion and is
 1378 rewritten to have suitable units for the K-L model as presented in Equation (73).

$$\frac{dX}{dt} = \frac{k_s S_0}{1 - e_0} X_N (1 - X)^{\frac{2}{3}} (C_{CO_2} - C_{CO_2,eq}) \quad (72)$$

$$K_{ri} = k_s \frac{X_N S_0 \rho_{CaO}}{M_{CaO}} (1 - X)^{\frac{2}{3}} \quad (73)$$

1379 In Equations (72) and (73), the intrinsic reaction rate constant (k_s) of $5.95 \times 10^{-10} \text{ m}^4/\text{mol-s}$
 1380 was found to be independent of temperature between 400°C and 725°C for the CO₂
 1381 volume fraction range of 0.1–0.42. The initial surface area of fresh CaO (S_0) was $40 \cdot 10^6$
 1382 m^2/m^3 with initial porosity (e_0) of 0.5. Additionally, it was assumed that if the maximum
 1383 carbonation conversion is reached, the chemical reaction rate becomes zero.

1384 Using TGA, Li et al. [181] have identified that the carbonation rate was independent of
 1385 temperature between 600°C and 700°C. Moreover, the maximum conversion of the
 1386 sorbent was found to be independent of the CO₂ concentration and increased with
 1387 temperature. Based on these findings, Fang et al. [135] proposed the following semi-
 1388 empirical equation for the carbonation rate. It accounts for the effect of the total
 1389 pressure on the rate of sorbent carbonation.

$$\frac{dX_N}{dt} = k_r \left(1 - \frac{X_N}{X_{max,N}}\right)^m (C_{CO_2} - C_{CO_2,eq})^{0.083 \frac{P}{P_0}} \quad (74)$$

1390 In this model, the exponent m was equal to 2/3 for the kinetic-controlled region and 4/3
 1391 for the diffusion-controlled region of the carbonation reaction. The corresponding kinetic
 1392 rate constants (k_r) were found to be $0.0025 \text{ m}^3/\text{mol-s}$ and $0.0021 \text{ m}^3/\text{mol-s}$ for kinetic-
 1393 and diffusion-controlled regions, respectively.

1394 Again, Fang et al. [135] proposed using the two-zone K-L model [179] to represent
 1395 carbonator hydrodynamics. The model is similar to the one adapted by Abanades et al.
 1396 [136], with a minor change to account for the solids present in the bubbles. Assuming
 1397 the volume fraction of solids dispersed in the bubbles (y_b) to be between 10^{-2} and 10^{-3} ,
 1398 the mass balance for the bubble phase is:

$$-\delta u_b^* \frac{dC_{CO_2,b}}{dz} = \delta K_{be}(C_{CO_2,b} - C_{CO_2,e}) + \delta y_b f_a K_r (C_{CO_2,b} - C_{CO_2,eq}) \quad (75)$$

1399 The carbonation rate constant in the units suitable for the K-L model and the active
 1400 fraction of CaO in the carbonation process were expressed as:

$$K_r = k_c \left(1 - \frac{X_N}{X_{max,N}}\right)^m \frac{\rho_{CaO}}{M_{CaO}} \quad (76)$$

$$f_a = X_{max,N} - X_N \quad (77)$$

1401 Finally, the overall conversion of CO₂ in the reactor was estimated as the average
 1402 concentration in the emulsion and the bubble phase.

$$X_{CO_2,exit} = 1 - \frac{\delta u_b^* C_{CO_2,b,exit} + (1 - \delta) u_{mf} C_{CO_2,e,exit}}{u_0 C_{CO_2,in}} \quad (78)$$

1403 Although the model by Shimizu et al. [28] provided a good representation of the CO₂
 1404 capture level in the carbonator, several improvements could be made to enhance
 1405 prediction accuracy. In the model developed by Abanades et al. [136], a semi-empirical
 1406 correlation was used to determine sorbent deactivation with the number of
 1407 carbonation/calcination cycles, which substituted the fixed conversion value after four
 1408 cycles used by Shimizu et al. [28]. Moreover, the overall kinetic rate constant defined by
 1409 the model by Abanades et al. [136] accounted for both the chemical reaction rate and
 1410 the mass transfer rate, resulting in a further improvement in prediction accuracy. A
 1411 further improvement in the semi-predictive carbonator model was achieved by Fang et
 1412 al. [135] whose model is capable of predicting process performance separately in the
 1413 chemically- and diffusion-controlled regions of the carbonation reaction. Unfortunately,
 1414 these semi-predictive models do not account for sorbent sulphation and ash

1415 accumulation in the system and this may cause under-estimation of the solids looping
1416 rates and, thus the heat requirement in the calciner.

1417 **4.3.3 Semi-predictive model with three-zone K-L hydrodynamics**

1418 Romano [84] has developed a model for a CFB carbonator by combining the improved
1419 three-zone K-L model [182; 183] with the maximum conversion expression proposed by
1420 Grasa and Abanades [143] and the carbonation kinetics developed by Grasa et al.
1421 [171]. The model developed by Romano [84] is the first one that accounts for the impact
1422 of sulphation on average sorbent conversion. This is achieved through estimation of the
1423 decay constant and the residual sorbent conversion by fitting Equation (4) to the
1424 experimental data from Grasa et al. [153].

1425 In the carbonator model, the uniform riser temperature, particle size distribution and
1426 superficial velocity were assumed, along with no gas side mass transfer resistance and
1427 perfect solid mixing. The model considered two statistical distributions. The first
1428 determines the carbonation/calcination cycle number that a given particle has already
1429 experienced using the correlations provided by Abanades [145] and Rodríguez et al.
1430 [11]. These, in combination of the maximum sorbent conversion correlation by Grasa
1431 and Abanades [143] with fitting parameters adjusted to consider sulphation, allow
1432 determining the maximum average sorbent conversion. The second characterises the
1433 fraction of particles of a given residence time in the carbonator, for which the average
1434 residence time is defined as in the model by Alonso et al. [30]. The active solid
1435 inventory is defined in Equation (80) to account for sulphation and ash accumulation
1436 effects.

$$f_t = \frac{1}{\tau} \exp\left(-\frac{t}{\tau}\right) \quad (79)$$

$$N_{Ca} = \frac{W_s}{M_s} (1 - x_{ash} - x_{CaSO_4}) \quad (80)$$

1437 The actual average conversion of the sorbent for a given CO₂ concentration (C_{CO₂*}) and
1438 the average carbonation level are determined as:

$$X_{ave} = \sum_{N_{age}=1}^{\infty} r_{N_{age}} \int_0^{\infty} f_t X(t, N, C_{CO_2}^*) dt \quad (81)$$

$$f_{carb} = \frac{X_{ave}}{X_{max,ave}} \quad (82)$$

1439 Using the same approach, the average kinetic constant in suitable units for the K-L
1440 model is computed as:

$$K_{ri,ave} = \frac{\rho_s}{M_s} \sum_{N_{age}=1}^{\infty} r_{N_{age}} \int_0^{\infty} f_t k_s S_N [1 - X(t, N, C_{CO_2}^*)]^{\frac{2}{3}} dt \quad (83)$$

1441 The CO₂ capture level in the carbonator model is then separately calculated from the
1442 carbonator mass balance and the K-L model:

$$E_{carb} = \frac{F_R X_{ave}}{F_{CO_2}} = \frac{F_{CO_2} - V_{g,out} C_{CO_2,out}}{F_{CO_2}} \quad (84)$$

1443 Since both the actual average conversion determined using Equation (81) and the outlet
1444 CO₂ concentration computed using the K-L model with the average kinetic constant
1445 estimated in Equation (83) depend on C_{CO₂}^{*}, the model is solved in an iterative process
1446 by varying C_{CO₂}^{*} until Equation (84) is satisfied. This approach was found to reliably
1447 predict the performance of the carbonator reactor for the INCAR-CSIC and IFK test
1448 units.

1449 The model developed recently by Romano [84] is the most advanced carbonator semi-
1450 predictive model available currently as it considers the effect of reactor hydrodynamics
1451 on the CO₂ capture level, reaction kinetics, the influence of sulphation on sorbent
1452 conversion and ash accumulation. Although it does not consider the diffusion region of
1453 the carbonation process, this region is usually neglected in industrial applications, to
1454 allow for a compact design of the CFB reactor [84; 145].

1455 4.4 Calciner reactor modelling

1456 4.4.1 Semi-predictive model with simple hydrodynamics

1457 Martínez et al. [134] have proposed a model to predict the performance of the
1458 calcination process that is based on the steady-state overall mass balance of the
1459 calciner.

$$F_{CO_2,calc} = N_{Ca} \cdot r_{calc} = (F_{Ca} + F_0)(X_{carb,ave} - X_{calc}) \quad (85)$$

1460 The average $CaCO_3$ content in the total flow entering the calciner ($X_{carb,ave}$) is
1461 determined based on solid flow from the carbonator (F_{Ca}) and fresh limestone make-up
1462 (F_0). The kinetic rate of the calcination reaction was developed in the earlier work by
1463 Martínez et al. [184]. It was based on the grain model and is similar to the calciner
1464 model by Fang et al. [135].

$$\frac{d(X_{carb} - X_{calc})}{dt} = k_{calc} \left(1 - \frac{X_{carb} - X_{calc}}{X_{carb}}\right)^{\frac{2}{3}} (C_{CO_2,eq} - C_{CO_2}) \quad (86)$$

1465 The time required for complete calcination can be determined by integrating Equation
1466 (86).

$$t_{calc}^* = \frac{3 \cdot X_{carb}}{k_{calc} (C_{CO_2,eq} - C_{CO_2})} \quad (87)$$

1467 Martínez et al. [184] determined that the calcination rate is constant and independent of
1468 the $CaCO_3$ content in the particle. Therefore, the average calcination rate was
1469 expressed as:

$$r_{calc} = \begin{cases} \frac{X_{carb,ave}}{t_{calc}^*} = \frac{k_{calc} (C_{CO_2,eq} - C_{CO_2})}{3} & \text{for } t < t_{calc}^* \\ 0 & \text{for } t \geq t_{calc}^* \end{cases} \quad (88)$$

1470 Based on the assumption that the solid phase in the calciner is perfectly mixed and
1471 considering the average particle residence time in the calciner, the fraction of particles

1472 that has a residence time lower than the time required for complete calcination can be
1473 estimated as:

$$f_a = 1 - \exp\left(-\frac{t_{calc}^*}{\tau}\right) \quad (89)$$

$$\tau = \frac{N_{Ca}}{F_{Ca} + F_0} \quad (90)$$

1474 Using these definitions, the amount of CaCO_3 that disappeared from the solid phase
1475 and the amount of CO_2 released in the calciner are given as:

$$(F_{Ca} + F_0)(X_{carb,ave} - X_{calc}) = (F_{Ca} + F_0)X_{carb,ave} \frac{f_a}{\ln\left[\frac{1}{1-f_a}\right]} \quad (91)$$

$$N_{Ca} \cdot r_{calc} = N_{Ca} \cdot f_a \cdot \frac{k_{calc}(C_{CO_2,eq} - C_{CO_2})}{3} \quad (92)$$

1476 Finally, the efficiency of the calciner (E_{calc}) can be estimated as:

$$E_{calc} = \frac{X_{carb} - X_{calc}}{X_{carb}} = \frac{f_a}{\ln\left[\frac{1}{1-f_a}\right]} \quad (93)$$

1477 To solve the model an approach similar to the one proposed by Romano [84] needs to
1478 be applied. Namely, the value of the C_{CO_2} concentration for which Equation (85) will be
1479 satisfied needs to be found in an iterative process.

1480 The calciner semi-predictive model proposed by Martínez et al. [134], has the same
1481 level of complexity as the carbonator semi-predictive model by Alonso et al. [30].
1482 Therefore, these models should be used together to represent CaL performance. The
1483 model has the same disadvantages that it does not consider sorbent sulphation and ash
1484 accumulation in the system.

1485 4.4.2 Semi-predictive model with two-zone K-L hydrodynamics

1486 As for the carbonator model, Fang et al. [135] used experimental data generated by Li
1487 et al. [181] to develop an apparent kinetic model for the calcination reaction.

$$\frac{dX_{calc}}{dt} = k_{calc}(1 - X_{calc})^{\frac{2}{3}}(C_{CO_2,eq} - C_{CO_2}) \quad (94)$$

1488 The TGA conducted under 90% CO₂ revealed that conversion during the calcination
 1489 process is inhibited by both temperature and CO₂ concentration. Therefore, the
 1490 calcination rate constant (k_{calc}) was given in the Arrhenius equation form with the pre-
 1491 exponential factor ($k_{0,calc}$) of 23 797 and the activation energy (E_a) of 150 kJ/mol.

1492 Unlike other calciner models, the model proposed by Fang et al. [135] accounted for the
 1493 reactor hydrodynamics using the same K-L model [179] as presented for the carbonator
 1494 model. In this model, the calcination rate constant and the fraction of CaCO₃ that was
 1495 not regenerated in the calcination stage are represented as:

$$k_r = k_{calc}(1 - X_{calc})^{\frac{2}{3}} \frac{\rho_{CaCO_3}}{M_{CaCO_3}} \quad (95)$$

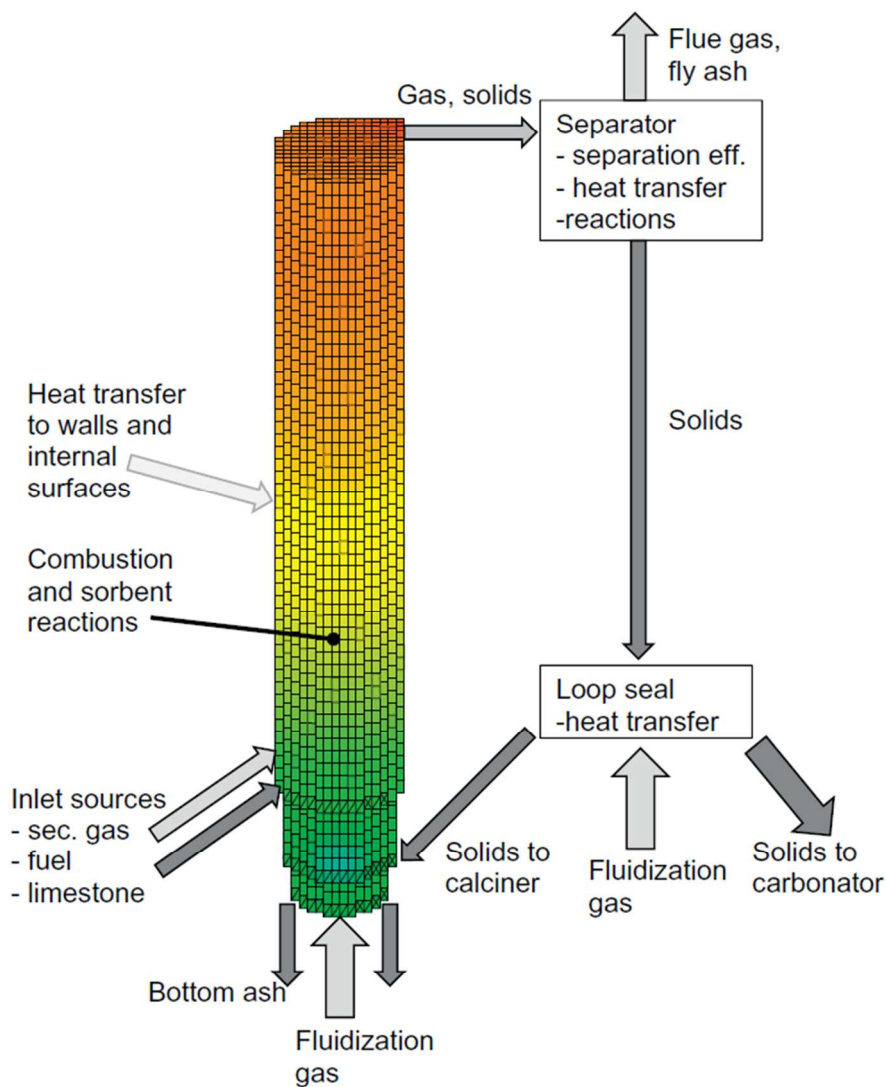
$$f_a = (1 - X_{calc})X_{max} \quad (96)$$

1496 The semi-predictive model for the calciner proposed by Fang et al. [135] provides an
 1497 enhanced prediction of process performance over the model by Martínez et al. [134], as
 1498 it considers the detailed hydrodynamics of the reactor. Moreover, the model takes both
 1499 the chemically- and diffusion-controlled regions into account. However, no correlation
 1500 was made with sorbent sulphation and ash accumulation in the system, which appears
 1501 to be the common issue in the process models reviewed here.

1502 4.4.3 Predictive model with CFD hydrodynamics

1503 Ylätaalo et al. [150] have adapted the CFB3D model code developed by Myöhänen et al.
 1504 [185] to model a three-dimensional oxy-fired calciner reactor (Figure 19). The
 1505 calcination reaction rate is expressed using the kinetic constant provided by Silcox et al.
 1506 [186] and the CO₂ equilibrium pressure by Barin [187].

$$r_{calc} = 1.22 \cdot \exp\left(-\frac{4026}{T}\right) S_m M_{CaCO_3} (p_{CO_2,eq} - p_{CO_2}) \quad (97)$$



1507

1508 **Figure 19: Three-dimensional CFB calciner model frame (Reprinted with permission from**
 1509 **Ylätaalo et al. [150]. Copyright 2015 Elsevier.)**

1510 The model included detailed modelling of sulphur dioxide and calcium sulphate in the
 1511 calciner using the correlations developed by Myöhänen et al. [185] that account for the
 1512 specific reaction surface area ($S_{m,i}$) of component i .

$$r_{sulf} = 0.001 \exp\left(-\frac{2400}{T}\right) \exp(-8X_{CaSO_4}) C_{SO_2} C_{O_2} S_{m,CaO} M_{CaO} \quad (98)$$

$$r_{dir,sulf} = 0.01 \exp\left(-\frac{3031}{T}\right) C_{SO_2}^{0.9} C_{CO_2}^{-0.75} C_{SO_2}^{0.001} S_{m,CaCO_3} M_{CaCO_3} \quad (99)$$

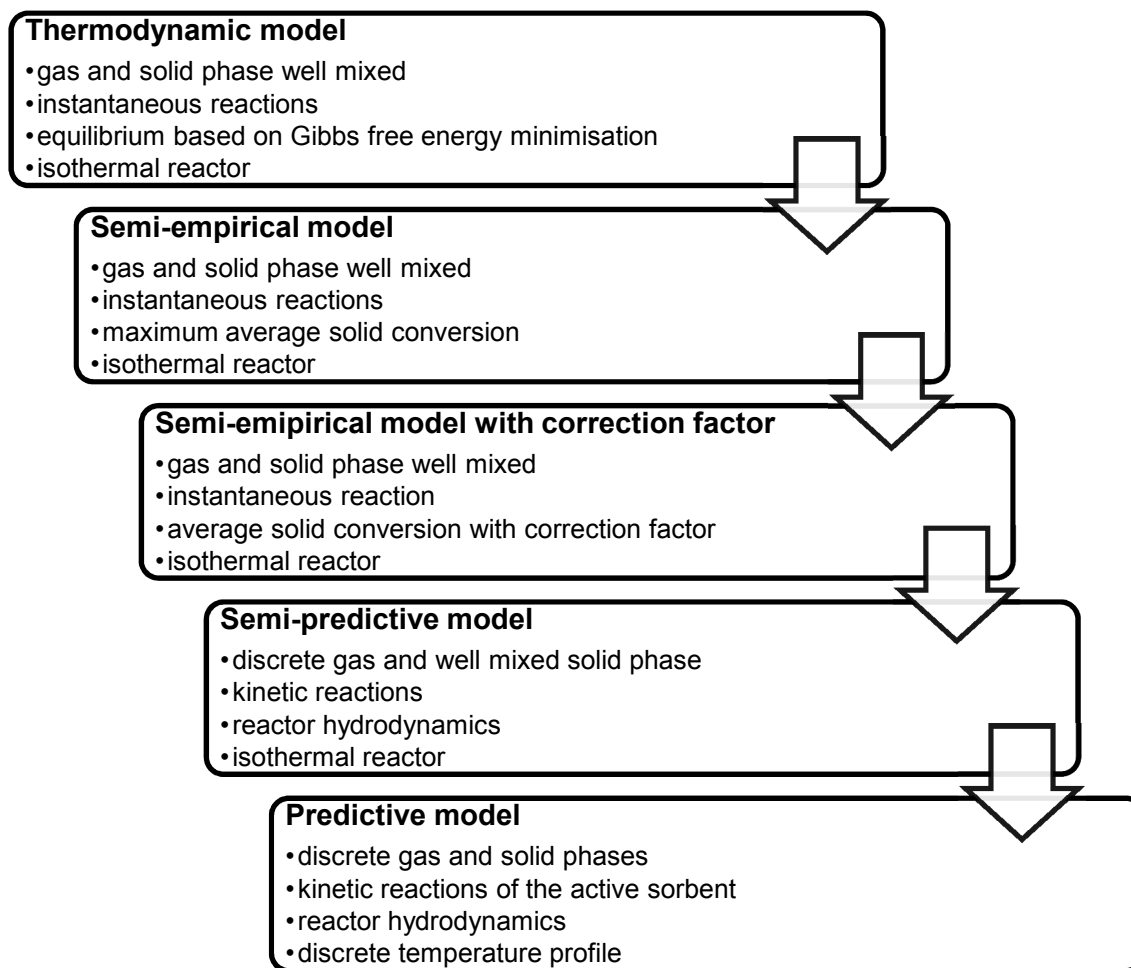
$$r_{de-sulf} = 0.005 \exp\left(-\frac{10000}{T}\right) C_{CO} S_{m, CaSO_4} M_{CaSO_4} \quad (100)$$

1513 In contrast to the calciner models presented previously, the CFD model proposed by
1514 Ylätaalo et al. [150] provides detailed information on how sulphation and sorbent
1515 properties could affect the calciner performance. Although more demanding
1516 computationally, such models will deliver more reliable predictions of calciner operating
1517 conditions as they are capable of predicting the temperature and the solids distribution
1518 across the reactor. Not only could the CFD models be used to reliably predict and/or
1519 optimise performance of the CFB reactor, they can be integrated into the process wide
1520 simulation. Recently, Atsonios et al. [188] have proposed to use the CFD model to
1521 generate information on CFB hydrodynamics (carbonator and calciner) and CO₂
1522 distribution in the bed (calciner), which is then fed to the carbonator and the calciner
1523 kinetic models in the process simulation.

1524 **4.5 Summary**

1525 The review of the carbonator reactor models undertaken in this section revealed that
1526 there are several approaches available in the open literature. However, some of the
1527 assumptions or formulations behind these models impose important limitations that may
1528 affect the accuracy of their predictions.

1529 The review findings show that five main complexity levels can be distinguished (Figure
1530 20). Models in the first level are based on first principles, energy and material
1531 conservation laws. At an early stage of concept development, which could include
1532 uncertainties related to process operating conditions and/or sorbent properties,
1533 thermodynamic models would perform well and could be used to estimate performance
1534 limited by equilibrium. The greatest limitation of such models is lack of correlation to the
1535 physical size of the reactor and the assumption of instantaneous reactions. Additionally,
1536 in most cases the equilibrium composition in the reactor, hence the sorbent conversion,
1537 is based on minimisation of Gibbs free energy at specified operating conditions and
1538 does not depend on what happens upstream of the unit.

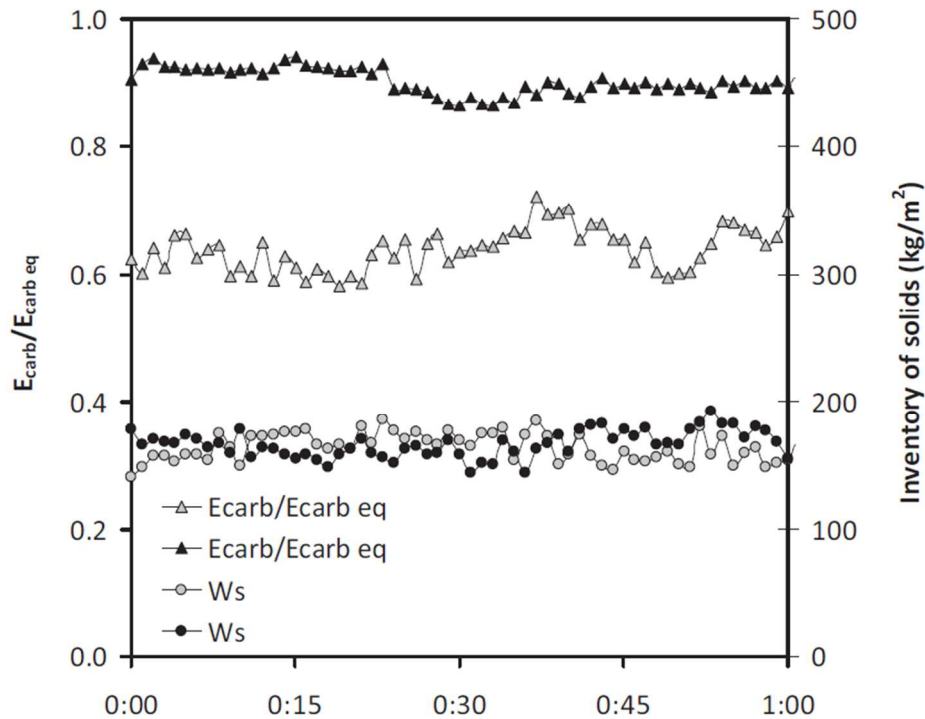


1539

1540 **Figure 20: Different levels of calcium looping model complexity**

1541 The last limitation of the thermodynamic models is partially eliminated in the semi-
 1542 empirical models, which allow determination of the maximum average sorbent
 1543 conversion depending on the solid looping rate and fresh sorbent make-up rate, as well
 1544 as carbonator and calciner performance [11; 39; 139]. These models, however, assume
 1545 that the sorbent achieves its maximum average conversion under certain operating
 1546 conditions, predicting actual reactor performance close to equilibrium performance.
 1547 Although the results from experimental trials using the 1.7 MW_{th} pilot plant at INCAR-
 1548 CSIC showed that this assumption is valid for systems operating with high sorbent
 1549 conversions, which require high fresh sorbent make-up rates, systems operating with

1550 low average conversions achieve around 60-90% of equilibrium performance (Figure
1551 21).



1552

1553 **Figure 21: Comparison of the actual and the equilibrium performance of 1.7 MW_{el} pilot**
1554 **plant at INCAR-CSIC operating at carbonator temperature of 660-690°C with $X_{ave}=0.11$**
1555 **(grey) and $X_{ave}=0.21$ (black) (Reprinted with permission from Arias et al. [96]. Copyright**
1556 **2015 Elsevier.)**

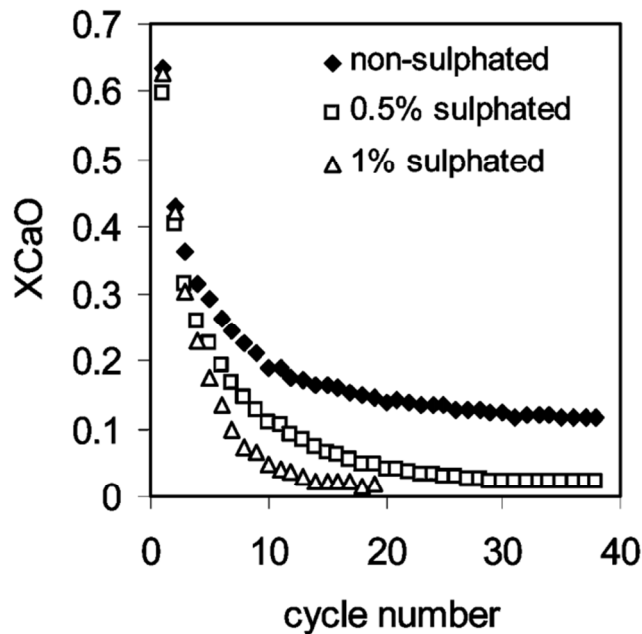
1557 To improve model accuracy, actual average sorbent conversion is determined by
1558 applying a correction factor to the maximum average sorbent conversion in the third
1559 level models. This factor can be either assumed [133; 146], as presented in Section 5,
1560 or calculated based on the actual and average residence times of the sorbent in the
1561 reactor [30; 134]. The former approach greatly enhances model prediction as the
1562 determined correction factor accounts for the solid inventory and the reaction kinetics in
1563 the reactor.

1564 The fourth level is achieved through a detailed consideration of reaction kinetics and
1565 hydrodynamics in determining the performance of the reactor. Most of the semi-

1566 predictive models developed to predict the performance of the calciner [135] and the
1567 carbonator [28; 84; 135; 136] used the hydrodynamic formulations developed by Kunii
1568 and Levenspiel [178; 179; 182; 183], which offer an analytical solution. This approach
1569 improves the prediction as the gas concentration depends on the operating conditions
1570 and location in the reactor, as well as the sorbent properties. A number of parameters in
1571 the K-L model need to be specified, but their values have not been substantiated
1572 experimentally and could affect the accuracy of the model.

1573 This, and other assumptions such as isothermal operation and well-mixed solid phase,
1574 can be eliminated by applying the predictive models that combine industrial CFD codes
1575 with experimentally-determined reaction kinetics to evaluate the reactor [150; 189] or
1576 the whole CaL plant [188] performance. Such models are the most complex and,
1577 therefore, computationally demanding. Although predictive models give the closest
1578 representation of the CaL process, they are not applicable at the early stage of concept
1579 design because any change in the process design would be followed by a long
1580 simulation period required to assess the impact of that change.

1581 In addition to presenting the current approaches for modelling of the CaL processes and
1582 identifying their limitations, this review has identified that neither sorbent sulphation nor
1583 ash accumulation are widely considered in the models currently developed. The only
1584 models accounting for sorbent sulphation were the carbonator model by Romano [84]
1585 and the calciner model by Ylätaalo et al. [150] described in Section 4.3.3 and Section
1586 4.4.3, respectively. Although it was claimed by Abanades et al. [136] that sorbent
1587 sulphation will have a minor effect on carbonation, the experimental analysis by Grasa
1588 et al. [153] suggests that even a change in the sulphation level of 0.5% in each cycle
1589 affects the sorbent decay curve (Figure 22).



1590

1591 **Figure 22: Decay in the carbonation conversion with the number of**
1592 **carbonation/calcination cycles under different sulphation conversions (Reprinted with**
1593 **permission from Grasa et al. [153]. Copyright 2015 American Chemical Society.)**

1594 Despite the fact that ash presence in the system would increase the inert solid looping
1595 rate and the bed inventory required to achieve a given CO₂ capture efficiency, the effect
1596 of ash accumulation in the system was only included in the model by Romano [84].
1597 Moreover, none of the reviewed models account for sorbent attrition and fragmentation,
1598 which was identified as another challenge of the CaL process [13]. Therefore, in
1599 addition to the sulphation effect on sorbent performance and ash accumulation, loss of
1600 sorbent due to attrition and fragmentation should also be considered in the future
1601 modelling attempts. This can be done, for example, by implementing the semi-empirical
1602 model for sorbent attrition developed by Fennell et al. [190] or by adapting the semi-
1603 detailed model developed for coal fragmentation by Senneca et al. [191].

1604

1605 **5 INTEGRATION OF CALCIUM LOOPING TO POWER PLANTS**

1606 A key reason for development of computational models for CO₂ capture processes is
1607 the ease with which they can be used to analyse retrofit scenarios of existing power
1608 plants, or to develop novel concepts for cleaner power generation systems. Models can
1609 be a cost-efficient complement to experimental trials of a particular system design under
1610 various operating conditions. The greatest advantage of using computational models is
1611 the ease of conducting a process-wide analysis for determining optimal overall process
1612 performance by indicating the possible integration points.

1613 Since 1999, when the CaL integration was proposed as a viable option for CO₂ capture
1614 from CFPPs [28], a number of studies have investigated different aspects of process
1615 integration aiming at improvement of the overall process performance. These included
1616 enhancement of process integration through heat exchange network analyses and
1617 reduction of CaL process energy requirements through implementation of alternative
1618 configurations. The applicability of the CaL process for CO₂ capture from combined
1619 cycle power plants was also investigated.

1620 The greatest disadvantage of conventional CO₂ capture systems is a relatively high
1621 projected efficiency penalty leading to increased fuel consumption and cost. This
1622 section reviews process integration and conceptual studies to quantify efficiency
1623 penalties in CFPPs and combined cycle power plants. In addition, the modelling
1624 approach for both the power cycle and the CaL process are identified and limitations are
1625 analysed to provide a guide for further modelling attempts.

1626 **5.1 Conventional coal-fired power plants**

1627 **5.1.1 Feasibility study for calcium looping for conventional power** 1628 **generation systems**

1629 A conceptual study by Shimizu et al. [28] analysed the impact of CaL plant integration
1630 on a supercritical CFPP. High-pressure steam generated in air-combustion of
1631 bituminous coal was used to generate electricity in the primary steam cycle, which

1632 operates with gross thermal efficiency of 46.6%_{HHV}. Flue gas was treated in the CaL
1633 plant with the carbonator operating at 650°C and the calciner operating at 950°C with
1634 100% efficiency. The performance of the carbonation process was predicted using the
1635 carbonator model described in Section 4.3.2.

1636 With a Ca:C ratio of 8.29, which is slightly smaller than values reported in the pilot-plant
1637 tests, and average conversion of 11%, CO₂ capture of 83% was reached in the
1638 carbonator, leading to an overall CO₂ capture level of 90.4%. The waste heat in the CaL
1639 plant was recovered to produce superheated and reheated steam at subcritical
1640 conditions of 172.25 bar/566°C and 30.4 bar/538°C, respectively. The gross thermal
1641 efficiency of the secondary steam cycle was assumed to be 42.6%_{HHV}. With the gross
1642 and net power outputs of the integrated system of 1000 MW_{el} and 817 MW_{el},
1643 respectively, the net efficiency was estimated to be 33.4%_{HHV}. This was 1.4% points
1644 higher than for an oxy-fired combustor with a primary steam cycle of the same gross
1645 power output and thus indicated feasibility of the CaL process for reducing CO₂
1646 emissions from the CFPPs.

1647 Unfortunately, Shimizu et al. [28] provided no benchmark to the reference CFPP without
1648 CO₂ capture plant, which would provide insight into how the retrofit affected the overall
1649 performance of the system. Also, sorbent decay was ignored as only four
1650 carbonation/calcination cycles were considered in determining sorbent conversion.
1651 Furthermore, the performance of both steam cycles was assumed rather than estimated
1652 using thermodynamic calculation or process simulation. Although this assumption could
1653 be valid for a CFPP operating at a fixed load, it does not allow prediction of part-load
1654 operation without knowledge of the gross efficiency correlation. Additionally, by
1655 assuming the gross thermal efficiency, the analysis did not account for the power
1656 consumption of the CFPP auxiliary equipment, with only ASU and CO₂ compression
1657 unit (CCU) considered in estimation of the net thermal efficiency. The power
1658 requirements for the CFPP and the CaL plant auxiliary equipment need to be
1659 considered to improve the prediction reliability and avoid over-estimating the net thermal
1660 efficiency of the integrated system.

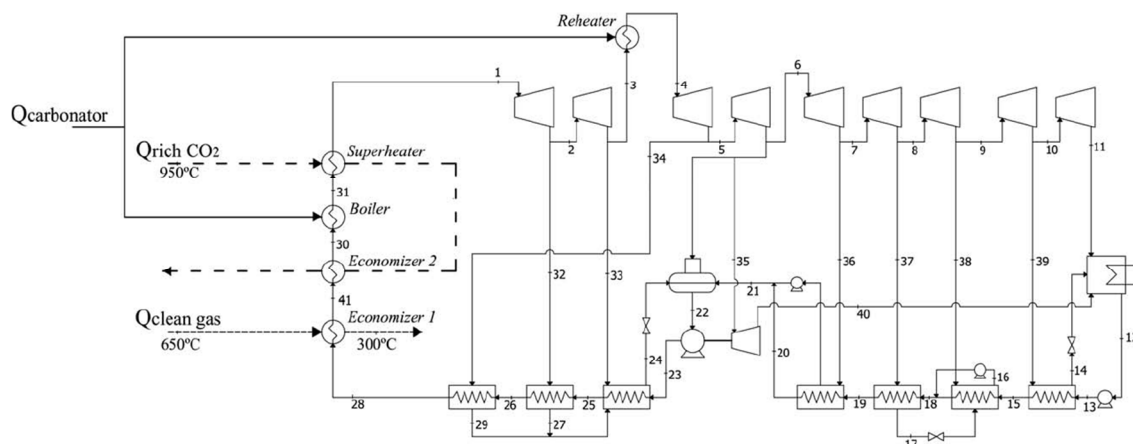
1661 **5.1.2 Heat integration with the primary and secondary steam cycle**

1662 High-temperature operation of the CaL process allows recovering high-grade heat to
1663 produce an additional amount of steam. Therefore, there are two options for integrating
1664 the CaL process with the existing CFPPs: steam can be utilised either in the primary
1665 steam cycle with the assumption that the steam generation rate in the boiler is reduced
1666 and the gross power output of the integrated system kept constant, or in the secondary
1667 steam cycle leading to higher gross power output. Yang et al. [16] investigated both
1668 integration options. In the first case, the CaL plant was integrated with the primary
1669 steam cycle of an existing 600 MW_{el} CFPP operating with net thermal efficiency of
1670 40.6%_{LHV}. Performance of a carbonator operated at 650°C was represented using the
1671 correlation by Abanades et al. [145], with a maximum conversion of 20% to reach 85%
1672 CO₂ capture level at Ca:C ratio of 5. It needs to be highlighted that compared to the
1673 Ca:C values reported in the pilot-plant tests reviewed in Section 3, the assumed Ca:C
1674 ratio is 1.5–3 times lower. This would cause underestimation of the solid looping rate
1675 and thus, heat requirement in the calciner. In this study, the calciner was operated at
1676 900°C and heat for sorbent regeneration was provided through oxy-combustion of coal.
1677 The parasitic load stemmed only from the ASU power requirement as no CCU was
1678 considered.

1679 Yang et al. [16] first proposed using heat in the CaL system to substitute the feedwater
1680 heating train in the primary steam cycle. Although this is a valid approach for integrated
1681 systems, which has been often proposed for integration of amine-based CO₂ capture
1682 plants [60; 73; 192-194], its applicability to existing CFPPs could be limited by the
1683 swallowing capacity of the steam turbines and/or the electric generator. Moreover, the
1684 suggestion by Yang et al. [16] that these extractions reduce the thermal efficiency of
1685 CFPPs is invalid from the thermodynamic point of view, as they increase the average
1686 temperature of heat addition in the boiler leading to an increase in thermal efficiency
1687 [195]. Yet, the indicated power output increase of 148.8 MW_{el} and increase in the net
1688 thermal efficiency from 19.4%_{LHV} to 25.3%_{LHV}, which stems from a higher degree of
1689 waste heat utilisation in the integrated system leading to minimisation of steam

1690 extractions, could not be achievable in reality due to operational limitations of the
1691 existing system. In another integration option, part of the boiler heat load was replaced
1692 by heat load from the CaL plant. The boiler in the CaL plant can provide 43.1% of the
1693 heat required by the system to operate with gross power output of 600 MW_{el} and net
1694 thermal efficiency of 34.1%_{LHV}. However, a further study on how such off-design
1695 operation conditions would affect the boiler performance needs to be conducted.
1696 Furthermore, in evaluating other integration options, the highest net thermal efficiency of
1697 36.8%_{LHV} and gross power output of 1000 MW_{el} were reached when the waste heat
1698 from the CaL plant was utilised to generate high-pressure steam to drive the secondary
1699 steam cycle. This result revealed that implementation of a secondary steam cycle and
1700 its integration with the CaL plant provides superior performance compared to the other
1701 CFPP integration options. This is also beneficial in terms of long-term revenue and
1702 meeting market demand. However, the estimated minimum net efficiency penalty of
1703 3.8% points (excluding power requirement for CO₂ compression) may not be a
1704 representative result, due to low Ca:C ratio assumed in the carbonator.

1705 In addition to evaluating different integration options, the effect of CaL integration to
1706 CFPPs operating with different steam conditions was investigated. Martínez et al. [83]
1707 analysed integration of a CaL plant to an existing 350 MW_{el} subcritical CFPP with net
1708 efficiency of 36%_{LHV}. The flue gas leaving the boiler, which contained 14.5%_{vol} CO₂, was
1709 desulphurised and then entered the CaL plant at typical stack conditions (1.16
1710 bar/180°C). Performance of the carbonator, which was operated at 650°C, was
1711 represented using the model proposed by Alonso et al. [30] described in Section 4.3.1
1712 with the kinetic expression proposed by Grasa et al. [196]. The sorbent was
1713 regenerated in the calciner operating at 950°C and complete calcination was assumed.
1714 The temperature in the calciner was maintained through oxy-combustion of South
1715 African coal. Even though this coal contains a relatively small amount of sulphur and the
1716 flue gas was desulphurised, an additional amount of CaCO₃ ($F_{Ca}/F_S = 3$) was provided
1717 with the make-up stream to account for sorbent sulphation losses. Moreover, part of the
1718 captured CO₂ was recycled to maintain the O₂ concentration in the oxidizing gas at
1719 25%_{mol}.



1720

1721 **Figure 23: Reference integration configuration for the CaL plant and supercritical steam**
 1722 **cycle (Reprinted with permission from Martínez et al. [83]. Copyright 2015 John Wiley**
 1723 **and Sons.)**

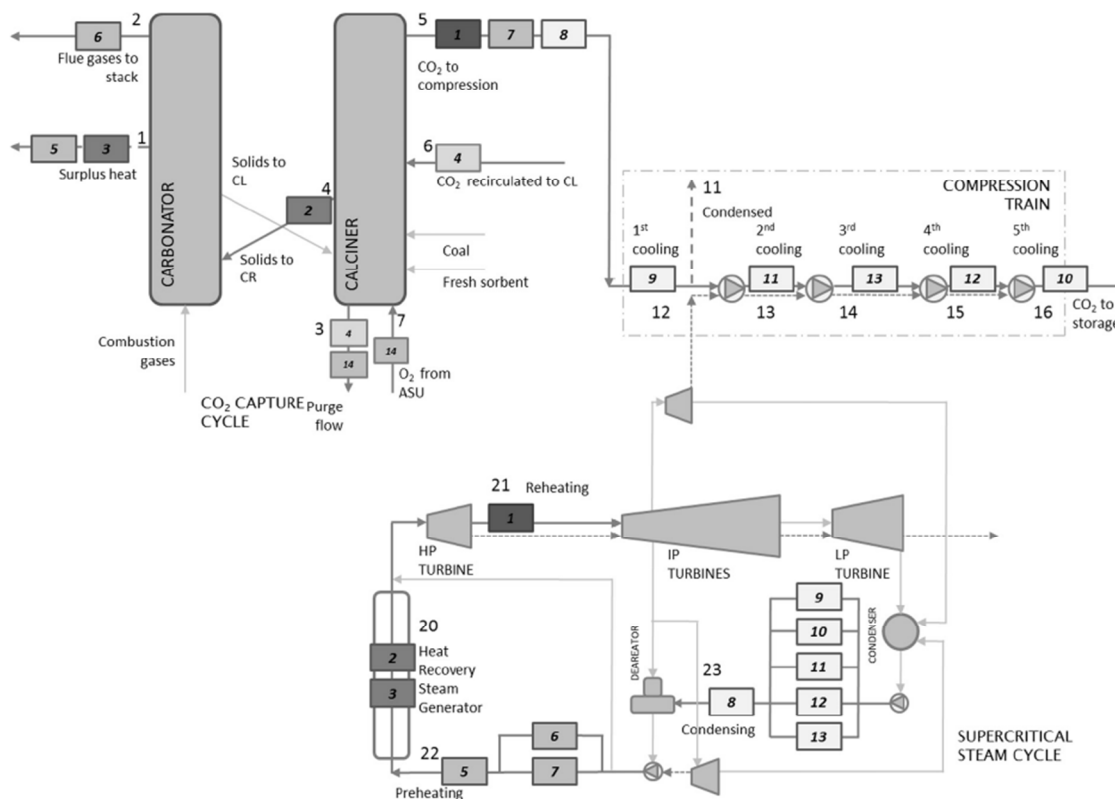
1724 Heat in the carbonator, the clean gas stream and the CO₂ stream was used to generate
 1725 steam to run the secondary steam cycle (Figure 23), the gross thermal efficiency of
 1726 which was assumed to be 45%_{LHV}. After deducting the auxiliary power consumption of
 1727 the plant, the net thermal efficiency was 36%_{LHV}. By adjusting the solid circulation rate,
 1728 the CO₂ capture level in the carbonator was maintained at 70%–90%, leading to
 1729 maximum net thermal efficiency of 33.1%_{LHV}–33.4%_{LHV}. Although an increase in the
 1730 CO₂ capture level required higher solid circulation rates, the increase in steam
 1731 generation exceeded the increased heat requirement in the calciner leading to a rise in
 1732 net thermal efficiency. The make-up rate was found to be a critical parameter as its
 1733 increase led to reduction in net thermal efficiency, since more heat was required for
 1734 fresh sorbent preheating. However, operation at low make-up rates would result in low
 1735 conversion of the sorbent and thus high circulation rates requiring a larger reactor.
 1736 Nevertheless, the viability of a CaL plant for subcritical CFPPs, for which the projected
 1737 efficiency penalties ranged between 8.3% and 10.3% points, has been confirmed.
 1738 Interestingly, if part of the spent sorbent was utilised in the cement plant as raw
 1739 material, the amount of energy required for sorbent calcination was not accounted for in
 1740 the net thermal efficiency calculation, leading to efficiency penalties between 7.5% and
 1741 9% points. The study clearly showed that this retrofit would be beneficial for the existing

1742 fleet of subcritical power plants, increasing their life span and environmental
1743 performance without a drastic net thermal efficiency drop, as is the case for
1744 conventional CO₂ capture plants. Nevertheless, performance of the steam cycle, ASU
1745 and CCU is determined based on assumed performance indicators that may not be
1746 valid for part-load operation. Also, Martínez et al. [37] benchmarked the performance of
1747 the integrated system against a hypothetical system rather than an existing power plant,
1748 which results in misleading conclusions regarding the projected efficiency penalty
1749 imposed on the retrofitted system. The performance of an integrated system should be
1750 benchmarked against the performance of an existing system to identify the net effect of
1751 the CaL plant integration.

1752 Romeo et al. [86] have investigated the integration of a secondary supercritical steam
1753 cycle (280 bar/600°C/600°C) with a CaL plant retrofitted to an existing 450 MW_{el}
1754 supercritical CFPP. In the CaL plant design, the temperatures in the carbonator and the
1755 calciner were kept at 650°C and 875°C, respectively. The performance of the system
1756 was represented by assuming 5% purge leading to average sorbent conversion of about
1757 20%. Heat for sorbent recovery was added through combustion of low-sulphur high-rank
1758 coal in pure O₂-stream produced in the ASU with specific power of 220 kWh/t-O₂.
1759 Romeo et al. [86] claimed that no CO₂ recirculation was needed to control the
1760 temperature in the calciner because of the large solid inflow at 650°C and the
1761 endothermic character of the calcination reaction. Despite the fact that the pure O₂
1762 stream will be diluted by CO₂ liberated in the calcination reaction, the local temperature
1763 of coal particles can be higher than the average bed temperature due to their
1764 combustion in a high-O₂-concentration environment [197; 198]. Such high temperatures
1765 can lead to local hot spots in the calciner on contact of the coal and sorbent particles
1766 and cause enhanced sintering and, thus deactivation of the sorbent [199].

1767 Analysing the CaL process, Romeo et al. [86] have proposed an integration
1768 configuration comprising five heat integration zones, in which waste heat from the
1769 carbonator, CO₂ stream, clean gas stream and purge stream were utilised to generate
1770 live and reheated steam, as well as to preheat the feedwater. The secondary

1771 supercritical steam cycle driven by heat recovered in the CaL plant generated an
 1772 additional 193.6 MW_{el} of net power output with net efficiency of 26.7%_{LHV}. Although this
 1773 increased the net power output of the integrated system by 45.3%, the net thermal
 1774 efficiency dropped by 7.9% points, from 44.9%_{LHV} for the reference CFPP to 37.0%_{LHV}
 1775 for the integrated system.

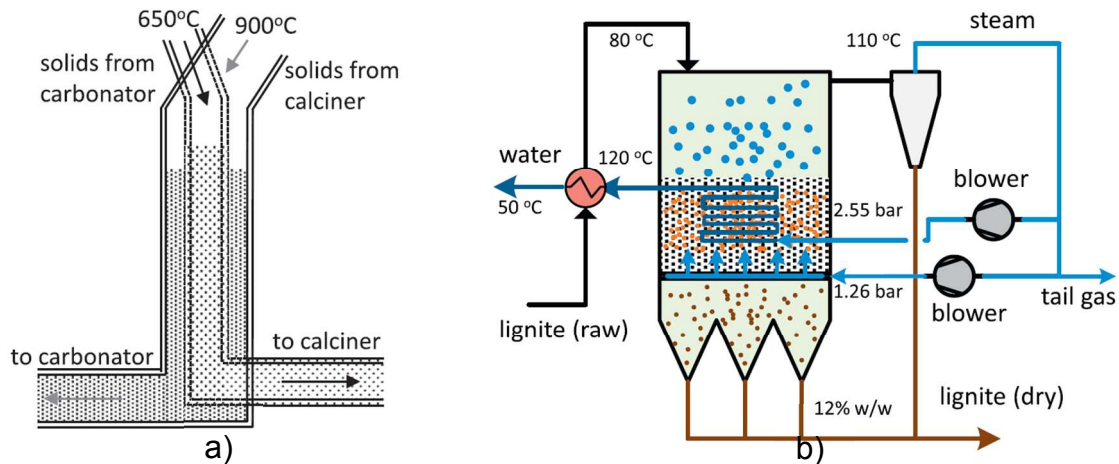


1776

1777 **Figure 24: Economically favourable heat exchanger network design for CaL integration**
 1778 **(Reprinted with permission from Lara et al. [200]. Copyright 2015 Elsevier.)**

1779 Further improvement of the integrated system efficiency can be reached through
 1780 development of integration schemes characterised with higher heat utilisation levels
 1781 using a systematic HEN analysis, which is commonly applied in different industries.
 1782 Such analysis has been used by Lara et al. [200; 201] to design the heat recovery
 1783 system for waste heat recovery from the CaL plant, which captures CO₂ from a 500
 1784 MW_{el} CFPP with net thermal efficiency of 38.2%_{LHV}, to generate steam to drive the
 1785 secondary steam cycle (290bar/600°C/620°C). Unfortunately, no information was

1786 provided on the assumptions made to assess the performance of the carbonator and
 1787 the calciner. Among different HEN configurations proposed, the economically favoured
 1788 configuration was reached when the streams were matched in such a way that they
 1789 were exhausted in a single heat exchanger (Figure 24). This configuration resulted in a
 1790 net thermal efficiency increase of 0.2% points [201] and 1.2% points [200].



1791
 1792 **Figure 25: Design of a) solid-solid heat exchanger and b) lignite bubbling fluidised bed**
 1793 **dryer (Reprinted with permission from Vorrias et al. [132]. Copyright 2015 Elsevier.)**

1794 In contrast to most previous studies, Vorrias et al. [132] have investigated integration of
 1795 a CaL plant to a lignite-fired power plant (235.4 bar/540°C/540°C) that delivers 330
 1796 MW_{el} of gross power output with net thermal efficiency of 39.1%_{LHV}. In this study the
 1797 conventional CaL plant configuration, which comprises the carbonator and the calciner
 1798 reactors interconnected with solid lines and operating at 650°C and 900°C, respectively,
 1799 was used. Having assumed that the carbonation reaction reached chemical equilibrium,
 1800 sorbent conversion in the carbonator was represented using the maximum average
 1801 conversion model by Abanades et al. [39] without the correction factor. The
 1802 performance of the calciner was represented using the chemical and phase equilibrium
 1803 through the Gibbs free energy minimization at a given temperature. Also, the heat for
 1804 sorbent regeneration is provided through oxy-combustion of lignite in an oxidizing
 1805 medium containing 80%_{vol} O₂. Although Vorrias et al. [132] claimed that this

1806 concentration was sufficient to avoid hot spots in the calciner that would increase the
1807 sorbent sintering rate, experimental and other modelling trials [33; 98; 100; 104; 133]
1808 suggested that the O₂ concentration should be below 50%_{vol} to avoid hot-spots in the
1809 reactor and thus excessive degradation of the sorbent performance.

1810 Further to utilise high-grade heat to generate additional steam to run the secondary
1811 supercritical steam cycle (235.4 bar/540°C/540°C), Vorrias et al. [132] proposed to
1812 integrate two systems for increased heat-utilisation in the CaL plant. The first is a solid
1813 recirculation heat exchanger which is proposed to be a set of concentric L-valves as
1814 illustrated in Figure 25a. It is assumed that the system performs as a co-current heat
1815 exchanger with a temperature approach of 10°C. However, the performance of such a
1816 system at a large scale has not yet been demonstrated. Moreover, as lignite consists of
1817 a considerable amount of moisture (36.8%_{wt}), oxy-combustion performance would be
1818 affected. Therefore, the second system, a BFB lignite dryer (Figure 25b) which uses
1819 recompressed water vapour as a fluidising medium, was proposed to reduce the
1820 moisture content in lignite to 12%_{wt}, comparable to the average moisture content of hard
1821 coal [202].

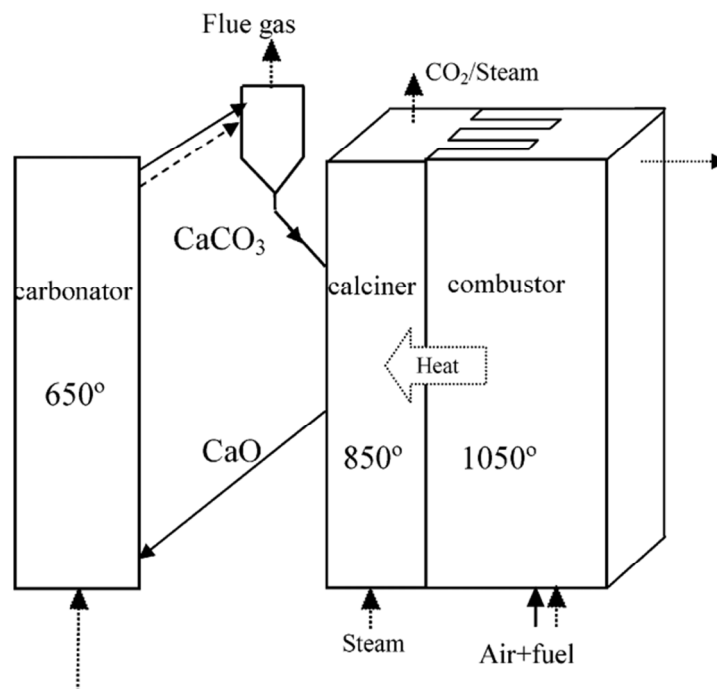
1822 Analysis of the overall process performance revealed that the net thermal efficiency of
1823 the integrated system reached 34.1%_{LHV} if both the solid-solid heat exchanger and the
1824 BFB lignite dryer were implemented. This falls to 34.0%_{LHV} and 32.5%_{LHV}, respectively,
1825 if only the first or second system is implemented. Nevertheless, the net projected
1826 efficiency penalty imposed on integration of the CaL plant reached the lowest value of
1827 5.0% points, which is considerably lower than in previous studies. It is not known if such
1828 improvement results from implementing the proposed systems or using no correction
1829 factor to determine the actual average sorbent conversion and high O₂ concentration in
1830 the oxidising medium. The net projected efficiency penalty due to CaL plant integration
1831 was found to be 2.9% points higher than for a corresponding MEA plant, but only 0.9%
1832 points higher for an oxy-fuel lignite-fired power plant.

1833 **5.1.3 Alternative configurations for efficiency improvement**

1834 Although most studies of the CaL process focus on the conventional process
1835 configuration proposed by Shimizu [28], other configurations, which aim to improve the
1836 overall process efficiency mainly through reduction of the O₂ requirement, were
1837 proposed by Abanades et al. [39] and Martínez et al. [133].

1838 In the first study proposing alternative configurations for efficiency improvement,
1839 Abanades et al. [39] investigated integration of a 100 MW_{el} supercritical CFPP with an
1840 assumed net thermal efficiency of 46%_{LHV}. In the basic configuration, the flue gas was
1841 treated in the carbonator operated at 650°C, the performance of which is modelled
1842 using Equation (8) and Equation (9). A complete sorbent regeneration was conducted at
1843 950°C using oxy-combustion of coal. In addition, the overall CO₂ capture level was
1844 assumed to be 90% and the captured CO₂ was compressed to 100 bar prior to being
1845 transported. Considering the power requirement to run the CCU and the ASU, the
1846 efficiency of the integrated system dropped by 7.2% points, to 38.8%.

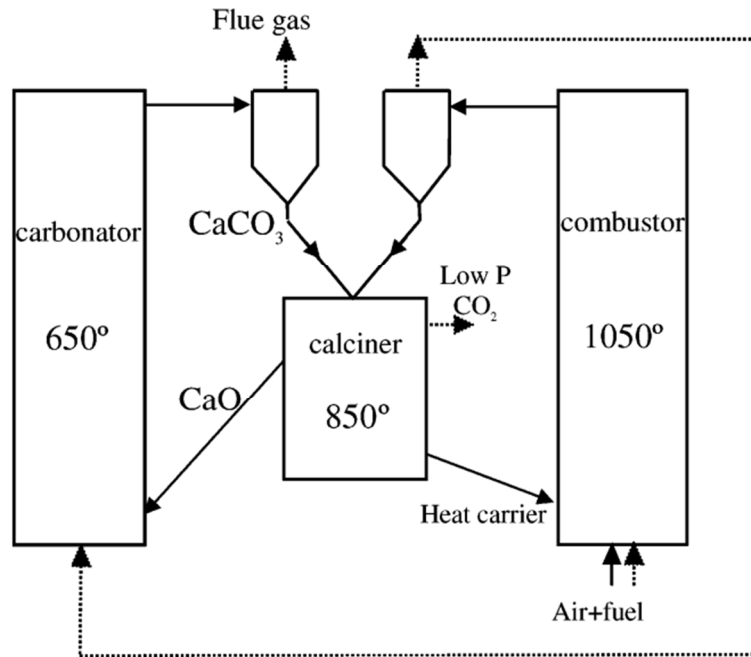
1847 As the efficiency penalty in the CaL process stems mainly from the O₂ production for
1848 oxy-fuel combustion in the calciner, Abanades et al. [39] have proposed an alternative
1849 calciner design in which the heat for the sorbent regeneration is supplied through the
1850 metallic walls from an external source (Figure 26). Their study assumed that the heat
1851 source is a fluidised bed combustor fuelled with an air and fuel mixture that operates at
1852 1050°C. Steam is used as a fluidising medium in the calciner operated at 850°C,
1853 leading to a CO₂ partial pressure of 0.4 bar. Although this configuration would be
1854 characterised by higher thermal efficiency and no requirement for O₂ production, it
1855 would require materials that have not yet been tested in practice. Also, a close
1856 integration of the combustor and the calciner is required, as a considerable heat transfer
1857 area of 800 m² is required. Despite the engineering challenges, this configuration was
1858 reported to have a net thermal efficiency of 39.4%, resulting in a projected efficiency
1859 penalty of 6.6% points. This is 1.6% points less than for the basic configuration.



1860

1861 **Figure 26: Heat transfer-integrated calciner and combustor (Reprinted with permission**
 1862 **from Abanades et al. [39]. Copyright 2015 American Chemical Society.)**

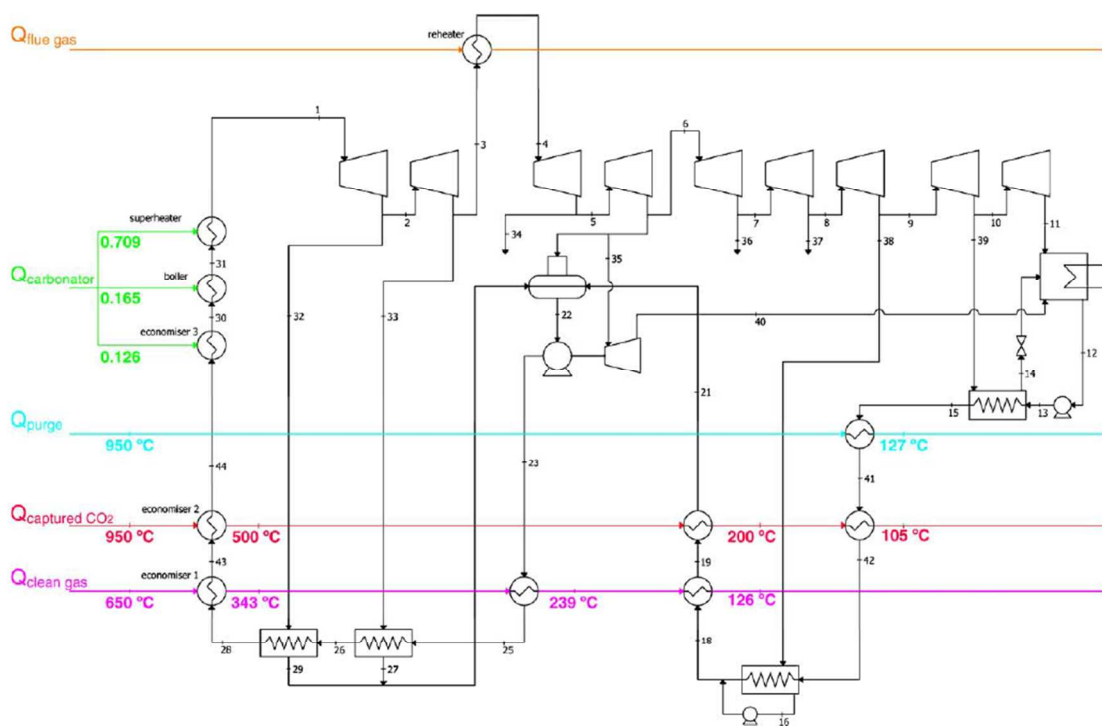
1863 To avoid application of untested materials, Abanades et al. [39] proposed that the heat
 1864 requirement of the calcination reaction could be satisfied using a solid heat carrier
 1865 (Figure 27). In this configuration, CO_2 partial pressure of 0.4 bar, which is required to
 1866 lower the calcination temperature to 850°C , is achieved through utilisation of a vacuum.
 1867 The process involves a common CFB combustor that is fired with an air and fuel
 1868 mixture. The solid bed material, which is a dense material, such as Al_2O_3 or deteriorated
 1869 CaO , is heated in the combustor, separated from the combustion gas stream and finally
 1870 fed to the calciner. However, as this configuration assumes that the heat carrier
 1871 particles would be mixed with the CO_2 sorbent in the calciner, it is still not clear whether
 1872 a continuous separation of these particles based on differences in their densities would
 1873 be possible at the required scale. Nevertheless, this configuration offers net thermal
 1874 efficiency of $40.0\%_{\text{LHV}}$, which is 2.2% points over the basic CaL configuration.



1875

1876 **Figure 27: Indirect heat transfer from combustor to the calciner (Reprinted with**
 1877 **permission from Abanades et al. [39]. Copyright 2015 American Chemical Society.)**

1878 This configuration was also investigated by Martínez et al. [148] who studied its
 1879 integration with the supercritical steam cycle (600°C/280 bar). The coal combustion took
 1880 place at 1030°C, with 15%_{vol} of excess air that entered the combustor at 400°C. The
 1881 energy input to the system through the coal combustion was assumed to be 1 GW_{th}.
 1882 The flue gas, which contained 15.7%_{vol} CO₂, was used to reheat the steam in the steam
 1883 cycle and to preheat the combustion air, and eventually entered the carbonator at
 1884 380°C. The carbonator, which operated at 650°C, was modelled using the carbonator
 1885 model developed by Alonso et al. [30] with the kinetic model for the multiple reaction
 1886 cycles by Grasa et al. [196]. Under given operating conditions, the CO₂ capture
 1887 efficiency in the carbonator was estimated to be 89%. Again, a complete calcination
 1888 process took place in the calciner operated at 950°C, which corresponds to partial
 1889 pressure of 1.93 bar. Heat for the sorbent regeneration came from the solid stream
 1890 heated in the combustor. The pressure of the separated CO₂ was increased to 150 bar
 1891 in the CCU comprising the five-stage compressor and the pump, and then it was cooled
 1892 to 40°C.



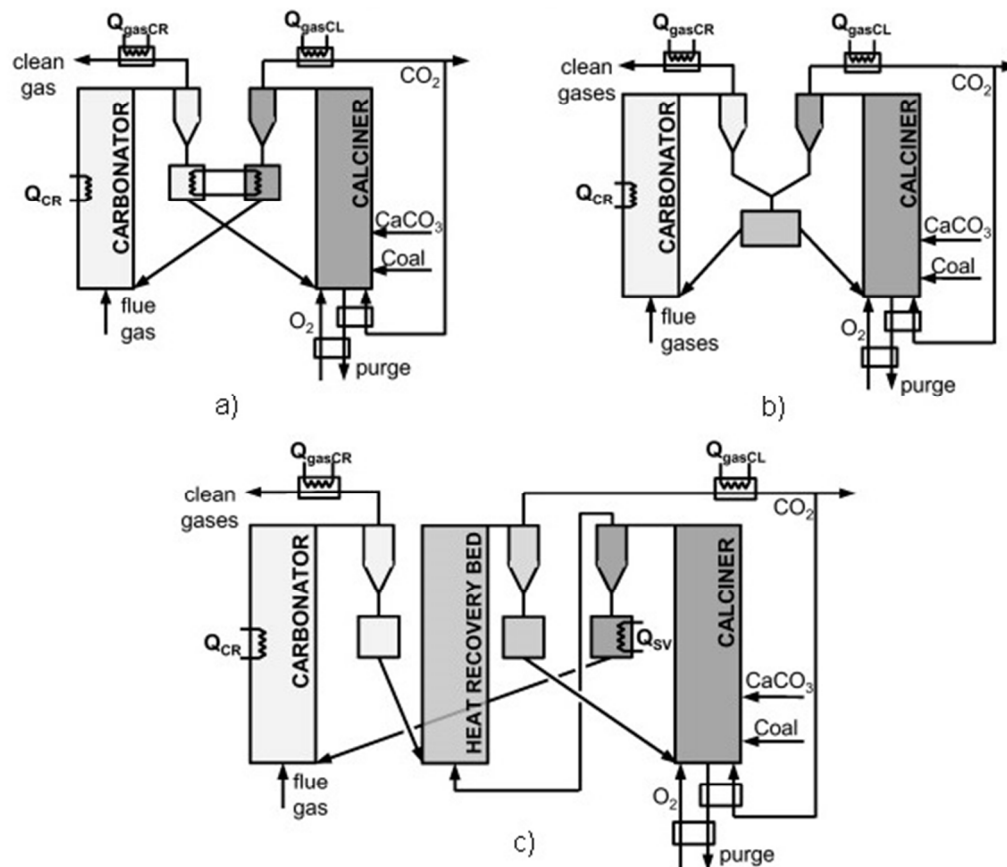
1893

1894 **Figure 28: Heat integration of the three-fluidised-bed combustion system with CaL CO₂**
 1895 **capture with the supercritical steam cycle (Reprinted with permission from Martínez et al.**
 1896 **[148]. Copyright 2015 Elsevier.)**

1897 Martínez et al. [148] have identified five possible heat sources in the analysed CaL
 1898 plant, which were heat released in the carbonator and heat carried with the clean gas,
 1899 purge, flue gas and CO₂ process streams. Having integrated these sources as
 1900 illustrated in Figure 28 and considering the power requirement for CO₂ compression, the
 1901 net power output of 378 MW_{el}, corresponding to net thermal efficiency of 37.8%, was
 1902 obtained. This was 4.3% points higher than a comparable oxy-fired CFPP.

1903 More recently, Martínez et al. [133] have proposed several process configurations that
 1904 aim to reduce the efficiency penalty in a CaL plant integrated to a 500 MW_{el} CFPP of
 1905 gross thermal efficiency of 44.4%_{LHV}. The temperature in the carbonator and calciner
 1906 were set at 650 °C and 930 °C. The performance of the carbonator was represented by
 1907 the maximum average conversion of the sorbent determined using the expression
 1908 proposed by Abanades [145] and Grasa et al. [171], and a correction factor of 0.8 to
 1909 estimate the actual average conversion. Complete calcination was assumed in the

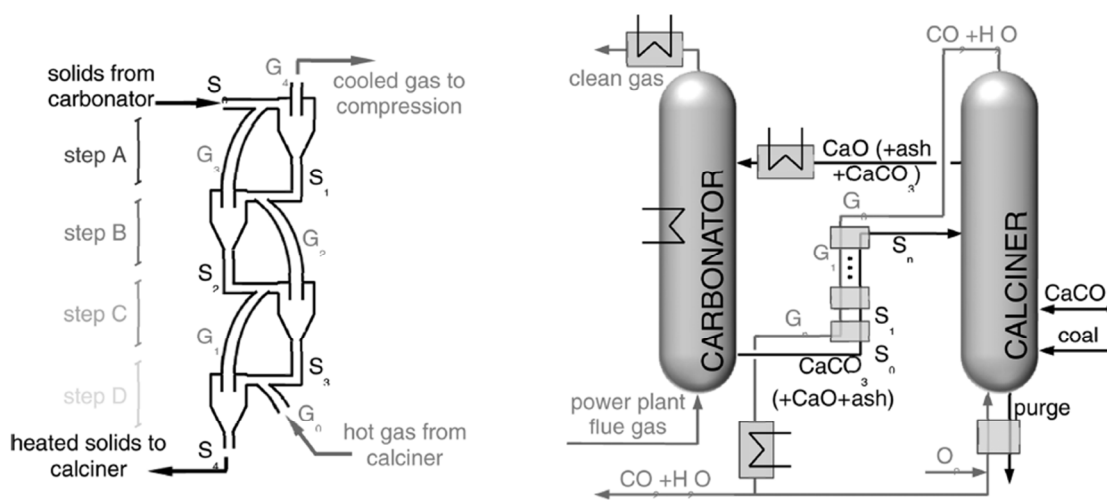
1910 calciner. As heat for sorbent regeneration was provided through oxy-combustion of coal,
 1911 O_2 was produced in the ASU, which was characterised with specific power consumption
 1912 of 220 kWh/t- O_2 . Recirculated CO_2 amounted to 40% of the inlet gas to control the
 1913 temperature in the calciner.



1914
 1915 **Figure 29: Alternative calcium looping process configurations including: a) seal valve**
 1916 **indirect heat exchanger, b) mixing seal valve and c) heat recovery fluidised bed**
 1917 **(Adapted with permission from Martínez et al. [133]. Copyright 2015 Elsevier.)**

1918 The first configuration (Figure 29a) assumes that heat is transferred from the solids
 1919 leaving the calciner to the solids leaving the carbonator by means of an indirect
 1920 heat exchanger integrated with the seal valves of the reactors. It is assumed that the solids
 1921 leave both seal valves at the same temperature. However, this is not achievable in
 1922 practice as there is no developed technology to carry out this process. To overcome this
 1923 engineering challenge, Martínez et al. [133] proposed using a single mixing seal valve

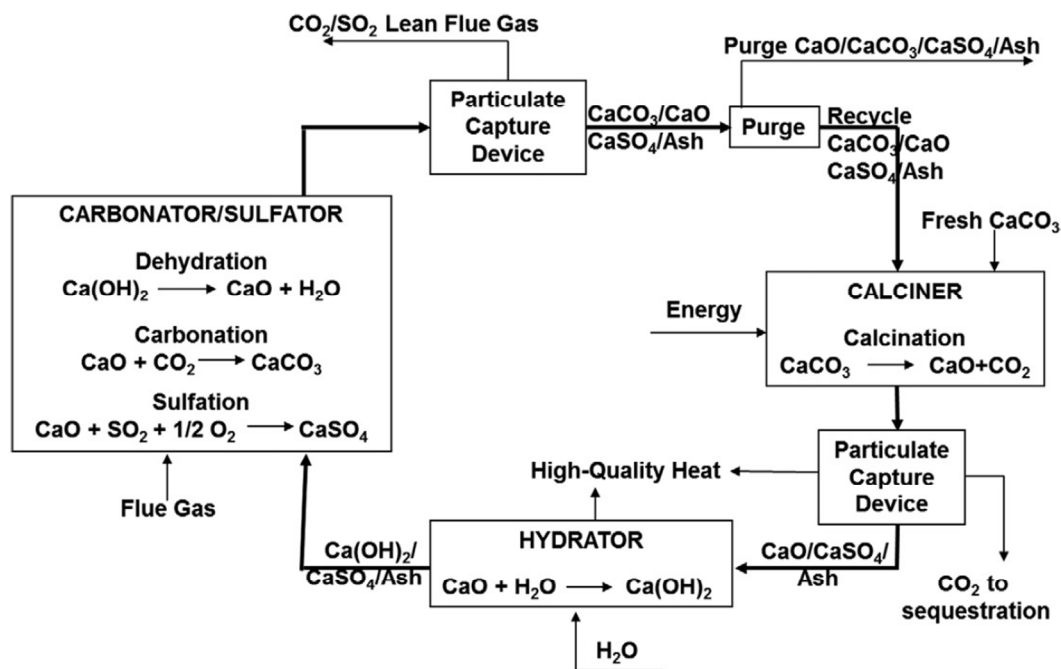
1924 for both reactors (Figure 29b). Although in this configuration solids can directly
 1925 exchange heat, the fraction of the active CaO entering the carbonator is reduced due to
 1926 solid mixing. In the last configuration, the sensible heat of the CO₂ stream leaving the
 1927 calciner is recovered to preheat the solid particles from the carbonator in an additional
 1928 heat recovery fluidised bed (Figure 29c). Although the flue gas acts as a fluidising
 1929 medium and mixes with the partially carbonated sorbent particles, no carbonation
 1930 reaction could occur in the heat recovery bed. This is because the fast carbonation
 1931 reaction cannot proceed, as the active CaO was trapped in the core of each solid
 1932 particle, the surface of which has been covered with the CaCO₃ layer formed in the
 1933 carbonator [203]. Although in this configuration the heat required by the calcination
 1934 process is satisfied through oxy-fuel combustion, it is expected to increase the thermal
 1935 efficiency of the CaL process by 1.4% points with a subsequent reduction in fuel
 1936 consumption of 9%.



1937
 1938 **Figure 30: Improvement of the calcium looping process performance through**
 1939 **implementation of the cyclonic preheater (Reprinted with permission from Martínez et al.**
 1940 **[204]. Copyright 2015 American Chemical Society.)**

1941 Another configuration proposed by Martínez et al. [204] utilises a multi-step cyclonic
 1942 preheater, which is similar to the ones used in the cement industry (Figure 30). In this
 1943 additional piece of equipment heat available in the CO₂ stream leaving the calciner is
 1944 utilised to preheat solids leaving the carbonator to around 725°C prior to entering the

1945 calciner. The temperature in the carbonator and calciner were set at 650°C and 950°C.
 1946 The performance of the carbonator and the calciner were represented by the Charitos et
 1947 al. [149] (Section 4.3.1) and Martínez et al. [134] (Section 4.4.1) models, respectively.
 1948 Although implementation of the cyclonic preheater has not changed the energetic
 1949 efficiency of the integrated system, it reduced the energy requirement of the calciner.
 1950 This was shown in reduction of the coal consumption by up to 13.3% and the oxygen
 1951 consumption by 13.6%. Finally, following the successful demonstration of the sub-pilot
 1952 facility described in Section 3.5, Wang et al. [26; 32] have investigated a CFPP retrofit
 1953 with the CaL plant involving a sorbent regeneration stage through hydration. Compared
 1954 to the conventional CaL process, the proposed CCR process comprises an additional
 1955 reactor which aims to improve conversion of the sorbent.



1956
 1957 **Figure 31: Conceptual design of hydrated calcium looping process (Reprinted with**
 1958 **permission from Wang et al. [32]. Copyright 2015 Elsevier.)**

1959 The performance of the calciner and hydrator reactors was computed based on the
 1960 assumption that the systems reach equilibrium state at 1000°C and 500°C, respectively.
 1961 In the conventional CaL process, a high calcination temperature would cause an

1962 excessive sintering of the sorbent leading to a reduction in the sorbent carrying capacity
1963 [13]. This is not the case in the CCR process as the sorbent is reactivated on contact
1964 with steam in the hydrator. Probably the lack of CO₂ recirculation to control the O₂
1965 concentration in the calciner was also due to the sorbent regeneration potential of the
1966 CCR process. Furthermore, in the experimental campaign using the sub-pilot CCR plant
1967 the CO₂ capture level of 90% in the carbonator was achieved at a Ca:C of 1.3. In the
1968 carbonator model used by Wang et al. [26; 32], a Ca:C ratio of 1.4 was used to
1969 determine the solid looping rate required to capture 90% of CO₂ and 100% of SO₂ at
1970 625°C.

1971 Wang et al. [32] have analysed integration of the CCR process into the 561 MW_{el}
1972 subcritical CFPP operating with an assumed net thermal efficiency of 33.5%_{HHV}. As
1973 mentioned above, although this approach works relatively well at full-load operation, any
1974 deviation from this point would reduce the prediction accuracy. Waste heat from the
1975 CCR process was used to generate high-quality steam that is sent to the primary cycles
1976 and replaced part of the steam generated in the power boiler. This means that the
1977 existing boiler would need to operate in part-load mode. Analysing the integration
1978 impact on the overall process efficiency, they have found that a maximum net efficiency
1979 of 26.9%_{HHV} was reached if the calciner was indirectly heated using the flue gas from
1980 the combustion process. On the other hand, when the calciner was directly heated
1981 through oxy-combustion of coal or natural gas, the net efficiency decreased to 26.5%_{HHV}
1982 and 26.1%_{HHV}, respectively. Such values for net thermal efficiency are considerably
1983 lower than in previous integration analyses reviewed. The main reason behind this is
1984 low net thermal efficiency of the reference power plant. The maximum projected
1985 efficiency penalty was estimated to be 7.4% points, which is considerably less than the
1986 9–12% points estimated for amine-based or oxy-combustion systems. Furthermore,
1987 Wang et al. [26] have shown that the projected efficiency penalty for the CCR process is
1988 22.2% lower than for a traditional CaL process. As the latter process operates on higher
1989 average conversions, this reduction can be associated with reduction of the solid
1990 looping rates between the reactors, which leads to a decrease in the heat requirement
1991 in the calciner.

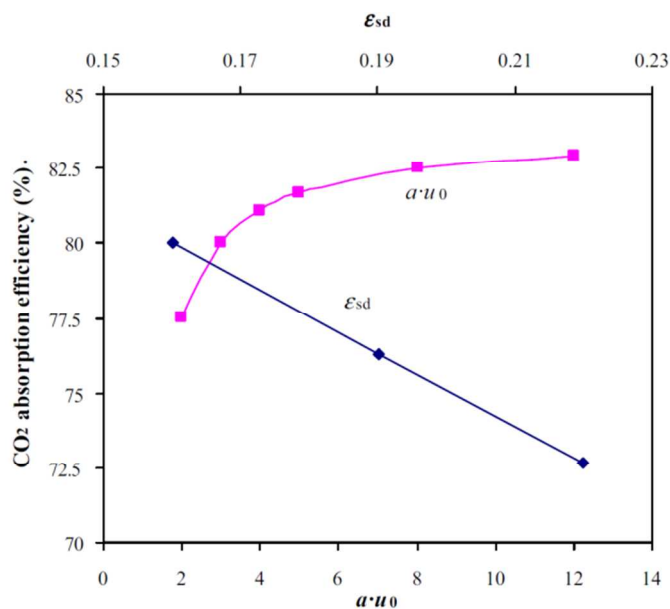
1992 **5.1.4 Comparison between the average conversion and semi-predictive** 1993 **calcium looping model**

1994 A review of the integration and process improvement studies revealed that different
1995 models have been used to represent the carbonator performance, with the average
1996 conversion and semi-predictive models being most commonly applied. On the other
1997 hand the calciner performance has been represented using equilibrium-based model in
1998 all studies reviewed. Therefore, it is important to highlight the impact of the carbonator
1999 model selection on the prediction of the integrated process performance.

2000 Ströhle et al. [147] and Lasheras et al. [31] have analysed integration of a CaL plant to a
2001 1000 MW_{el} ultra-supercritical CFPP (285 bar/600°C/620°C), which had a net thermal
2002 efficiency of 45.6%, with the aim of optimising overall process performance They
2003 assumed that a conventional CaL plant configuration was retrofitted to the existing FGD
2004 plant, thus the sulphation effect was kept to a minimum. Waste heat from the CaL plant
2005 was used to generate additional steam for the secondary steam cycle with an assumed
2006 net thermal efficiency of 49.98%. The performance of the calciner, operated at 900°C,
2007 was determined using a Gibbs reactor and the heat for sorbent regeneration was
2008 provided through oxy-combustion of coal ($w_{ASU} = 184 \text{ kWh/t-O}_2$). The carbonator was
2009 operated at 650°C with an assumed pressure drop of 100-200 mbar and SO₂
2010 conversion of 99% due to the large Ca/S ratio.

2011 Ströhle et al. [147] have compared two commonly applied approaches for carbonator
2012 modelling, the maximum average conversion of sorbent model by Abanades et al. [39]
2013 and the 1D carbonator model by Abanades et al. [136] and evaluated the differences
2014 between these approaches in terms of overall process performance. Assuming a CO₂
2015 capture level in the carbonator of 80%, application of the maximum average conversion
2016 model led to underestimation of the O₂ input to the calciner, solid looping rates and heat
2017 available for steam generation. However, in contrast to studies by Martínez et al. [133]
2018 and Berstad et al. [146], no correction was made to the maximum average conversion
2019 to determine the actual average conversion of the sorbent. Nevertheless, net thermal
2020 efficiencies were estimated to be 42.9% and 42.4% for the maximum average

2021 conversion and the predictive 1D carbonator model, respectively. It can be concluded,
 2022 therefore, that application of the maximum average conversion model with a reasonable
 2023 correction factor would give a reasonable prediction of the overall process performance.



2024
 2025 **Figure 32: Effect of KL CFB model uncertainty on the CO₂ capture level in the carbonator**
 2026 **(Reprinted with permission from Lasheras et al. [31]. Copyright 2015 Elsevier.)**

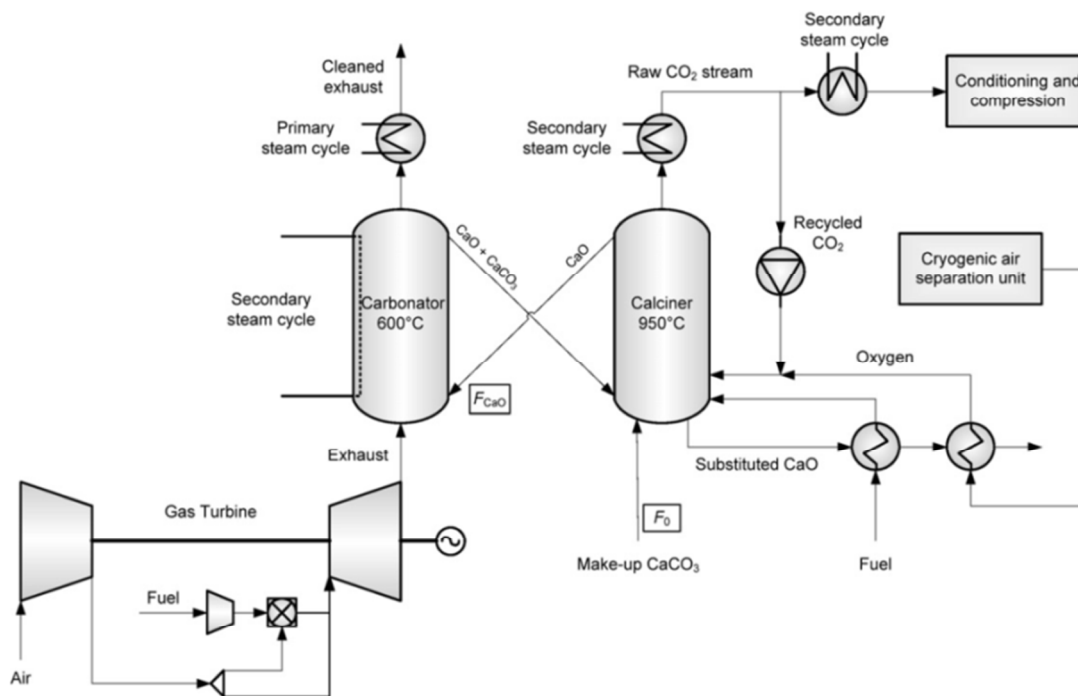
2027 In a study by Lasheras et al. [31], the effect of the uncertainty in the K-L CFB model,
 2028 which requires specification of the decay constant (a) and the solid fraction in the dense
 2029 region (ϵ_d), on the overall process performance was assessed. The analysis revealed
 2030 that variation in the key input parameters led to 10% variation of the CO₂ capture level
 2031 in the carbonator. This indicates that further experimental studies are required to identify
 2032 the K-L model parameters.

2033 5.2 Combined cycle power plants

2034 5.2.1 Feasibility of calcium looping process for natural gas-fired power 2035 plants

2036 Conversely to previous studies that analysed integration of a CaL plant to a CFPP,
 2037 Berstad et al. [146] have analysed the applicability of this CO₂ capture technology to
 2038 decarbonise a natural gas combined-cycle power plant (NGCC). The reference NGCC

2039 delivers 416.4 MW_{el} with net thermal efficiency of 52.6%_{HHV}. To account for the gas
 2040 pressure losses in the carbonator, the gas turbine discharge pressure was increased by
 2041 0.02 bar, resulting in a discharge temperature of 611°C. Such a temperature makes it
 2042 more feasible to retrofit the CaL plant right after the gas turbine island (Figure 33).



2043

2044 **Figure 33: Conceptual design of integration of calcium looping plant to natural gas**
 2045 **combined cycle power plant (Reprinted with permission from Berstad et al. [146].**
 2046 **Copyright 2015 Elsevier.)**

2047 CO₂ capture from NGCCs is more difficult than from CFPPs, as the CO₂ concentration
 2048 in the flue gas is approximately 4%_{vol}. Therefore, to achieve a CO₂ capture level
 2049 between 85% and 86% in the carbonator, its operating temperature needs to be 600°C.
 2050 To represent the performance of the carbonator, the maximum average conversion
 2051 model proposed by Rodríguez et al. [11; 40] was used. As the actual carbonation
 2052 conversion (X_{carb}) is usually lower than the maximum value, a correction factor of 0.75,
 2053 expressed as the X_{carb}/X_{ave} ratio, was adapted to enhance the accuracy of the model
 2054 prediction. Such a conservative assumption is in agreement with the experimental
 2055 results as presented in Section 3. To reach the actual carbonation conversion of 0.2, a

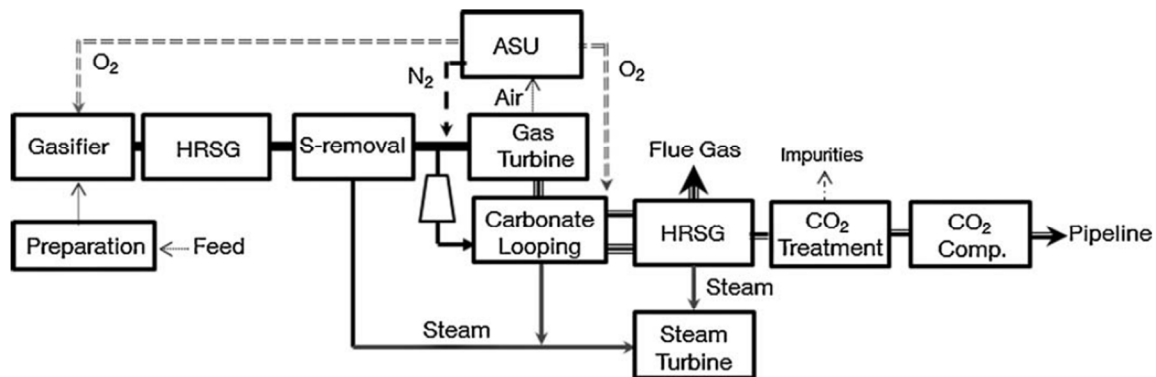
2056 F_0/F_{CaO} ratio of 0.06 was used. The sorbent is regenerated in the calciner, which is
2057 modelled as an equilibrium reactor with a calcination efficiency of 100%. A temperature
2058 of 950°C is maintained in the calciner by means of oxy-combustion of natural gas. The
2059 95%_{mol}-purity O₂ stream is produced in the cryogenic ASU and mixed with the recycled
2060 CO₂ to maintain 25%_{mol} O₂ concentration in the oxidising gas. The pressure drop in the
2061 calciner is accounted for through an increase of the recycled CO₂ pressure of 0.03 bar.
2062 The remaining CO₂ is directed to the CCU, which is modelled as four compression
2063 stages and one pumping stage with intercooling to 28°C, where it is compressed to 150
2064 bar before being transported.

2065 The waste heat from the CaL plant was utilised to generate an additional amount of
2066 steam that was then used to drive the secondary steam cycle. As the solids transported
2067 from the calciner to the carbonator carry a considerable amount of energy, the effect of
2068 the heat recuperation between the solid streams on the energy requirement in the
2069 calciner was investigated. Overall, three options for steam conditions (120
2070 bar/560°C/560°C, 120 bar/610°C/610°C and 202 bar/610°C/610°C) were analysed for
2071 two CaL process configurations (with and without solid-solid heat recuperation). The
2072 study revealed that in the best case scenario, where solid-solid heat recuperation was
2073 implemented and the HP steam was generated at 610°C and 202 bar, the projected
2074 efficiency penalty amounted to 9.1% points. This was found to be 1.3% points higher
2075 than for the reference NGCC with a conventional MEA CO₂ capture plant. Therefore, a
2076 CaL plant may not be a preferable option for NGCCs, which can be attributed to low
2077 CO₂ concentration in flue gas that results in lower driving force for the carbonation
2078 reaction. In turn, to reach the desired CO₂ capture level, the carbonator operating
2079 temperature needed to be lowered to 600°C. The primary steam cycle location
2080 upstream of the CaL plant contributed to the efficiency penalty as less flue gas was fed
2081 to the primary waste heat steam generator. A possible solution for both issues was
2082 presented by Biliyok and Yeung [205] who showed that exhaust gas recirculation and/or
2083 supplementary firing could increase the flue gas temperature, flow rate and CO₂
2084 concentration. However, feasibility of the former solution is doubtful as it would further

2085 increase the capital cost by 20%, while reducing the levelised cost of electricity by only
 2086 4%.

2087 5.2.2 High-reliability and high-efficiency coal-gasification power generation 2088 systems

2089 The need for high-efficiency and environmentally friendly fossil-fuel power generation
 2090 systems led to development of IGCC as an alternative to CFPPs. Kunze et al. [131]
 2091 considered the reference 510 MW_{el} IGCC plant having net thermal efficiency of
 2092 39.4%_{LHV}, in which coal is gasified in the O₂-rich environment. Produced syngas is then
 2093 cleaned to remove impurities, such as metals, sulphur and nitrogen compounds, and
 2094 CO is converted to CO₂ in the water/gas shift reaction, which is then removed through a
 2095 pre-combustion system using acid gas removal (AGR) based on an amine (MDEA)
 2096 process. Finally, the purified syngas, which at this stage consists mostly of H₂, is
 2097 combusted in a gas turbine coupled with an electric generator. The waste heat from the
 2098 discharge gas is used to generate high-pressure steam at 170 bar, which then
 2099 generates electricity in the bottoming steam cycle.



2100

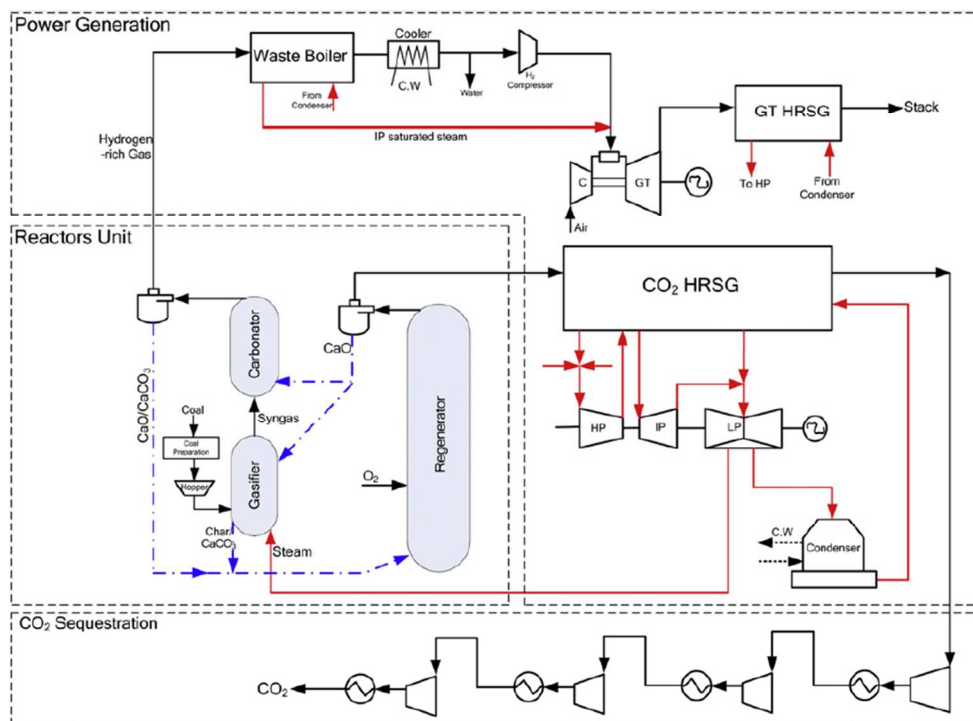
2101 **Figure 34: Conceptual design of integration of calcium looping plant to IGCC (Reprinted**
 2102 **with permission from Kunze et al. [131]. Copyright 2015 Elsevier.)**

2103 Kunze et al. [131] have proposed substituting a pre-combustion AGR system with a
 2104 post-combustion CaL plant (Figure 34). The carbonator was modelled as a
 2105 stoichiometric reactor with conversion of 20% and operating temperature of 650°C. The
 2106 desired CO₂ capture level in the carbonator of 90% was assured through adjusting the

2107 solids looping rate in the system. In contrast to the other studies, the calciner, which
2108 operated at 950°C, was modelled as a stoichiometric reactor with conversion of 95% to
2109 account for sorbent sintering. The heat requirement for sorbent regeneration was met
2110 through direct oxy-combustion of syngas in the calciner. It was proposed that O₂ was
2111 produced using the oxygen transfer membrane, which separates O₂ from the high-
2112 pressure air diverted from the gas turbine compressor at temperatures of 850–900°C,
2113 and then mixed with recycled CO₂ to control the calcination temperature. The remaining
2114 CO₂ was sent to purification and compression to 110 bar.

2115 The waste heat available in the CaL plant was utilised to generate high-pressure steam
2116 (250 bar/630°C/650°C) that was fed to a bottoming dual-pressure supercritical steam
2117 cycle. This substitution of a subcritical bottoming steam cycle in the conventional IGCC
2118 plant led to improvement in net thermal efficiency of 3.8% points, to 43.2%_{LHV} and a
2119 9.5% increase in the net thermal power, to 462 MW_{el}. Such performance is in the range
2120 for the supercritical CFPPs without a CO₂ capture plant [206; 207]. For this reason, the
2121 IGCC plants with CaL could be a feasible option for production of clean power from
2122 coal, with an increased reliability due to the lack of complicated chemical plant as in the
2123 conventional systems.

2124 Alternative process configuration for a H₂-fuelled IGCC power plant that comprises a
2125 DFB system has been proposed by Wang et al. [130] (Figure 35). The performance of
2126 each reactor in the system was based on the assumption that chemical and phase
2127 equilibrium is reached. The gasifier reactor is composed of the BFB gasifier, in which
2128 allothermal steam gasification of coal takes place at 700°C, integrated with a carbonator
2129 riser operated at 600°C. As the gasifier is assumed to operate with 50% conversion of
2130 coal, the unreacted char and sorbent are fed to the calciner, which operates at 900°C.
2131 The heat required to sustain the calcination reaction stems from the oxy-combustion of
2132 char. The H₂-rich gas is used to fuel an F-class gas turbine, in which the compressor
2133 operates at a pressure ratio of 17 and expander temperature of 1350°C.



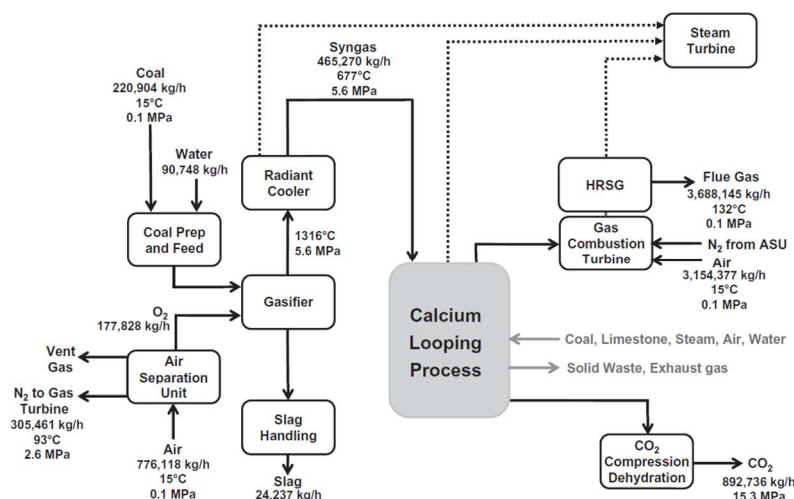
2134

2135 **Figure 35: Conceptual design of integration of calcium looping plant to IGCC (Reprinted**
 2136 **with permission from Wang et al. [130]. Copyright 2015 Elsevier.)**

2137 The waste heat available in the integrated system is utilised to sustain the gasification
 2138 reaction by diverting part of the regenerated sorbent to the gasifier and to generate the
 2139 steam for the bottoming subcritical steam cycle (125 bar/565°C/565°C). The net thermal
 2140 efficiency of the proposed process was 42.7%_{LHV}, while a CO₂ capture level of 95% was
 2141 reached. The efficiency was considerably higher than for a supercritical CFPP retrofitted
 2142 with an ammonia-based CO₂ capture plant (net thermal efficiency of 27.9%_{HHV}) [208].
 2143 This is also 5.7% points higher than for a CFPP retrofitted with the CaL plant analysed
 2144 by Romeo et al. [86] (Section 5.1.2).

2145 It is also important to benchmark the process performance improvements through
 2146 substitution of the dual stage Selexol process, which is commonly considered in the
 2147 IGCC power plants, with the CaL plant. Connell et al. [129] have evaluated such
 2148 performance improvement in an IGCC power plant, which comprises two F-class gas
 2149 turbines (Case 2 in Black et al. [209]). In the considered CaL configuration, which was
 2150 based on the double looping CCR process developed and successfully demonstrated

2151 by Wang et al. [26; 32], each reactor was assumed to reach chemical and phase
 2152 equilibrium at a given operating temperature. In contrast to previous studies, the
 2153 carbonator was operated at 33 bar, which required a temperature of 700°C to allow
 2154 $\text{Ca}(\text{OH})_2$ dissociation and hence the water/gas shift reaction. To increase the average
 2155 sorbent conversion, and hence operate the system at Ca:C ratio of 1.3 that was
 2156 identified in the pilot-plant testing to allow reaching more than 90% CO_2 capture, the
 2157 sorbent is hydrated at 2 bar and 493°C. The reason for the hydrator being operated at
 2158 an elevated pressure was to increase its operating temperature and allow for more
 2159 waste heat recovery in the system. An operating temperature of more than 875°C in the
 2160 calciner is maintained through oxy-combustion of coal. The conceptual IGCC design
 2161 assumes that the heat from the CaL plant is utilised to generate steam for the bottoming
 2162 steam cycle (Figure 36).

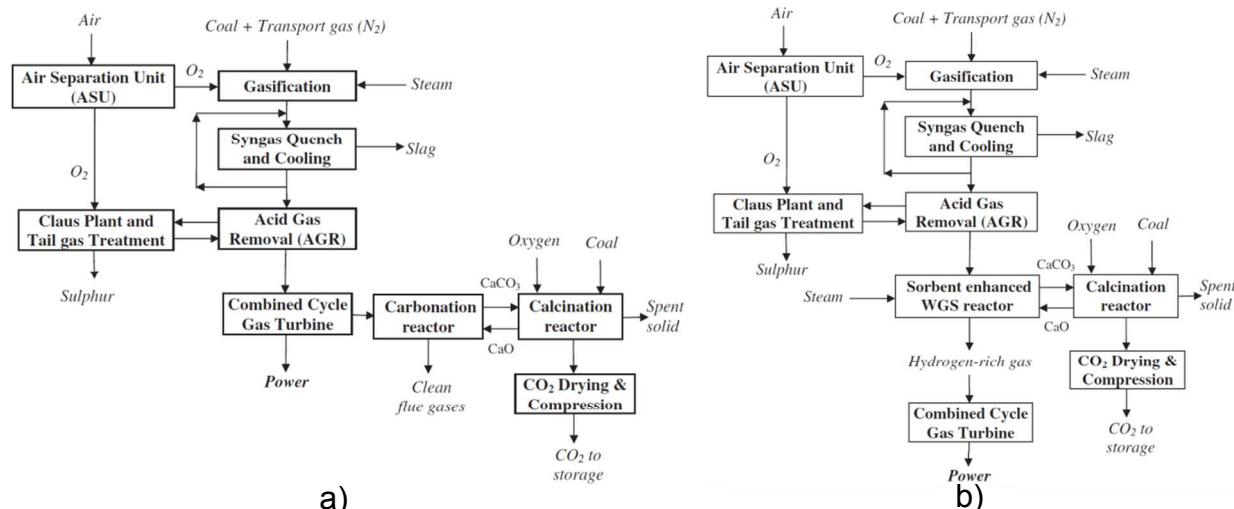


2163
 2164 **Figure 36: Conceptual design of integration of calcium looping plant to IGCC (Reprinted**
 2165 **with permission from Connell et al. [129]. Copyright 2015 Elsevier.)**

2166 Having compared the performance of the IGCC with the CCR process and the
 2167 conventional IGCC with dual stage Selexol process, Connell et al. [129] have found that
 2168 net thermal efficiency increased by 0.4% points, from 32.7%_{HHV} to 33.1%_{HHV}, with the
 2169 coal oxy-combustion accounting for 41% of the total heat input to the process. This
 2170 performance was 6.5% points higher than for a comparable subcritical CFPP retrofitted

2171 with an MEA scrubbing system [209]. More importantly, the net power output of the
2172 system increased by 41.8%, from 543.2 MW_{el} to 932.9 MW_{el}.

2173 In the IGCC power plant, the CaL process can be used as either post-combustion, with
2174 the standard AGR process used for syngas treatment, or pre-combustion technology.
2175 Cormos and Cormos [128] have investigated the difference between these approaches
2176 for a 561.15 MW_{el} IGCC power plant of 44.36%_{LHV} net thermal efficiency. The
2177 performance of all reactors in the system was determined based on thermodynamic
2178 equilibrium, as no significant differences were found when the kinetics of the calcination
2179 and carbonation processes were considered. In the investigated CaL plant, the
2180 carbonator and the calciner were operated at 650-700°C and 900-950°C, respectively.
2181 The temperature in the calciner was maintained through oxy-combustion of coal. It was
2182 also assumed that the CaL plant was fully heat integrated with the rest of the plant.



2183
2184 **Figure 37: Conceptual design of integration of a) post-combustion and b) pre-**
2185 **combustion calcium looping plant to IGCC (Adapted with permission from Cormos and**
2186 **Comros [128]. Copyright 2015 Elsevier.)**

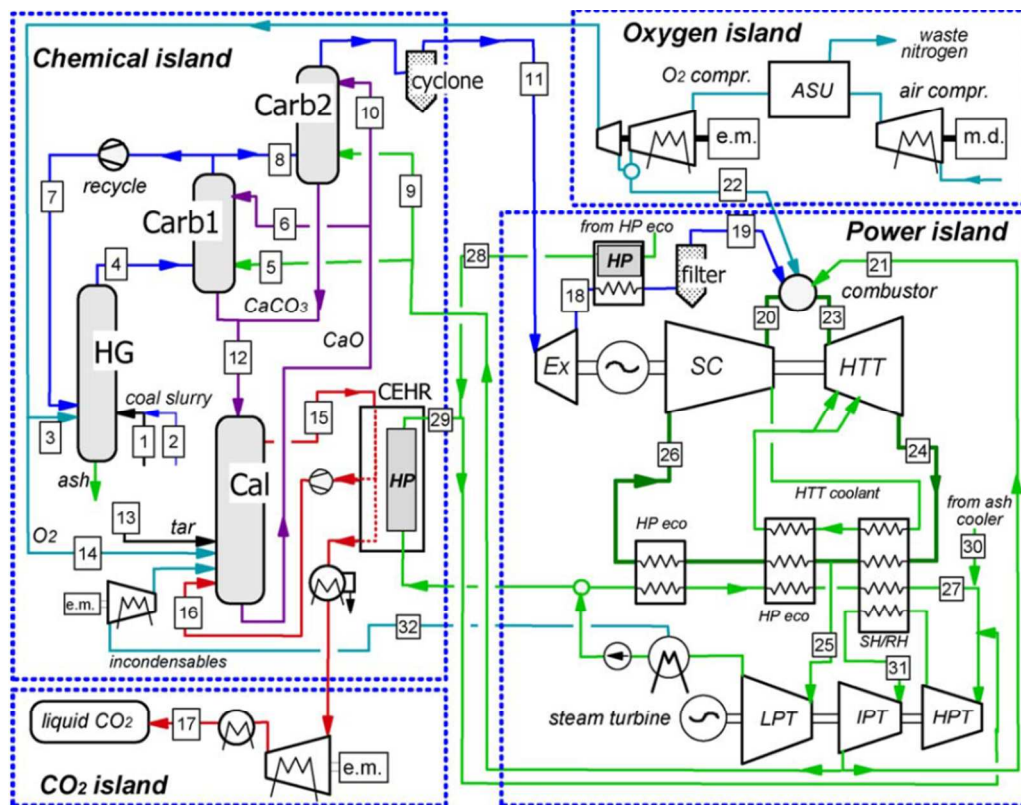
2187 In the first configuration, the CaL plant was proposed to be retrofitted after the power
2188 block (Figure 37a), which would provide a flexible integrated system. Conversely, the
2189 second configuration assumes that the carbonator was located after the AGR plant

2190 (Figure 37b). Steam is supplied directly to the calciner to facilitate the water/gas shift
2191 reaction allowing the H₂-rich stream to be fed to the power block.

2192 Analysis of the overall plant performance indicators revealed that on integration of the
2193 CaL plant the net thermal efficiency dropped by 10.1% points for the post-combustion
2194 configuration and by 7.3% points for the pre-combustion configuration. With utilisation of
2195 the waste heat to produce high-pressure steam, which was then used to produce power
2196 in the bottoming steam cycle, the net power output increased by 14.6% and 19.4% for
2197 the post-combustion and pre-combustion configurations, respectively. Although such
2198 results show that the former configuration is more promising in terms of overall process
2199 performance, its higher integration degree would affect plant flexibility. Moreover,
2200 Cormos and Cormos [128] have concluded that the net efficiency penalty of the post-
2201 combustion configuration is comparable with the one associated with conventional post-
2202 combustion scrubbing technologies. Hence application of CaL as a post-combustion
2203 CO₂ capture plant will not bring any benefit in terms of process performance. However,
2204 the pre-combustion configuration was found to result in a net efficiency penalty 1–2%
2205 points lower than conventional pre-combustion scrubbing technologies.

2206 **5.2.3 Zero-emissions coal-based power generation systems**

2207 Due to high-temperature operation of the CaL process, it can serve as a base for
2208 development of novel highly-efficient and low-emission power generation systems. Two
2209 alternative coal-fasification combined cycle power plants, which utilise the CaL process
2210 as both a pre-combustion CO₂ capture technology and heat source, have been
2211 investigated by Romano and Lozza [127; 210]. Both zero-emissions coal mixed
2212 technology (ZECOMIX) (Figure 38) and zero-emissions coal mixed technology with air
2213 gas turbine (ZECOMAG) (Figure 39) can be divided into four sections – chemical island,
2214 oxygen island, CO₂ island and power island – and they only differ in the power island
2215 configuration.

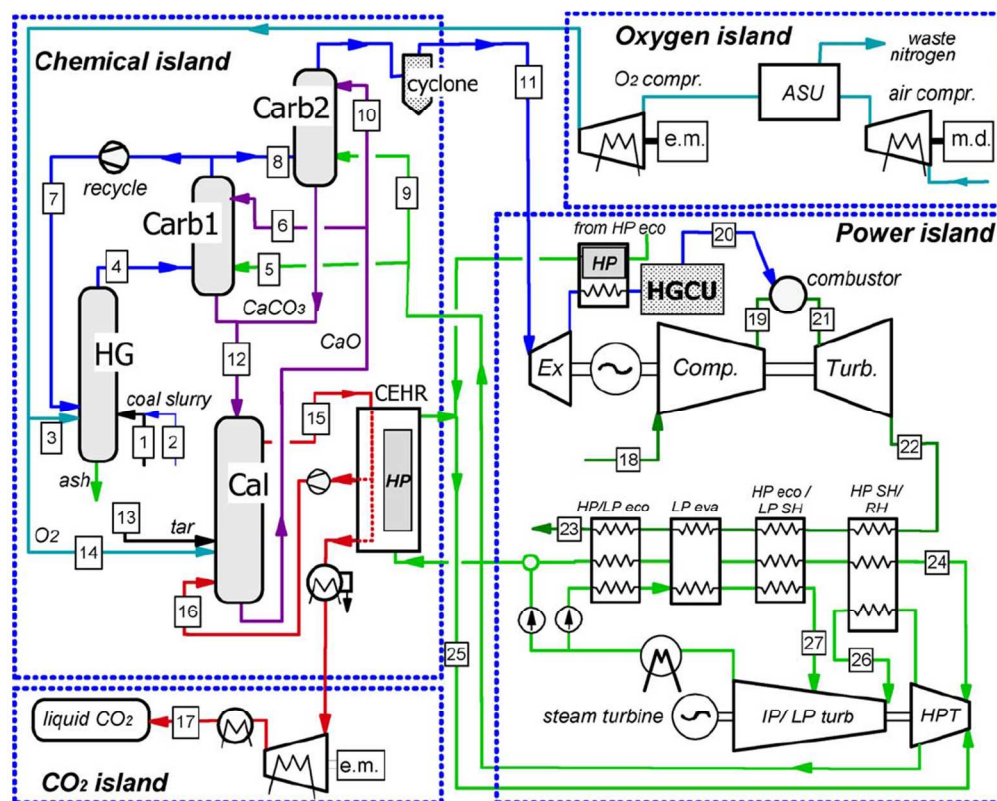


2216

2217 **Figure 38: Conceptual design of Zero-Emissions COal MIXed technology (Reprinted with**
 2218 **permission from Romano and Lozza [210]. Copyright 2015 Elsevier.)**

2219 In the chemical island, where each reactor was assumed to operate under equilibrium
 2220 conditions, coal slurry is gasified under an H₂ atmosphere in a hydrogasifier producing
 2221 syngas that is then shifted to the H₂-rich stream in the carbonator. A small amount of O₂
 2222 is utilised to sustain the operating temperature at 700°C–1000°C, depending on the
 2223 operating pressure ranging between 30 bar and 70 bar. The overall chemical reaction
 2224 taking place in the hydrogasifier and the carbonator is presented in Equation (101). This
 2225 reaction was found to be exothermal, as the heat released on the exothermal CO₂
 2226 removal from the syngas was enough to sustain the steam reforming reaction. Part of
 2227 the H₂-rich stream is recycled from the carbonator to the hydrogasifier.





2228

2229 **Figure 39: Conceptual design of Zero-Emissions COal Mixed technology with Air Gas**
 2230 **turbine (Reprinted with permission from Romano and Lozza [127]. Copyright 2015**
 2231 **Elsevier.)**

2232 It was assumed that the carbonator operates with an average conversion of 50% that
 2233 was substantiated with the expected progress in sorbent treatment, production and
 2234 reactivation [210]. Sorbent regeneration was assumed to be conducted at an elevated
 2235 pressure and temperatures ranging between 920°C and 1250°C, regardless of sorbent
 2236 sintering and degradation. Such high temperatures were achieved through oxy-
 2237 combustion of the refinery residuals with 90% oxygen excess, as usage of the produced
 2238 syngas would reduce the net thermal efficiency of the process, while usage of coal at
 2239 such a high temperature would result in ash melting.

2240 The power island of ZECOMIX technology comprises a semi-closed Joule cycle, in
 2241 which heat from the syngas oxy-combustion and the combustion gases are mixed with
 2242 compressed steam to control the combustor outlet temperature. Such a mixture is

2243 expanded in a high-temperature steam turbine and then used for supercritical steam
2244 generation in the bottoming steam cycle. The incondensable species, such as CO₂ and
2245 O₂, are removed from the condenser and from the deaerator with part of the steam sent
2246 to the calciner. This approach allows the ASU load to be minimised as unreacted O₂ is
2247 recycled to the calciner. Conversely, ZECOMAG technology has a more conventional
2248 power island, in which the syngas is burned with air in an open gas turbine cycle, and
2249 the discharged flue gas is used to generate supercritical steam in the dual-pressure
2250 heat recovery steam generator for the steam cycle [127]. Despite its more conventional
2251 configuration, ZECOMAG cannot be considered as a zero-emissions technology as the
2252 gas turbine flue gas, which consists of CO₂, NO_x and SO_x, is exhausted to the
2253 environment.

2254 Analysis of the overall process performance revealed that ZECOMIX and ZECOMAG
2255 yield similar maximum net thermal efficiencies of 46.69%_{LHV} and 46.74%_{LHV},
2256 respectively. The analysis also revealed that the net efficiency of ZECOMIX was
2257 degraded by 0.59% points on increase of the steam compressor pressure from 25 bar
2258 to 48.5 bar, and by 2.32% points on reduction of the calciner temperature to 920°C. In
2259 addition, reduction of the average sorbent conversion in the carbonator from 66.7% to
2260 20.0% was found to reduce the net thermal efficiency of ZECOMIX by 3% points and of
2261 ZECOMAG by 2.5%. This indicates that sorbent performance is critical in terms of the
2262 overall process efficiency. Finally, the net power output of 667.5 MW_{el} for ZECOMIX
2263 when the steam compressor is operated with a pressure ratio of 25, was found to be
2264 25.2% higher than for ZECOMAG with the gas turbine compressor operated with a
2265 pressure ratio of 20. The maximum net power output achievable by ZECOMIX was
2266 found to be 1242.2 MW_{el} if the steam compressor inlet pressure was increased from
2267 1.02 bar to 1.9 bar.

2268 **5.3 Summary**

2269 **5.3.1 Integration impact on the overall process performance**

2270 Depending on the power plant type, the net projected efficiency penalty imposed by
2271 post-combustion CaL plant integration was 2.6 [37]–7.9% [86] points for a CFPP and
2272 9.1–11.4% [146] points for a combined cycle power plant.

2273 A very low net projected efficiency penalty of 2.6% points was estimated by Martínez et
2274 al. [37] in investigating a subcritical CFPP retrofit with a CaL plant and supercritical
2275 secondary steam cycle. This shows that implementation of CaL plants into subcritical
2276 units, the majority of the current CFPP fleet, would result in a minor net efficiency
2277 penalty compared to conventional CO₂ capture technologies. Nevertheless, the mean
2278 net projected efficiency penalty for a CFPP was 6–7% points with 2.5–3% points
2279 associated with the CaL plant itself and the remainder caused by the CCU. Yang et al.
2280 [16] have estimated an extremely low net thermal efficiency of 21.2% for a CaL plant
2281 integrated into a CFPP without any heat recovery system. This implies that as high-
2282 grade heat is available in the CaL plant, it needs to be recovered efficiently to reach
2283 high overall performance.

2284 The studies by Berstad et al. [146] and Cormos and Cormos [128] revealed that
2285 integration of a CaL plant as a post-combustion technology into the NGCC and the
2286 IGCC power plant would result in a net efficiency penalty comparable to conventional
2287 CO₂ capture systems. This could be associated with low partial pressure of CO₂ in the
2288 flue gas, and thus lower driving force for the carbonation reaction. However, in studies
2289 where a CaL plant was used as a substitute for a complex gas processing plant
2290 integrated as a pre-combustion CO₂ capture technology into an IGCC system, the net
2291 thermal efficiency increased by 0.4 [129]–3.8% [131] points, and reached 43.2%_{LHV}
2292 [131]. The study by Romano and Lozza [127; 210] revealed that development of new
2293 coal-based power generation systems based on the CaL process, which are
2294 characterised by net thermal efficiencies of 46.69%_{LHV} for CO₂ capture higher than 95%,
2295 is feasible. Such values for net thermal efficiency, which are in the range of supercritical

2296 and ultra-supercritical CFPPs without CO₂ capture plants, and increased process
2297 reliability due to the lack of complicated chemical plant indicate that gasification-based
2298 power plants with pre-combustion CaL could become a cost-efficient and
2299 environmentally-friendly technology for coal-based power generation, and could allow
2300 further coal utilisation.

2301 It is important to highlight that all of the reviewed studies use different initial set of
2302 assumptions regarding the reference power plant. Moreover, the reference net thermal
2303 efficiencies of the CFPPs gathered in Table 7 vary between 32.7–44.6%_{HHV} (studies
2304 using higher heating value basis), and 36.0–46.0%_{LHV} (studies using lower heating value
2305 basis). However, as mentioned in the introduction, the average net thermal efficiency of
2306 the existing global fleet has been identified to be 33%_{LHV}, which corresponds to 30–
2307 31%_{HHV} depending on fuel composition [211]. As the sub-critical units, which operate
2308 with low net thermal efficiencies and yet account for around 75% of the global CFPP
2309 capacity [6], can be expected to be still in operation in the nearest future, the further
2310 analyses of the CaL process integration should focus on a portfolio of steam conditions
2311 to assure prediction accuracy and realism. This implies that baseline reference models
2312 for CaL process integration need to be established, what can be done, for example, by
2313 replicating CFPP (subcritical and supercritical), NGCC and IGCC models from the
2314 revised NETL report [209] and developing ultra-supercritical CFPP model based on the
2315 European Benchmarking Task Force documents [212; 213] Table 7 reveals that not
2316 only are the reference CFPPs are based on different steam conditions, from sub-critical
2317 to ultra-supercritical, but also their gross power outputs and net thermal efficiencies vary
2318 considerably. The performance of the reference IGCC plants vary significantly as well.
2319 As this makes an comparison of results across different analyses impossible, a set of
2320 baseline reference, which should include models for CFPP, NGCC and IGCC plants
2321 with consideration of different steam conditions, needs to be established. Such a
2322 baseline reference models would allow for a reliable comparison of further process
2323 developments using process simulations.

2324

2325 **Table 7: Summary of the process integration studies**

Reference	Power plant type	Gross power output (MW _{el})	Reference net thermal efficiency (% _{LHV})	Net thermal efficiency of integrated system (% _{LHV})	Efficiency penalty (% points)
Shimizu et al. [28]	SC-CFPP*	1000	N/A	33.4 ****	N/A
Yang et al. [16]	SC-CFPP*	600	40.6	25.3–36.8	3.8–15.3
Abanades et al. [39]	USC-CFPP*	100	46	38.8–40.0	6–7.2
Martínez et al. [83]	SubC-CFPP*	350	36	30.3–33.4	2.6–5.7
Martínez et al. [148]	SC-CFPP*	433.7	N/A	37.8	N/A
Martínez et al. [133]	CFPP**	500	44.35		N/A
Romeo et al. [86]	SC-CFPP*	450	44.93	37.0	7.93
Lara et al. [200]	SC-CFPP*	500	38.2	33.0	5.2
Lara et al. [201]	SC-CFPP*	500	38.2	34.0	6.2
Ströhle et al. [147]	USC-CFPP*	1100	45.6	42.4–42.8	2.8–3.2
Lasheras [31]	USC-CFPP*	1000	45.6	42.7	2.9
Wang et al. [32]	USC-CFPP*	561	44.6****	37.2–38.0****	6.6–7.4
Wang et al. [26]	SubC-CFPP*	500*****	35.8****	N/A	N/A
Wang et al. [26]	SC-CFPP*	500*****	39.0****	N/A	N/A
Vorrias et al. [132]	SC-LFPP***	330	42.5	37.5	5.0
Berstad et al. [146]	NGCC	418.8	52.6****	41.2–43.5****	9.1–11.4
Kunze et al. [131]	IGCC	510	39.4	43.2	-3.8
Wang et al. [130]	IGCC	N/A	N/A	42.7	N/A
Connel et al. [129]	IGCC	734	32.7****	33.1****	-0.4
Cormos and Cormos [128]	IGCC	561.2	44.4	34.2–37.0	7.4–10.2
Romano and Lozza [210]	ZECOMIX	N/A	N/A	44.4–46.7	N/A
Romano and Lozza [127]	ZECOMAG	N/A	N/A	46.7	N/A

*SC - Supercritical; USC - Ultra-supercritical ; SubC – Subcritical, **Steam conditions not specified, ***Supercritical lignite-fired power plant, ****HHV basis, ***** Net power output.

2326 Moreover, the reference net thermal efficiencies of the CFPPs gathered in Table 7 vary
 2327 between 32.7–44.6%_{HHV} (studies using higher heating value basis), and 36.0–46.0%_{LHV}
 2328 (studies using lower heating value basis). However, as mentioned in the introduction,
 2329 the average net thermal efficiency of the existing global fleet has been identified to be
 2330 33%_{LHV}, which corresponds to 30–31%_{HHV} depending on fuel composition [211]. As the
 2331 sub-critical units, which operate with low net thermal efficiencies and yet account for
 2332 around 75% of the global CFPP capacity [6], can be expected to be still in operation in
 2333 the nearest future, the further analyses of the CaL process integration should focus on a

2334 portfolio of steam conditions to assure prediction accuracy and realism. This implies that
2335 baseline reference models for CaL process integration need to be established, what can
2336 be done, for example, by replicating CFPP (subcritical and supercritical), NGCC and
2337 IGCC models from the revised NETL report [209] and developing ultra-supercritical
2338 CFPP model based on the European Benchmarking Task Force documents [212; 213].

2339 **5.3.2 Modelling approaches, assumptions and limitations**

2340 This review identified limitations in the approaches for modelling CaL plants and their
2341 integration into the power plants (Table 8). Firstly, it was found that in several studies
2342 the net or gross thermal efficiency of the secondary steam cycle [26; 28; 31; 32; 37; 39;
2343 83; 147], as well as specific power consumptions of ASU [26; 28; 31; 32; 83; 86; 128;
2344 130; 133; 146; 147; 200; 201] and CCU [26; 28; 32; 83] were assumed rather than
2345 estimated using thermodynamic or process models. Although this approach could be
2346 valid for a particular system operating at a fixed load, any deviation from the operating
2347 point, such as part-load operation, would reduce the accuracy of the prediction.
2348 Moreover, such approach applied to represent the performance of the secondary steam
2349 cycle, ASU and CCU, restricts applicability of a detailed design of the HEN of the entire
2350 process.

2351 Secondly, the studies reviewed assumed that total calcination is achieved in the
2352 calciner, with the exception of the study by Kunze et al. [131] who assumed 95%
2353 conversion in the calciner to account for less favourable calcination conditions. Thirdly,
2354 all the studies utilised thermodynamic models to represent the calcination process,
2355 mostly achieving chemical equilibrium through Gibbs free energy minimisation. Most of
2356 the studies analysing the combined cycle power plants used thermodynamic models
2357 also for the carbonator, with the exception of Berstad et al. [146], while more complex
2358 models, such as average conversion models [16; 39; 132; 133; 147] and 1D carbonator
2359 models based on K-L hydrodynamics [28; 31; 147] were used in analysing the CFPPs.
2360 Interestingly, the study by Ströhe et al. [147], in which both models have been
2361 compared, revealed that, although application of the maximum average conversion
2362 model without the correction factor resulted in underestimation of several process

2363 parameters, the overall process performance of a CFPP with a CaL process was the
2364 same for both models. Furthermore, the sensitivity study performed by Lasheras et al.
2365 [31] revealed that the uncertainty in the K-L model can affect CaL plant performance by
2366 up to 10%. As this can have a significant effect on estimation of overall process
2367 performance, further experimental tests are necessary to identify the required
2368 parameters.

2369 It is worth pointing out that lower operating temperature (600°C) of the carbonator in the
2370 CaL linked with the NGCC compared to studies reviewed in Section 5.1 (650°C), which
2371 assessed integration of the CFPP and the CaL process, results in slower carbonation
2372 reaction, hence larger units are required. Moreover, low CO₂ partial pressure in the
2373 NGCC flue gas makes the carbonation process more difficult, and thus the maximum
2374 CO₂ capture level of 86% in the carbonator was achieved. Although the carbonator
2375 temperature could be further lowered, favouring chemical equilibrium at expense of the
2376 reaction kinetics, the desired high-pressure steam temperature of 550-560°C [146]
2377 would not be achievable.

2378 Finally, although the operating temperatures of the carbonator and the calciner were
2379 found to be similar in all studies reviewed selection of several important parameters
2380 seem to be inconsistent (Table 8). Namely, some studies assume that the O₂ in the
2381 calciner fluidising gas is diluted with recycled CO₂, and its concentration varies from
2382 25%_{vol} [83; 146] to 80%_{vol} [132]. In addition, several studies claimed that no CO₂ recycle
2383 is required and 95%_{vol}-purity O₂ can be directly fed to the calciner [26; 32; 86]. Current
2384 pilot-plant testing activities were conducted with the O₂ concentration below 50%_{vol} [33;
2385 98; 100; 104]. Therefore, to limit the sorbent deterioration, further integration studies
2386 should include the CO₂ recycle to control the temperature in the calciner. Another
2387 important parameter is Ca:C ratio that has been assumed to be between 5–8.29 to
2388 reach the CO₂ capture levels in the carbonator up to 90% using non-pretreated sorbent.
2389 It needs to be highlighted that the pilot-plant tests reviewed in Section 3 claimed that to
2390 reach such reduction in the CO₂ emissions in the carbonator, the Ca:C ratio should be
2391 higher than 8-11.6 [98; 103; 107]. For this reason, in the studies where low Ca:C ratios

2392 were used to reach high CO₂ capture level in the carbonator, prediction of the process
2393 performance may be overly optimistic due to under-estimated solids looping rate, and
2394 thus heat requirement in the calciner. Moreover, the excess O₂ and the relative
2395 limestone make-up rate, which is represented using F_0/F_R ratio, were found to vary
2396 between 1.03–1.10 and 0.025–0.06, respectively. This implies the need for establishing
2397 baseline design parameters for the CaL process that would allow comparing process
2398 performance across analyses.

2399

2400 Table 8: Summary of modelling approaches and assumptions in investigating calcium looping integration to power plants

Reference	Carbonator assumptions		Calciner assumptions		Modelling approach for other system components		
	Model	Operating conditions	Model	Operating conditions	ASU	CCU	Secondary steam cycle
Shimizu et al. [28]	Semi-predictive model with KL hydrodynamics	T = 650°C Ca:C = 8.29 E _{carb} = 83%	Equilibrium	T = 950°C X _{calc} = 100%	Assumed w _{ASU} = 25.9 MJ/kmol-O ₂	Assumed w _{CCU} = 24.5 MJ/kmol-CO ₂	Assumed η _g = 42.6% _{HHV}
Yang et al. [16]	Average conversion w/o correction	T = 650°C Ca:C = 5 E _{carb} = 85%	Equilibrium	T = 900°C	Assumed w _{ASU} = 220 kWh/t-O ₂	Not considered	Thermodynamic model
Abanades et al. [39]	Average conversion w/o correction	T = 650°C E _{carb} = 75.2%	Equilibrium	T = 950°C X _{calc} = 100%	Estimated using process model	Estimated using process model	N/A
Martínez et al. [83]	Semi-predictive model with simple hydrodynamics	T = 650°C E _{carb} = 70-90% u ₀ = 6 m/s	Equilibrium	T = 950°C λ _{O2} = 1.05 X _{calc} = 100% y _{O2,fluidising gas} = 25% _{vol}	Assumed w _{ASU} = 160 kWh/t-O ₂	Assumed w _{CCU} = 100 kWh/t-CO ₂	Assumed η _g = 45%
Martínez et al. [148]	Semi-predictive model with simple hydrodynamics	T = 650°C E _{carb} = 89%	Equilibrium	T = 950°C E _{calc} = 100%	Not specified	Estimated using adiabatic compression model with η _a = 75%	Thermodynamic model
Martínez et al. [133]	Average conversion with correction	T = 650°C X _{carb} /X _{ave} = 0.8 E _{carb} = 90%	Equilibrium	T = 930°C X _{calc} = 100%	Assumed w _{ASU} = 220 kWh/t-O ₂	N/A	N/A
Romeo et al. [86]	Average conversion w/o correction	T = 650°C X _{carb} = 20% E _{carb} = 85%	Equilibrium	T = 875–950°C X _{calc} = 100% y _{O2,fluidising gas} = 95% _{vol}	Assumed w _{ASU} = 220 kWh/t-O ₂	N/A	Thermodynamic model
Lara et al. [200; 201]	Average conversion w/o correction	T = 650°C Ca:C = 5	Equilibrium	T = 950°C F ₀ /F _R = 0.025	Assumed w _{ASU} = 220 kWh/t-O ₂	Estimated using isentropic compression model with η _i = 80%	Thermodynamic model
Ströhle et al. [147], Lasheras et al. [31]	Average conversion w/o correction and Semi-predictive mode with K-L hydrodynamics	T = 650°C E _{carb} = 80% E _{SO2} = 99%	Equilibrium	T = 900°C λ _{O2} = 1.10 X _{coal} = 0.995	Assumed w _{ASU} = 184.8 kWh/t-O ₂	N/A	Assumed η _g = 50.3% _{LHV}

2401

2402 **Table 8 (cont): Summary of modelling approaches and assumptions in investigating calcium looping integration to power**
 2403 **plants**

Reference	Carbonator assumptions		Calciner assumptions		Modelling approach for other system components		
	Model	Operating conditions	Model	Operating conditions	ASU	CCU	Secondary steam cycle
Wang et al. [26; 32]	Equilibrium	T = 625°C Ca:C = 1.4 E _{carb} = 90% E _{SO2} = 100%	Equilibrium	T = 1000°C Y _{O2,fluidising gas} = 95% _{vol}	Assumed w _{ASU} = 200 kWh/t-O ₂	Assumed w _{ASU} = 119 kWh/t-CO ₂	Assumed η _g = 42% _{HHV}
Vorrias et al. [132]	Average conversion w/o correction	T = 650°C Ca:C = 7 E _{carb} = 90%	Equilibrium	T = 950°C F _O /F _{CO2} = 0.1 Y _{O2,fluidising gas} = 80% _{vol}	Estimated using process model	Estimated using process model	Thermodynamic model
Berstad et al. [146]	Average conversion with correction	T = 600°C X _{carb} /X _{ave} = 0.75 E _{carb} = 85–86%	Equilibrium	T = 950°C F _O /F _R = 0.06 λ _{O2} = 1.03 X _{calc} = 100% Y _{O2,fluidising gas} = 25% _{vol}	Assumed w _{ASU} = 200 kWh/t-O ₂	Estimated using polytrophic compression model with η _p = 75–80%	Thermodynamic model
Kunze et al. [131]	Average conversion w/o correction	T = 650°C X _{carb} = 0.2 E _{carb} = 90%	Equilibrium	T = 950°C X _{calc} = 95%	Assumed w _{ASU} = 28 kWh/t-O ₂	Assumed w _{ASU} = 83 kWh/t-CO ₂	N/A
Wang et al. [130]	Equilibrium	T = 600°C	Equilibrium	T = 900°C	Assumed w _{ASU} = 245 kWh/t-O ₂	Estimated using isentropic compression model with η _i = 75%	Thermodynamic model
Connel et al. [129]	Equilibrium	T = 700°C E _{carb} > 90%	Equilibrium	T > 875°C	N/A	N/A	N/A
Cormos and Cormos [128]	Equilibrium	T = 650 – 700°C	Equilibrium	T = 900 – 950°C	Assumed w _{ASU} = 225 kWh/t-O ₂	Estimated using process model	Thermodynamic model
Romano and Lozza [127; 210]	Equilibrium	T = 875 – 882°C X _{carb} = 0.5	Equilibrium	T = 1250	Estimated	Estimated using isentropic compression model with η _i = 89.5%	Thermodynamic model

2404

2405

2406 **6 THE FUTURE OF CALCIUM LOOPING IN POWER** 2407 **GENERATION SYSTEMS**

2408 In light of increasing environmental concerns, the power sector seems to be the first in
2409 line to be completely decarbonised by 2050. High reliance on coal, however, makes this
2410 a challenging task requiring implementation of CO₂ capture technologies in the existing
2411 coal-based power generation fleet. Unfortunately, conventional technologies, which
2412 utilise chemical sorbents and oxy-fuel combustion, result in a considerable drop in
2413 system efficiency, leading to an increase in the cost of electricity. The CaL process is
2414 regarded as a feasible alternative to conventional technologies because not only is it
2415 characterised by lower loss in power plant efficiency, but it is also capable of increasing
2416 the power output of the system.

2417 CaL process viability and performance have been widely investigated in bench- and
2418 pilot-scale facilities the size of which varies between 1 kW_{th} and 1.9 MW_{th}. The test
2419 campaigns reported in the open literature provide valuable insight into the process
2420 operation that can be used for process model development. Nevertheless, this review
2421 has shown that the available data were not detailed enough for any test facility to be
2422 useful for detailed process model validation. This is caused by, for example, the
2423 uncertainty associated with the solid looping rate measurements. To allow detailed
2424 process model validation, however, more detailed data should be reported for future
2425 tests.

2426 The CaL experimental trials have revealed that the actual CO₂ capture level can be
2427 close to that determined by equilibrium provided sufficient solids inventory of moderate
2428 conversion and looping rate are maintained. However, deterioration of the sorbent
2429 performance, triggered mainly by sintering and sulphation, requires relatively high
2430 make-up rates to reach the desired level of average sorbent conversion, which affects
2431 the economic performance of the system. Therefore, the further developments of the
2432 sorbent performance enhancement measures and/or novel sorbents experiencing lower
2433 performance deterioration need to be pursued in the near to mid-term timescale.

2434 To date, the predictions of process performance have been modelled with different
2435 levels of complexity. Five levels can be distinguished, which differ in application of the
2436 kinetic or equilibrium reactions, considering the concentration changes in the gas and
2437 solid phases and implementation of FB hydrodynamics. Importantly, the effect of
2438 sulphation on the sorbent activity and inert solids accumulation in the system were
2439 rarely included in the models available in the literature. Therefore, to improve the
2440 accuracy and reliability of the overall process performance prediction, future models
2441 should account for sorbent sulphation and ash accumulation.

2442 Application of the CaL plant to typical coal-based power generation systems was found
2443 to impose lower efficiency penalties (6–7% points), compared to conventional CO₂
2444 capture systems, proving the technology viability. Moreover, novel power generation
2445 systems that are based on the CaL process have been proposed, and reach net thermal
2446 efficiencies close to those of ultrasupercritical CFPPs without CO₂ capture. This implies
2447 that the CaL plant can serve as a base system for development of state-of-the-art power
2448 generation systems that could be implemented on a large scale in place of current
2449 technologies. Nevertheless, it is highlighted that the analyses performed to date used
2450 not only different CaL modelling approaches, but more importantly they employed
2451 different reference power plants and sets of CaL operating conditions. As this restricts
2452 the accuracy of process performance comparison across these analyses, the baseline
2453 reference models for the power plant and CaL plant need to be developed. In the near
2454 term, such baseline models would allow a reliable comparison of the process
2455 performances of the further analyses of the CaL process improvements.

2456

2457 **LIST OF ABBREVIATIONS**

AGR	Acid gas removal
ASU	Air separation unit
BFB	Bubbling fluidised bed
CaL	Calcium looping
CaRS-CO ₂	Calcium-based reaction separation for CO ₂
CCR	Carbonation-calcination reaction process
CCS	Carbon capture and storage

CCU	CO ₂ compression unit
CFB	Circulating fluidised bed
CFD	Computational fluid dynamics
CFPP	Coal-fired power plant
DFB	Dual fluidised bed
EB	Entrained bed
FGD	Flue gas desulphurisation unit
HEN	Heat exchanger networks
IFK	The Institute of Combustion and Power Plant Technology (Institut für Feuerungs-und Kraftwerkstechnik)
IGCC	Integrated-gasification combined cycle power plant
INCAR-CSIC	The Instituto Nacional del Carbón - Consejo Superior de Investigaciones Científicas
ITRI	The Industrial Technology Research Institute
K-L	Kunii and Levenspiel model
MB	Moving bed
MDEA	Methyldiethanolamine
MEA	Monoethanolamine
NGCC	Natural gas combined cycle power plant
OSCAR	The Ohio State carbonation ash reactivation process
PZ	Piperazine
RK	Rotary kiln
SER	Sorption-enhanced reforming process
SME	Sorption-enhanced methane steam reforming
TGA	Thermo-gravimetric analyser
ZECOMAG	Zero-emissions coal mixed technology with air gas turbine
ZECOMIX	Zero-emissions coal mixed technology

2458

2459 **NOMENCLATURE****Latin symbols**

A	Bed cross-section area	m ²
a_1	Fitting parameter in Li and Cai [133] correlation	-
a_2	Fitting parameter in Li and Cai [133] correlation	-
c_0	Freundlich isotherm characteristic	-
C_i	Concentration of species i	kmol/m ³
D	Diffusivity coefficient	m ² /s
d_b	Bubble diameter	m/s
E	Activation energy	J/kmol
E_{carb}	CO ₂ capture level in the carbonator	-
E_{calc}	Efficiency of the calciner	-
f	Extent of calcination or carbonation	-
F_0	CaCO ₃ makeup rate	kmol/s
f_1	Fitting parameter in Li and Cai [133] correlation	-
f_2	Fitting parameter in Li and Cai [133] correlation	-

f_a	Active fraction of particles	-
F_{CO_2}	CO ₂ flow rate in the flue gas	kmol/s
F_H	Sorbent rate diverted to the hydrator	kmol/s
F_R	CaO looping rate	kmol/s
h	CaCO ₃ layer thickness	nm
H_D	Height of the dense phase	m
k	Kinetic rate constant or sorbent deactivation constant or proportionality constant	1/s, m ³ /mol-s, m ⁴ /mol-s, -
K_{be}	Bubble and emulsion interchange coefficient	-
k_g	Mass transfer coefficient	m/s
N	Number of calcination/carbonation cycle	-
n	Sorbent sintering exponent or number of active sites in Langmuir-Hinshelwood mechanism	-
N_{Ca}	Mole inventory of CaO in the bed	kmol
M_i	Molar mass of species i	kg/kmol
P_{CO_2}	Partial pressure of CO ₂	atm
r	Reaction rate	kmol/m ³ s, 1/s
R	Particle radius	m
r_0	Mole fraction of particles that has never been calcined or initial grain radius	- or m
$r_{C/S}$	Molar ratio of carbon and sulphur in the fuel	-
Re	Reynolds number	-
R_g	Gas constant	J/kmolK
r_N	Mass fraction of particles that has undergone N carbonation/calcination cycles	-
r_i	Un-reacted radius of CaO grain	M
S	Particle surface area	m ² /m ³
Sc	Schmidt number	-
Sh	Sherwood number	-
T	Temperature	K
t^*	Actual residence time	s
u_0	Superficial gas velocity	m/s
u_b	Bubble rise velocity	m/s
u_b^*	Rising bubble gas velocity	m/s
v_{CO_2}	Volume fraction of CO ₂ in the gas phase	-
$V_{M,i}$	Molar volume of species i	m ³ /kmol
W_{CaO}	Mass inventory of CaO in the bed	kg
X	Sorbent conversion	-
y_{comb}	mass ratio between fuel going to the main combustor and total fuel into the plant	-
Greek symbols		
δ	Volume of bubbles per unit bed volume	-
ε	Porosity of sorbent particle or solid fraction in the reactor	-
θ	Fraction of the active sites	-

ρ_i	Mass density of species i	kg/m ³
τ	Average residence time	s
φ_e	Effectivity factor	-
Φ_s	Particle sphericity	-
Ψ	Sorbent pore structural parameter	-

Superscripts

H Hydrated sorbent

Subscripts

0 Initial conditions

ave, max Refer to maximum average sorbent conversion

b Refer to bubble zone

$calc$ Variable related to calciner operating conditions or stream leaving calciner

$carb$ Variable related to carbonator operating conditions or stream leaving carbonator

e Refer to emulsion zone

eq Equilibrium conditions

mf Refer to minimum fluidising conditions

max Refer to maximum sorbent conversion

r Refer to residual sorbent conversion

s Refer to intrinsic kinetic constant

2460

2461 **REFERENCES**

2462 [1] European Commission (2010), *Communication from the Commission to the*
 2463 *European Parliament, the Council, the European Economic and Social Committee*
 2464 *and the Committee of the Regions, International climate policy post-Copenhagen:*
 2465 *Acting now to reinvigorate global action on climate change*, COM(2010) 86,
 2466 Commission of the European Communities, Brussels, Belgium.

2467 [2] European Commission (2014), *Communication from the Commission to the*
 2468 *European Parliament, the Council, the European Economic and Social Committee*
 2469 *and the Committee of the Regions, A policy framework for climate and energy in the*
 2470 *period from 2020 to 2030*, COM(2014) 15, European Commission, Brussels,
 2471 Belgium.

2472 [3] European Council (2014), *European Council 23/24 October 2014 – Conclusions*,
 2473 EUCO gv 169/14 CO EUR 13 CONCL 5, European Commission, Brussels,
 2474 Belgium.

2475 [4] European Commission (2011), *Communication from the Commission to the*
 2476 *European Parliament, the Council, the European Economic and Social Committee*
 2477 *of the Regions - Energy Roadmap 2050*, COM(2011) 885/2, European
 2478 Commission, Brussels, Belgium.

- 2479 [5] UNEP (2012), *The Emissions Gap Report 2012*, United Nations Environment
2480 Programme (UNEP), Nairobi, Kenya.
- 2481 [6] IEA (2013), *Tracking Clean Energy Progress 2013. IEA Input to the Clean Energy*
2482 *Ministerial*, IEA Publications, Paris, France.
- 2483 [7] IEA (2010), *Power generation from coal: Measuring and reporting efficiency*
2484 *performance and CO₂ emissions*, IEA Publications, Paris, France.
- 2485 [8] EIA (2011), *International Energy Outlook 2011*, DOE/EIA-0484(2011), U.S.
2486 Energy Information Administration, Washington, USA.
- 2487 [9] IEA (2013), *Technology Roadmap: Carbon capture and storage*, IEA Publications,
2488 Paris, France.
- 2489 [10] Stéphenne, K. (2014), "Start-up of world's first commercial post-combustion coal
2490 fired ccs project: Contribution of Shell CANSOLV to Saskpower Boundary Dam
2491 ICCS project", in Dixon T., Twining S. and Herzog H. (eds.), *12th International*
2492 *Conference on Greenhouse Gas Control Technologies, GHGT 2014*, vol. 63, 5-9
2493 October 2014, Austin, TX, USA, pp. 6106.
- 2494 [11] Rodríguez, N., Alonso, M. and Abanades, J. C. (2010), "Average activity of CaO
2495 particles in a calcium looping system", *Chemical Engineering Journal*, vol. 156, no.
2496 2, pp. 388-394.
- 2497 [12] Bhowan, A. S. and Freeman, B. C. (2011), "Analysis and status of post-
2498 combustion carbon dioxide capture technologies", *Environmental Science and*
2499 *Technology*, vol. 45, no. 20, pp. 8624-8632.
- 2500 [13] Blamey, J., Anthony, E., Wang, J. and Fennell, P. (2010), "The calcium looping
2501 cycle for large-scale CO₂ capture", *Progress in Energy and Combustion Science*,
2502 vol. 36, no. 2, pp. 260-279.
- 2503 [14] Dean, C. C., Blamey, J., Florin, N. H., Al-Jeboori, M. J. and Fennell, P. S. (2011),
2504 "The calcium looping cycle for CO₂ capture from power generation, cement
2505 manufacture and hydrogen production", *Chemical Engineering Research and*
2506 *Design*, , no. 89, pp. 836-855.
- 2507 [15] Boot-Handford, M. E., Abanades, J. C., Anthony, E. J., Blunt, M. J., Brandani, S.,
2508 Mac Dowell, N., Fernandez, J. R., Ferrari, M. C., Gross, R., Hallett, J. P.,
2509 Haszeldine, R. S., Heptonstall, P., Lyngfelt, A., Makuch, Z., Mangano, E., Porter, R.
2510 T. J., Pourkashanian, M., Rochelle, G. T., Shah, N., Yao, J. G. and Fennell, P. S.
2511 (2014), "Carbon capture and storage update", *Energy & Environmental Science*, no.
2512 7, pp. 130-189.

- 2513 [16] Yang, Y., Zhai, R., Duan, L., Kavosh, M., Patchigolla, K. and Oakey, J. (2010),
2514 "Integration and evaluation of a power plant with a CaO-based CO₂ capture
2515 system", *International Journal of Greenhouse Gas Control*, vol. 4, no. 4, pp. 603-
2516 612.
- 2517 [17] Xu, G., Jin, H. G., Yang, Y. P., Xu, Y. J., Lin, H. and Duan, L. (2010), "A
2518 comprehensive techno-economic analysis method for power generation systems
2519 with CO₂ capture", *International Journal of Energy Research*, vol. 34, no. 4, pp.
2520 321-332.
- 2521 [18] Goto, K., Yogo, K. and Higashii, T. (2013), "A review of efficiency penalty in a
2522 coal-fired power plant with post-combustion CO₂ capture", *Applied Energy*, vol. 111,
2523 pp. 710-720.
- 2524 [19] Stanmore, B. R. and Gilot, P. (2005), "Review—calcination and carbonation of
2525 limestone during thermal cycling for CO₂ sequestration", *Fuel Processing
2526 Technology*, vol. 86, no. 16, pp. 1707-1743.
- 2527 [20] Harrison, D. P. (2008), "Sorption-Enhanced Hydrogen Production: A Review",
2528 *Industrial & Engineering Chemistry Research*, vol. 47, no. 17, pp. 6486–6501.
- 2529 [21] Florin, N. H. and Harris, A. T. (2008), "Enhanced hydrogen production from
2530 biomass with in situ carbon dioxide capture using calcium oxide sorbents",
2531 *Chemical Engineering Science*, vol. 63, no. 2, pp. 287-316.
- 2532 [22] Anthony, E. J. (2011), "Ca looping technology: Current status, developments and
2533 future directions", *Greenhouse Gases: Science and Technology*, vol. 1, no. 1, pp.
2534 36-47.
- 2535 [23] Liu, W., An, H., Qin, C., Yin, J., Wang, G., Feng, B. and Xu, M. (2012),
2536 "Performance enhancement of calcium oxide sorbents for cyclic CO₂ capture-a
2537 review", *Energy and Fuels*, vol. 26, no. 5, pp. 2751-2767.
- 2538 [24] Kierzkowska, A. M., Pacciani, R. and Müller, C. R. (2013), "CaO-based CO₂
2539 sorbents: From fundamentals to the development of new, highly effective
2540 materials", *ChemSusChem*, vol. 6, no. 7, pp. 1130-1148.
- 2541 [25] Romano, M. C., Martínez, I., Murillo, R., Arstad, B., Blom, R., Ozcan, D. C., Ahn,
2542 H. and Brandani, S. (2013), "Process simulation of Ca-looping processes: Review
2543 and guidelines", *11th International Conference on Greenhouse Gas Control
2544 Technologies, GHGT 2012*, Vol. 37, 18-22 November 2012, Kyoto, Japan, pp. 142.
- 2545 [26] Wang, W., Ramkumar, S. and Fan, L. (2013), "Energy penalty of CO₂ capture for
2546 the Carbonation–Calcination Reaction (CCR) Process: Parametric effects and
2547 comparisons with alternative processes", *Fuel*, vol. 104, pp. 561-574.

- 2548 [27] Hirama, T., Hosoda, H., Kitano, K. and Shimizu, T. (1996), *Method of separating*
2549 *carbon dioxide from carbon dioxide containing gas and combustion apparatus*
2550 *having function to separate carbon dioxide from the combustion gas*, UK Patent
2551 2291051A.
- 2552 [28] Shimizu, T., Hirama, T., Hosoda, H., Kitano, K., Inagaki, M. and Tejima, K.
2553 (1999), "A Twin Fluid-Bed Reactor for Removal of CO₂ from Combustion
2554 Processes", *Chemical Engineering Research and Design*, vol. 77, no. 1, pp. 62-68.
- 2555 [29] Hughes, R. W., Lu, D. Y., Anthony, E. J. and Macchi, A. (2005), "Design, process
2556 simulation and construction of an atmospheric dual fluidized bed combustion
2557 system for in situ CO₂ capture using high-temperature sorbents", *Fuel Processing*
2558 *Technology*, vol. 86, no. 14–15, pp. 1523-1531.
- 2559 [30] Alonso, M., Rodríguez, N., Grasa, G. and Abanades, J. C. (2009), "Modelling of
2560 a fluidized bed carbonator reactor to capture CO₂ from a combustion flue gas",
2561 *Chemical Engineering Science*, vol. 64, no. 5, pp. 883-891.
- 2562 [31] Lasheras, A., Ströhle, J., Galloy, A. and Epple, B. (2011), "Carbonate looping
2563 process simulation using a 1D fluidized bed model for the carbonator", *International*
2564 *Journal of Greenhouse Gas Control*, vol. 5, no. 4, pp. 686-693.
- 2565 [32] Wang, W., Ramkumar, S., Wong, D. and Fan, L. (2012), "Simulations and
2566 process analysis of the carbonation–calcination reaction process with intermediate
2567 hydration", *Fuel*, vol. 92, no. 1, pp. 94-106.
- 2568 [33] Lu, D. Y., Hughes, R. W. and Anthony, E. J. (2008), "Ca-based sorbent looping
2569 combustion for CO₂ capture in pilot-scale dual fluidized beds", *Fuel Processing*
2570 *Technology*, vol. 89, no. 12, pp. 1386-1395.
- 2571 [34] Valverde, J. M. (2013), "A model on the CaO multicyclic conversion in the Ca-
2572 looping process", *Chemical Engineering Journal*, vol. 228, pp. 1195-1206.
- 2573 [35] Yin, J., Qui, C., Feng, B., Ge, L., Luo, C., Liu, W. and An, H. (2014), "Calcium
2574 Looping for CO₂ Capture at a Constant High Temperature", *Energy & Fuels*, vol. 28,
2575 no. 1, pp. 307-318.
- 2576 [36] Baker, E. H. (1962), "The calcium oxide-carbon dioxide system in the pressure
2577 range 1-300 atmospheres", *Journal of the Chemical Society*, pp. 464-470.
- 2578 [37] Martínez, I., Murillo, R., Grasa, G. and Abanades, J. C. (2011), "Integration of a
2579 Ca-looping system for CO₂ capture in an existing power plant", *Energy Procedia*,
2580 vol. 4, pp. 1699-1706.

- 2581 [38] Valverde, J., Sanchez-Jimenez, P. E., Perejon, A. and Perez-Maqueda, L. A.
2582 (2013), "CO₂ multicyclic capture of pretreated/doped CaO in the Ca-looping
2583 process. Theory and experiments", *Physical Chemistry Chemical Physics*, vol. 15,
2584 pp. 11775-11793.
- 2585 [39] Abanades, J. C., Anthony, E. J., Wang, J. and Oakey, J. E. (2005), "Fluidized
2586 Bed Combustion Systems Integrating CO₂ Capture with CaO", *Environmental
2587 Science and Technology*, vol. 39, no. 8, pp. 2861–2866.
- 2588 [40] Rodriguez, N., Alonso, M., Grasa, G. and Abanades, J. C. (2008), "Heat
2589 requirements in a calciner of CaCO₃ integrated in a CO₂ capture system using
2590 CaO", *Chemical Engineering Journal*, vol. 138, no. 1–3, pp. 148-154.
- 2591 [41] Manovic, V. and Anthony, E. J. (2009), "Improvement of CaO-based sorbent
2592 performance for CO₂ looping cycles", *Thermal Science*, vol. 13, no. 1, pp. 89-104.
- 2593 [42] Abanades, C. J. and Alvarez, D. (2003), "Conversion limits in the reaction of CO₂
2594 with lime", *Energy & Fuels*, vol. 17, pp. 308-315.
- 2595 [43] Borgwardt, R. H. (1989), "Calcium oxide sintering in atmospheres containing
2596 water and carbon dioxide", *Industrial and Engineering Chemistry Research*, vol. 28,
2597 no. 4, pp. 493-500.
- 2598 [44] Zhen-Shan, L. and Ning-Sheng, C. (2008), "Process analysis of CO₂ capture
2599 from flue gas using carbonation/calcination cycles", *Environmental and Energy
2600 Engineering*, vol. 54, no. 7, pp. 1912-1925.
- 2601 [45] García-Labiano, F., Rufas, A., De Diego, L. F., Obras-Loscertales, M. D. L.,
2602 Gayán, P., Abad, A. and Adánez, J. (2011), "Calcium-based sorbents behaviour
2603 during sulphation at oxy-fuel fluidised bed combustion conditions", *Fuel*, vol. 90, no.
2604 10, pp. 3100-3108.
- 2605 [46] Duke, M. C., Ladewig, B., Smart, S., Rudolph, V. and Da Costa, J. C. D. (2010),
2606 "Assessment of post-combustion carbon capture technologies for power
2607 generation", *Frontiers of Chemical Engineering in China*, vol. 4, no. 2, pp. 184-195.
- 2608 [47] Maroto-Valer, M., (2010), *Developments and Innovation in Carbon Dioxide
2609 (CO₂) Capture and Storage Technology, Volume 1 - Carbon Dioxide (CO₂) Capture,
2610 Transport and Industrial Applications*, Woodhead Publishing, Cambridge, UK.
- 2611 [48] Rackley, S.A., (2010), *Carbon Capture and Storage*, Elsevier, Burlington, USA.
- 2612 [49] Zhao, B. and Su, Y. (2014), "Process effect of microalgal-carbon dioxide fixation
2613 and biomass production: A review", *Renewable and Sustainable Energy Reviews*,
2614 vol. 31, pp. 121-132.

- 2615 [50] Kheshgi, H. S., Thomann, H., Bhore, N. A., Hirsch, R. B., Parker, M. E. and
2616 Teletzke, G. F. (2012), "Perspectives on CCS cost and economics", *SPE*
2617 *Economics and Management*, vol. 4, no. 1, pp. 24-31.
- 2618 [51] Renner, M. (2014), "Carbon prices and CCS investment: A comparative study
2619 between the European Union and China", *Energy Policy*, vol. 75, pp. 327-340.
- 2620 [52] CSIRO (2012), *Assessing Post-Combustion Capture for Coal-fired Power*
2621 *Stations in Asia-Pacific Partnership Countries*, EP116217, CSIRO Advanced Coal
2622 Technology, Newcastle, NW, USA.
- 2623 [53] Rao, A. B. and Rubin, E. S. (2002), "A Technical, Economic, and Environmental
2624 Assessment of Amine-Based CO₂ Capture Technology for Power Plant
2625 Greenhouse Gas Control", *Environmental Science and Technology*, vol. 36, no. 20,
2626 pp. 4467-4475.
- 2627 [54] Bottoms, R.R., (1930), *Process for separating acidic gases*, U.S. Patent
2628 1783901, available online at: <http://bit.ly/1GIWnoS> (accessed 30/05/2015).
- 2629 [55] Kohl, L. and Nielsen, R. B. (1997), *Gas purification*, 5th ed, Gulf Publishing
2630 Company, Huston, Texas, USA.
- 2631 [56] Öi, L. E. (2010), "CO₂ removal by absorption: Challenges in modelling",
2632 *Mathematical and Computer Modelling of Dynamical Systems*, vol. 16, no. 6, pp.
2633 511-533.
- 2634 [57] Pires, J. C. M., Martins, F. G., Alvim-Ferraz, M. C. M. and Simões, M. (2011),
2635 "Recent developments on carbon capture and storage: An overview", *Chemical*
2636 *Engineering Research and Design*, vol. 89, no. 9, pp. 1446-1460.
- 2637 [58] Rubin, E. S., Mantripragada, H., Marks, A., Versteeg, P. and Kitchin, J. (2012),
2638 "The outlook for improved carbon capture technology", *Progress in Energy and*
2639 *Combustion Science*, vol. 38, no. 5, pp. 630-671.
- 2640 [59] Folger, P. (2013), *Carbon Capture: A Technology Assessment*, R41325,
2641 Congressional Research Service, available online at: <http://bit.ly/1esPfhA>
2642 (accessed 30/05/2015).
- 2643 [60] Hanak, D. P., Biliyok, C., Yeung, H. and Bialecki, R. (2014), "Heat integration
2644 and exergy analysis for a high ash supercritical coal-fired power plant integrated
2645 with a post-combustion carbon capture process", *Fuel*, vol. 134, pp. 126-139.
- 2646 [61] Kvamsdal, H. M., Romano, M. C., van der Ham, L., Bonalumi, D., van Os, P. and
2647 Goetheer, E. (2014), "Energetic evaluation of a power plant integrated with a

- 2648 piperazine-based CO₂ capture process", *International Journal of Greenhouse Gas*
2649 *Control*, vol. 28, no. 1, pp. 343-355.
- 2650 [62] Van Wagener, D. H., Liebenthal, U., Plaza, J. M., Kather, A. and Rochelle, G. T.
2651 (2014), "Maximizing coal-fired power plant efficiency with integration of amine-
2652 based CO₂ capture in greenfield and retrofit scenarios", *Energy*, vol. 72, pp. 824-
2653 831.
- 2654 [63] Strube, R. and Manfrida, G. (2011), "CO₂ capture in coal-fired power plants -
2655 Impact on plant performance", *International Journal of Greenhouse Gas Control*,
2656 vol. 5, no. 4, pp. 710-726.
- 2657 [64] Shao, R. and Stangeland, A. (2009), *Amines Used in CO₂ Capture - Health and*
2658 *Environmental Impacts*, The Bellona Foundation, available at: <http://bit.ly/1fpznvO>
2659 (accessed 30/05/2015).
- 2660 [65] Thitakamol, B., Veawab, A. and Aroonwilas, A. (2007), "Environmental impacts
2661 of absorption-based CO₂ capture unit for post-combustion treatment of flue gas
2662 from coal-fired power plant", *International Journal of Greenhouse Gas Control*, vol.
2663 1, no. 3, pp. 318-342.
- 2664 [66] Veltman, K., Singh, B. and Hertwich, E. G. (2010), "Human and Environmental
2665 Impact Assessment of Postcombustion CO₂ Capture Focusing on Emissions from
2666 Amine-Based Scrubbing Solvents to Air", *Environmental Science and Technology*,
2667 vol. 44, no. 4, pp. 1496-1502.
- 2668 [67] Bai, H. and Yeh, A. C. (1997), "Removal of CO₂ Greenhouse Gas by Ammonia
2669 Scrubbing", *Industrial & Engineering Chemistry Research*, vol. 36, no. 6, pp. 2490-
2670 2493.
- 2671 [68] Brown, T., Perry, C. C. and Manthey, B. (2009), *Pleasant Prairie carbon capture*
2672 *demonstration project*, Progress report, 8th October 2009, Alstom, Wisconsin.
- 2673 [69] Telikapalli, V., Kozak, F., Francois, J., Sherrick, B., Black, J., Muraskin, D., Cage,
2674 M., Hammond, M. and Spitznogle, G. (2011), "CCS with the Alstom chilled
2675 ammonia process development program—Field pilot results", *Energy Procedia*, vol.
2676 4, pp. 273-281.
- 2677 [70] Yu, H., Morgan, S., Allport, A., Cottrell, A., Do, T., McGregor, J., Wardhaugh, L.
2678 and Feron, P. (2011), "Results from trialling aqueous NH₃ based post-combustion
2679 capture in a pilot plant at Munmorah power station: Absorption", *Chemical*
2680 *Engineering Research and Design*, vol. 89, no. 8, pp. 1204-1215.

- 2681 [71] Ciferno, J. P., DiPietro, P. and Tarka, T. (2005), *An economic scoping study for*
2682 *CO₂ capture using aqueous ammonia*, National Energy Technology Laboratory;
2683 Advanced Resources International; Energetics Incorporated.
- 2684 [72] Gal, E. (2006), *Chilled-ammonia Post Combustion CO₂ Capture System–*
2685 *Laboratory and Economic Evaluation Results*, 1012797, EPRI, Palo Alto, CA, USA.
- 2686 [73] Romeo, L. M., Espatolero, S. and Bolea, I. (2008), "Designing a supercritical
2687 steam cycle to integrate the energy requirements of CO₂ amine scrubbing",
2688 *International Journal of Greenhouse Gas Control*, vol. 2, no. 4, pp. 563-570.
- 2689 [74] Wang, M., Lawal, A., Stephenson, P., Sidders, J. and Ramshaw, C. (2011),
2690 "Post-combustion CO₂ capture with chemical absorption: A state-of-the-art review",
2691 *Chemical Engineering Research and Design*, vol. 89, no. 9, pp. 1609-1624.
- 2692 [75] Resnik, K. P., Yeh, J. T. and Pennline, H. W. (2004), "Aqua ammonia process for
2693 simultaneous removal of CO₂, SO₂ and NO_x", *International Journal of*
2694 *Environmental Technology and Management*, vol. 4, no. 1-2, pp. 89-104.
- 2695 [76] Shakerian, F., Kim, K., Szulejko, J. E. and Park, J. (2015), "A comparative review
2696 between amines and ammonia as sorptive media for post-combustion CO₂
2697 capture", *Applied Energy*, vol. 148, pp. 10-22.
- 2698 [77] Zhao, B., Su, Y., Tao, W., Li, L. i. and Peng, Y. (2012), "Post-combustion CO₂
2699 capture by aqueous ammonia: A state-of-the-art review", *International Journal of*
2700 *Greenhouse Gas Control*, vol. 9, pp. 355-371.
- 2701 [78] Zhao, M., Minett, A. I. and Harris, A. T. (2013), "A review of techno-economic
2702 models for the retrofitting of conventional pulverised-coal power plants for post-
2703 combustion capture (PCC) of CO₂", *Energy and Environmental Science*, vol. 6, no.
2704 1, pp. 25-40.
- 2705 [79] Sutton, B. (2015), "Statement from Peabody Energy on the Department Of
2706 Energy's decision to suspend FutureGen", *Peabody Energy*, available online at:
2707 <http://bit.ly/1LsNh3d> (18/03/2015).
- 2708 [80] Marshall, C. and Quiñones, M. (2015), "Clean Coal Power Plant Killed, Again",
2709 *Scientific American*, available online at: <http://bit.ly/1DAqa2i> (18/03/2015).
- 2710 [81] Soundararajan, R. and Gundersen, T. (2013), "Coal based power plants using
2711 oxy-combustion for CO₂ capture: Pressurized coal combustion to reduce capture
2712 penalty", *Applied Thermal Engineering*, vol. 61, no. 1, pp. 115-122.
- 2713 [82] Soundararajan, R., Gundersen, T. and Ditaranto, M., (2014), *Oxy-combustion*
2714 *coal based power plants: Study of operating pressure, oxygen purity and*

- 2715 *downstream purification parameters*, Italian Association of Chemical Engineering -
2716 AIDIC.
- 2717 [83] Martínez, I., Murillo, R., Grasa, G. and Carlos Abanades, J. (2011), "Integration
2718 of a Ca looping system for CO₂ capture in existing power plants", *AIChE Journal*,
2719 vol. 57, no. 9, pp. 2599-2607.
- 2720 [84] Romano, M. C. (2012), "Modeling the carbonator of a Ca-looping process for
2721 CO₂ capture from power plant flue gas", *Chemical Engineering Science*, vol. 69, no.
2722 1, pp. 257-269.
- 2723 [85] Markusson, N. (2012), "The politics of FGD deployment in the UK (1980s-2009)",
2724 *Case study for the project CCS: Realising the potential*, University of Edinburgh,
2725 Edinburgh, Scotland.
- 2726 [86] Romeo, L. M., Abanades, J. C., Escosa, J. M., Paño, J., Giménez, A., Sánchez-
2727 Biezma, A. and Ballesteros, J. C. (2008), "Oxyfuel carbonation/calcination cycle for
2728 low cost CO₂ capture in existing power plants", *Energy Conversion and*
2729 *Management*, vol. 49, no. 10, pp. 2809-2814.
- 2730 [87] Abanades, J. C., Grasa, G., Alonso, M., Rodriguez, N., Anthony, E. J. and
2731 Romeo, L. M. (2007), "Cost structure of a postcombustion CO₂ capture system
2732 using CaO", *Environmental Science and Technology*, vol. 41, no. 15, pp. 5523-
2733 5527.
- 2734 [88] Cormos, C. C. (2014), "Economic evaluations of coal-based combustion and
2735 gasification power plants with post-combustion CO₂ capture using calcium looping
2736 cycle", *Energy*, vol. 78, pp. 665-673.
- 2737 [89] Cormos, C. C. (2015), "Assessment of chemical absorption/adsorption for post-
2738 combustion CO₂ capture from Natural Gas Combined Cycle (NGCC) power plants",
2739 *Applied Thermal Engineering*, vol. 82, pp. 120-128.
- 2740 [90] Huang, C., Hsu, H., Liu, W., Cheng, J., Chen, W., Wen, T. and Chen, W. (2011),
2741 "Development of post-combustion CO₂ capture with CaO/CaCO₃ looping in a bench
2742 scale plant", *Energy Procedia*, vol. 4, pp. 1268-1275.
- 2743 [91] Chang, M. H., Huang, C. M., Liu, W. H., Chen, W. C., Cheng, J. Y., Chen, W.,
2744 Wen, T. W., Ouyang, S., Shen, C. H. and Hsu, H. W. (2013), "Design and
2745 Experimental Investigation of Calcium Looping Process for 3-kW_{th} and 1.9-MW_{th}
2746 Facilities", *Chemical Engineering and Technology*, vol. 36, no. 9, pp. 1525-1532.
- 2747 [92] CCSA (2013), "Taiwan inaugurates advanced carbon capture plant", *CCSA*
2748 *Weekly Newsletter*, vol. 212, no. 2, pp. 4.

- 2749 [93] Rodríguez, N., Alonso, M. and Abanades, J. C. (2011), "Experimental
2750 investigation of a circulating fluidized-bed reactor to capture CO₂ with CaO", *AIChE*
2751 *Journal*, vol. 57, no. 5, pp. 1356-1366.
- 2752 [94] Alonso, M., Rodríguez, N., González, B., Grasa, G., Murillo, R. and Abanades, J.
2753 C. (2010), "Carbon dioxide capture from combustion flue gases with a calcium
2754 oxide chemical loop. Experimental results and process development", *International*
2755 *Journal of Greenhouse Gas Control*, vol. 4, no. 2, pp. 167-173.
- 2756 [95] Sánchez-Biezma, A., Ballesteros, J. C., Diaz, L., de Zárraga, E., Álvarez, F. J.,
2757 López, J., Arias, B., Grasa, G. and Abanades, J. C. (2011), "Postcombustion CO₂
2758 capture with CaO. Status of the technology and next steps towards large scale
2759 demonstration", *Energy Procedia*, vol. 4, pp. 852-859.
- 2760 [96] Arias, B., Diego, M. E., Abanades, J. C., Lorenzo, M., Diaz, L., Martínez, D.,
2761 Alvarez, J. and Sánchez-Biezma, A. (2013), "Demonstration of steady state CO₂
2762 capture in a 1.7MW_{th} calcium looping pilot", *International Journal of Greenhouse*
2763 *Gas Control*, vol. 18, pp. 237-245.
- 2764 [97] Sánchez-Biezma, A., Paniagua, J., Diaz, L., Lorenzo, M., Alvarez, J., Martínez,
2765 D., Arias, B., Diego, M. E. and Abanades, J. C. (2013), "Testing postcombustion
2766 CO₂ capture with CaO in a 1.7 MW_t pilot facility", *Energy Procedia*, vol. 37, pp. 1-8.
- 2767 [98] Ströhle, J., Junk, M., Kremer, J., Galloy, A. and Epple, B. (2014), "Carbonate
2768 looping experiments in a 1 MW_{th} pilot plant and model validation", *Fuel*, vol. 127,
2769 pp. 13-22.
- 2770 [99] Bates, L. (2008), "Screw conveyors", in McGlinchey, D. (ed.) *Bulk solids*
2771 *handling: equipment selection and operation*, 1st ed, Blackwell Publishing Ltd, UK,
2772 pp. 197-220.
- 2773 [100] Rodríguez, N., Alonso, M., Abanades, J. C., Charitos, A., Hawthorne, C.,
2774 Scheffknecht, G., Lu, D. Y. and Anthony, E. J. (2011), "Comparison of experimental
2775 results from three dual fluidized bed test facilities capturing CO₂ with CaO", *Energy*
2776 *Procedia*, vol. 4, pp. 393-401.
- 2777 [101] Charitos, A., Hawthorne, C., Bidwe, A. R., Korovesis, L., Schuster, A. and
2778 Scheffknecht, G. (2010), "Hydrodynamic analysis of a 10 kW_{th} Calcium Looping
2779 Dual Fluidized Bed for post-combustion CO₂ capture", *Powder Technology*, vol.
2780 200, no. 3, pp. 117-127.
- 2781 [102] Dieter, H., Bidwe, A. R., Varela-Duelli, G., Charitos, A., Hawthorne, C. and
2782 Scheffknecht, G. (2014), "Development of the calcium looping CO₂ capture
2783 technology from lab to pilot scale at IFK, University of Stuttgart", *Fuel*, vol. 127, pp.
2784 23-37.

- 2785 [103] Charitos, A., Hawthorne, C., Bidwe, A. R., Sivalingam, S., Schuster, A.,
2786 Spliethoff, H. and Scheffknecht, G. (2010), "Parametric investigation of the calcium
2787 looping process for CO₂ capture in a 10 kW_{th} dual fluidized bed", *International*
2788 *Journal of Greenhouse Gas Control*, vol. 4, no. 5, pp. 776-784.
- 2789 [104] Dieter, H., Hawthorne, C., Zieba, M. and Scheffknecht, G. (2013), "Progress in
2790 Calcium Looping Post Combustion CO₂ Capture: Successful Pilot Scale
2791 Demonstration", *Energy Procedia*, vol. 37, pp. 48-56.
- 2792 [105] Hawthorne, C., Dieter, H., Bidwe, A., Schuster, A., Scheffknecht, G.,
2793 Unterberger, S. and Käß, M. (2011), "CO₂ capture with CaO in a 200 kW_{th} dual
2794 fluidized bed pilot plant", *Energy Procedia*, vol. 4, pp. 441-448.
- 2795 [106] Dieter, H. (2012), "Design concepts, operating experiences and experimental
2796 results of the 200 kW_{th} calcium-looping pilot plant", *2nd International Workshop on*
2797 *Oxy-FBC Technology*, 28-29 June, Stuttgart, available at: <http://bit.ly/1aqVqok>
2798 (30/05/2015).
- 2799 [107] Varela, G., Charitos, A., Diego, M. E., Stavroulakis, E., Dieter, H. and
2800 Scheffknecht, G. (2015), "Investigations at a 10kW_{th} calcium looping dual fluidized
2801 bed facility: Limestone calcination and CO₂ capture under high CO₂ and water
2802 vapor atmosphere", *International Journal of Greenhouse Gas Control*, vol. 33, pp.
2803 103-112.
- 2804 [108] Ghosh-Dastidar, A. and Mahuli, S. (1998), *Calcium carbonate sorbent*
2805 *and methods of making and using same*, US Patent 5779464.
- 2806 [109] Mahuli, S. and Agnihotri, R. (2001), *Suspension carbonation process fo reaction*
2807 *of partially utilized sorbent*, US Patent 6309996 B1.
- 2808 [110] Gupta, H., Thomas, T. J., Park, A. A., Iyer, M. V., Gupta, P., Agnihotri, R.,
2809 Jadhav, R. A., Walker, H. W., Weavers, L. K., Butalia, T. and Fan, L. -. (2007),
2810 "Pilot-scale demonstration of the OSCAR process for high-temperature
2811 multipollutant control of coal combustion flue gas, using carbonated fly ash and
2812 mesoporous calcium carbonate", *Industrial and Engineering Chemistry Research*,
2813 vol. 46, no. 14, pp. 5051-5060.
- 2814 [111] Fan, L., Gupta, H. and Iyer, M. V. (2008), *Separation of carbon dioxide (CO₂)*
2815 *from gas mixtures by calcium based reaction reparation (CaRS-CO₂) process*, US
2816 patent 0233029.
- 2817 [112] Wang, W., Ramkumar, S., Li, S., Wong, D., Iyer, M., Sakadjian, B. B., Statnick,
2818 R. M. and Fan, L. (2010), "Subpilot demonstration of the carbonation-calcination
2819 reaction (CCR) process: High-temperature CO₂ and sulfur capture from coal-fired

- 2820 power plants", *Industrial and Engineering Chemistry Research*, vol. 49, no. 11, pp.
2821 5094-5101.
- 2822 [113] Symonds, R. T., Lu, D. Y., Hughes, R. W., Anthony, E. J. and Macchi, A.
2823 (2009), "CO₂ capture from simulated syngas via cyclic carbonation/calcination for a
2824 naturally occurring limestone: Pilot-plant testing", *Industrial and Engineering
2825 Chemistry Research*, vol. 48, no. 18, pp. 8431-8440.
- 2826 [114] Cotton, A., Finney, K. N., Patchigolla, K., Eatwell-Hall, R. E. A., Oakey, J. E.,
2827 Swithenbank, J. and Sharifi, V. (2014), "Quantification of trace element emissions
2828 from low-carbon emission energy sources: (I) Ca-looping cycle for post-combustion
2829 CO₂ capture and (II) fixed bed, air blown down-draft gasifier", *Chemical
2830 Engineering Science*, vol. 107, pp. 13-29.
- 2831 [115] Cotton, A. M. (2013), *Engineering scale-up and environmental effects of the
2832 calcium looping cycle for post-combustion CO₂ capture* (PhD thesis), Cranfield
2833 University, Cranfield, UK.
- 2834 [116] Kavosh, M. (2011), *Process engineering and development of post-combustion
2835 CO₂ separation from fuels using limestone in CaO-looping cycle* (PhD thesis),
2836 Cranfield University, Cranfield.
- 2837 [117] Geldart, D. (1973), "Types of gas fluidization", *Powder Technology*, vol. 7, no.
2838 5, pp. 285-292.
- 2839 [118] Fang, F., Li, Z. S. and Cai, N. S. (2009), "Continuous CO₂ capture from flue
2840 gases using a dual fluidized bed reactor with calcium-based sorbent", *Industrial and
2841 Engineering Chemistry Research*, vol. 48, no. 24, pp. 11140-11147.
- 2842 [119] Aigner, I., Pfeifer, C. and Hofbauer, H. (2011), "Co-gasification of coal and
2843 wood in a dual fluidized bed gasifier", *Fuel*, vol. 90, no. 7, pp. 2404-2412.
- 2844 [120] Pfeifer, C., Schmid, J. C., Pröll, T. and Hofbauer, H. (2010), "Next generation
2845 biomass gasifier", *Proceedings of the 19th European Biomass Conference and
2846 Exhibition*, June 6-10 2010, Berlin, Germany.
- 2847 [121] Broda, M., Manovic, V., Imtiaz, Q., Kierzkowska, A. M., Anthony, E. J. and
2848 Müller, C. R. (2013), "High-purity hydrogen via the sorption-enhanced steam
2849 methane reforming reaction over a synthetic CaO-based sorbent and a Ni catalyst",
2850 *Environmental Science and Technology*, vol. 47, no. 11, pp. 6007-6014.
- 2851 [122] Hufton, J. R., Mayorga, S. and Sircar, S. (1999), "Sorption-enhanced reaction
2852 process for hydrogen production", *AIChE Journal*, vol. 45, no. 2, pp. 248-256.

- 2853 [123] Rawadieh, S. and Gomes, V. G. (2009), "Steam reforming for hydrogen
2854 generation with in situ adsorptive separation", *International Journal of Hydrogen*
2855 *Energy*, vol. 34, no. 1, pp. 343-355.
- 2856 [124] Hofbauer, H., Rauch, R., Bosch, K., Koch, R. and Aichernig, C. (2003),
2857 "Biomass CHP Plant Güssing – A Success Story", in Bridgwater, A. V. (ed.),
2858 *Pyrolysis and Gasification of Biomass and Waste*, Newsbury, UK, CPL Press, pp.
2859 371-383.
- 2860 [125] Koppatz, S., Pfeifer, C., Rauch, R., Hofbauer, H., Marquard-Moellenstedt, T.
2861 and Specht, M. (2009), "H₂ rich product gas by steam gasification of biomass with
2862 in situ CO₂ absorption in a dual fluidized bed system of 8 MW fuel input", *Fuel*
2863 *Processing Technology*, vol. 90, no. 7–8, pp. 914-921.
- 2864 [126] Kirnbauer, F., Wilk, V. and Hofbauer, H. (2013), "Performance improvement of
2865 dual fluidized bed gasifiers by temperature reduction: The behavior of tar species in
2866 the product gas", *Fuel*, vol. 108, pp. 534-542.
- 2867 [127] Romano, M. C. and Lozza, G. G. (2010), "Long-term coal gasification-based
2868 power with near-zero emissions. Part B: Zecomag and oxy-fuel IGCC cycles",
2869 *International Journal of Greenhouse Gas Control*, vol. 4, no. 3, pp. 469-477.
- 2870 [128] Cormos, C. C. and Cormos, A. M. (2013), "Assessment of calcium-based
2871 chemical looping options for gasification power plants", *International Journal of*
2872 *Hydrogen Energy*, vol. 38, no. 5, pp. 2306-2317.
- 2873 [129] Connell, D. P., Lewandowski, D. A., Ramkumar, S., Phalak, N., Statnick, R. M.
2874 and Fan, L. (2013), "Process simulation and economic analysis of the Calcium
2875 Looping Process (CLP) for hydrogen and electricity production from coal and
2876 natural gas", *Fuel*, vol. 105, pp. 383-396.
- 2877 [130] Wang, D., Chen, S., Xu, C. and Xiang, W. (2013), "Energy and exergy analysis
2878 of a new hydrogen-fueled power plant based on calcium looping process",
2879 *International Journal of Hydrogen Energy*, vol. 38, no. 13, pp. 5389-5400.
- 2880 [131] Kunze, C., De, S. and Spliethoff, H. (2011), "A novel IGCC plant with
2881 membrane oxygen separation and carbon capture by carbonation-calcinations
2882 loop", *International Journal of Greenhouse Gas Control*, vol. 5, no. 5, pp. 1176-
2883 1183.
- 2884 [132] Vorrias, I., Atsonios, K., Nikolopoulos, A., Nikolopoulos, N., Grammelis, P. and
2885 Kakaras, E. (2013), "Calcium looping for CO₂ capture from a lignite fired power
2886 plant", *Fuel*, vol. 113, pp. 826-836.

- 2887 [133] Martínez, A., Lara, Y., Lisbona, P. and Romeo, L. M. (2012), "Energy penalty
2888 reduction in the calcium looping cycle", *International Journal of Greenhouse Gas*
2889 *Control*, vol. 7, pp. 74-81.
- 2890 [134] Martínez, I., Grasa, G., Murillo, R., Arias, B. and Abanades, J. C. (2013),
2891 "Modelling the continuous calcination of CaCO₃ in a Ca-looping system", *Chemical*
2892 *Engineering Journal*, vol. 215–216, pp. 174-181.
- 2893 [135] Fang, F., Li, Z. and Cai, N. (2009), "Experiment and modeling of CO₂ capture
2894 from flue gases at high temperature in a fluidized bed reactor with Ca-based
2895 sorbents", *Energy and Fuels*, vol. 23, no. 1, pp. 207-216.
- 2896 [136] Abanades, C. J., Anthony, E. J., Lu, D. Y., Salvador, C. and Alvarez, D. (2004),
2897 "Capture of CO₂ from combustion gases in a fluidized bed of CaO", *Environmental*
2898 *and Energy Engineering*, vol. 50, no. 7, pp. 1614-1622.
- 2899 [137] Arias, B., Grasa, G. S. and Abanades, J. C. (2010), "Effect of sorbent hydration
2900 on the average activity of CaO in a Ca-looping system", *Chemical Engineering*
2901 *Journal*, vol. 163, no. 3, pp. 324-330.
- 2902 [138] Lisbona, P., Martínez, A., Lara, Y. and Romeo, L. M. (2010), "Integration of
2903 carbonate CO₂ capture cycle and coal-fired power plants. A comparative study for
2904 different sorbents", *Energy and Fuels*, vol. 24, no. 1, pp. 728-736.
- 2905 [139] Li, Z., Cai, N. and Croiset, E. (2008), "Process analysis of CO₂ capture from flue
2906 gas using carbonation/calcination cycles", *AIChE Journal*, vol. 54, no. 7, pp. 1912-
2907 1925.
- 2908 [140] Valverde, J. M., Sanchez-Jimenez, P. E. and Perez-Maqueda, L. A. (2015),
2909 "Ca-looping for postcombustion CO₂ capture: A comparative analysis on the
2910 performances of dolomite and limestone", *Applied Energy*, vol. 138, pp. 202-215.
- 2911 [141] Wang, J. and Anthony, E. J. (2007), "A common decay behavior in cyclic
2912 processes", *Chemical Engineering Communications*, vol. 194, no. 11, pp. 1409-
2913 1420.
- 2914 [142] Wang, J. and Anthony, E. J. (2005), "On the decay behavior of the CO₂
2915 absorption capacity of CaO-based sorbents", *Industrial and Engineering Chemistry*
2916 *Research*, vol. 44, no. 3, pp. 627-629.
- 2917 [143] Grasa, G. S. and Abanades, J. C. (2006), "CO₂ capture capacity of CaO in long
2918 series of carbonation/calcination cycles", *Industrial and Engineering Chemistry*
2919 *Research*, vol. 45, no. 26, pp. 8846-8851.

- 2920 [144] Lysikov, A. I., Salanov, A. N. and Okunev, A. G. (2007), "Change of CO₂
2921 carrying capacity of CaO in isothermal recarbonation-decomposition cycles",
2922 *Industrial and Engineering Chemistry Research*, vol. 46, no. 13, pp. 4633-4638.
- 2923 [145] Abanades, J. C. (2002), "The maximum capture efficiency of CO₂ using a
2924 carbonation/calcination cycle of CaO/CaCO₃", *Chemical Engineering Journal*, vol.
2925 90, no. 3, pp. 303-306.
- 2926 [146] Berstad, D., Anantharaman, R. and Jordal, K. (2012), "Post-combustion CO₂
2927 capture from a natural gas combined cycle by CaO/CaCO₃ looping", *International*
2928 *Journal of Greenhouse Gas Control*, vol. 11, pp. 25-33.
- 2929 [147] Ströhle, J., Lasheras, A., Galloy, A. and Epple, B. (2009), "Simulation of the
2930 carbonate looping process for post-combustion CO₂ capture from a coal-fired power
2931 plant", *Chemical Engineering and Technology*, vol. 32, no. 3, pp. 435-442.
- 2932 [148] Martínez, I., Murillo, R., Grasa, G., Rodríguez, N. and Abanades, J. C. (2011),
2933 "Conceptual design of a three fluidised beds combustion system capturing CO₂ with
2934 CaO", *International Journal of Greenhouse Gas Control*, vol. 5, no. 3, pp. 498-504.
- 2935 [149] Charitos, A., Rodríguez, N., Hawthorne, C., Alonso, M., Zieba, M., Arias, B.,
2936 Kopanakis, G., Scheffknecht, G. and Abanades, J. C. (2011), "Experimental
2937 Validation of the Calcium Looping CO₂ Capture Process with Two Circulating
2938 Fluidized Bed Carbonator Reactors", *Industrial & Engineering Chemistry Research*,
2939 vol. 50, no. 16, pp. 9685-9695.
- 2940 [150] Ylätaalo, J., Parkkinen, J., Ritvanen, J., Tynjälä, T. and Hyppänen, T. (2013),
2941 "Modeling of the oxy-combustion calciner in the post-combustion calcium looping
2942 process", *Fuel*, vol. 113, pp. 770-779.
- 2943 [151] H. Borgwardt, R. (1989), "Sintering of nascent calcium oxide", *Chemical*
2944 *Engineering Science*, vol. 44, no. 1, pp. 53-60.
- 2945 [152] Sun, P., Grace, J. R., Lim, C. J. and Anthony, E. J. (2007), "Removal of CO₂ by
2946 calcium-based sorbents in the presence of SO₂", *Energy and Fuels*, vol. 21, no. 1,
2947 pp. 163-170.
- 2948 [153] Grasa, G. S., Alonso, M. and Abanades, J. C. (2008), "Sulfation of CaO
2949 particles in a carbonation/calcination loop to capture CO₂", *Industrial and*
2950 *Engineering Chemistry Research*, vol. 47, no. 5, pp. 1630-1635.
- 2951 [154] Anthony, E. J. and Granatstein, D. L. (2001), "Sulfation phenomena in fluidized
2952 bed combustion systems", *Progress in Energy and Combustion Science*, vol. 27,
2953 no. 2, pp. 215-236.

- 2954 [155] Lyngfelt, A. and Leckner, B. (1989), "Sulphur capture in fluidized bed boilers:
2955 The effect of reductive decomposition of CaSO₄", *The Chemical Engineering*
2956 *Journal*, vol. 40, no. 2, pp. 59-69.
- 2957 [156] Baker, R. (1973), "The reversibility of the reaction CaCO₃ ⇌ CaO+CO₂", *Journal*
2958 *of Applied Chemistry and Biotechnology*, vol. 23, no. 10, pp. 733-742.
- 2959 [157] Salvador, C., Lu, D., Anthony, E. J. and Abanades, J. C. (2003), "Enhancement
2960 of CaO for CO₂ capture in an FBC environment", *Chemical Engineering Journal*,
2961 vol. 96, no. 1–3, pp. 187-195.
- 2962 [158] Curran, G. P., Fink, C. E. and Gorin, E. (1967), "Carbon dioxide-acceptor
2963 gasification process: studies of acceptor properties", *Advanced Chemistry Services*,
2964 vol. 69, pp. 141-165.
- 2965 [159] Silaban, A., Narcida, M. and Harrison, D. P. (1996), "Characteristics of the
2966 reversible reaction between CO_{2(g)} and calcined dolomite", *Chemical Engineering*
2967 *Communications*, vol. 146, no. 1, pp. 149-162.
- 2968 [160] Aihara, M., Nagai, T., Matsushita, J., Negishi, Y. and Ohya, H. (2001),
2969 "Development of porous solid reactant for thermal-energy storage and temperature
2970 upgrade using carbonation/decarbonation reaction", *Applied Energy*, vol. 69, no. 3,
2971 pp. 225-238.
- 2972 [161] Manovic, V., Anthony, E. J., Grasa, G. and Abanades, J. C. (2008), "CO₂
2973 looping cycle performance of a high-purity limestone after thermal
2974 activation/doping", *Energy and Fuels*, vol. 22, no. 5, pp. 3258-3264.
- 2975 [162] Mantripragada, H. C. and Rubin, E. S. (2013), "Calcium looping cycle for CO₂
2976 capture - Performance, cost and feasibility analysis", *Energy Procedia*, vol. 63, pp.
2977 2199-2206.
- 2978 [163] Manovic, V. and Anthony, E. J. (2007), "Steam reactivation of spent CaO-based
2979 sorbent for multiple CO₂ capture cycles", *Environmental Science and Technology*,
2980 vol. 41, no. 4, pp. 1420-1425.
- 2981 [164] Fennell, P. S., Davidson, J. F., Dennis, J. S. and Hayhurst, A. N. (2007),
2982 "Regeneration of sintered limestone sorbents for the sequestration of CO₂ from
2983 combustion and other systems", *Journal of the Energy Institute*, vol. 80, no. 2, pp.
2984 116-119.
- 2985 [165] Hughes, R. W., Lu, D., Anthony, E. J. and Wu, Y. (2004), "Improved long-term
2986 conversion of limestone-derived sorbents for in situ capture of CO₂ in a fluidized
2987 bed combustor", *Industrial and Engineering Chemistry Research*, vol. 43, no. 18,
2988 pp. 5529-5539.

- 2989 [166] Grasa, G., Murillo, R., Alonso, M., González, B., Rodríguez, N. and Abanades,
2990 J. C. (2009), "Steam reactivation of CaO-based natural sorbents applied to a
2991 carbonation/calcination loop for CO₂ capture", *4th International Conference on
2992 Clean Coal Technologies*, Dresden, Germany, Cited in: Arias, B., Grasa, G.S. and
2993 Abanades, J.C (2010), "Effect of sorbent hydration on the average activity of CaO in
2994 a Ca-looping system", *Chemical Engineering Journal*, vol. 163, pp. 324-330, .
- 2995 [167] Blamey, J., Manovic, V., Anthony, E. J., Dugwell, D. R. and Fennell, P. S.
2996 (2015), "On steam hydration of CaO-based sorbent cycled for CO₂ capture", *Fuel*,
2997 vol. 150, pp. 269-277.
- 2998 [168] Lee, D. K. (2004), "An apparent kinetic model for the carbonation of calcium
2999 oxide by carbon dioxide", *Chemical Engineering Journal*, vol. 100, no. 1–3, pp. 71-
3000 77.
- 3001 [169] Bhatia, S. and Perlmutter, D. (1983), "Effect of the product layer on the kinetics
3002 of the CO₂-lime reaction", *AIChE Journal*, vol. 29, no. 1, pp. 79-86.
- 3003 [170] Gupta, G. and Fan, L. S. (2002), "Carbonation-calcination cycle using high
3004 reactivity calcium oxide for carbon dioxide separation from flue gas", *Industrial and
3005 Engineering Chemistry Research*, vol. 41, pp. 4035-4042.
- 3006 [171] Grasa, G. S., Abanades, J. C., Alonso, M. and González, B. (2008), "Reactivity
3007 of highly cycled particles of CaO in a carbonation/calcination loop", *Chemical
3008 Engineering Journal*, vol. 137, no. 3, pp. 561-567.
- 3009 [172] Yu, Y. S., Liu, W. Q., An, H., Yang, F. S., Wang, G. X., Feng, B., Zhang, Z. X.
3010 and Rudolph, V. (2012), "Modeling of the carbonation behavior of a calcium based
3011 sorbent for CO₂ capture", *International Journal of Greenhouse Gas Control*, vol. 10,
3012 pp. 510-519.
- 3013 [173] Mahuli, S. K., Agnihotri, R., Jadhav, R., Chauk, S. and Fan, L. (1999),
3014 "Combined calcination, sintering and sulfation model for CaCO₃-SO₂ reaction",
3015 *AIChE Journal*, vol. 45, no. 2, pp. 367-381.
- 3016 [174] Sun, P., Grace, J. R., Lim, C. J. and Anthony, E. J. (2008), "Determination of
3017 intrinsic rate constants of the CaO-CO₂ reaction", *Chemical Engineering Science*,
3018 vol. 63, no. 1, pp. 47-56.
- 3019 [175] Borgwardt, R. H. (1985), "Calcination kinetics and surface area of dispersed
3020 limestone particles", *AIChE Journal*, vol. 31, no. 1, pp. 103-111.
- 3021 [176] García-Labiano, F., Abad, A., de Diego, L. F., Gayán, P. and Adánez, J. (2002),
3022 "Calcination of calcium-based sorbents at pressure in a broad range of CO₂
3023 concentrations", *Chemical Engineering Science*, vol. 57, no. 13, pp. 2381-2393.

- 3024 [177] Dennis, J. S. and Hayhurst, A. N. (1987), "The effect of CO₂ on the kinetics and
3025 extent of calcination of limestone and dolomite particles in fluidised beds", *Chemical*
3026 *Engineering Science*, vol. 42, no. 10, pp. 2361-2372.
- 3027 [178] Kunii, D. and Levenspiel, O. (1991), *Fluidization engineering*, 2nd ed,
3028 Butterworth-Heinemann, Stoneham, MA, USA.
- 3029 [179] Kunii, D. and Levenspiel, O. (1990), "Fluidized reactor models. 1. For bubbling
3030 beds of fine, intermediate, and large particles. 2. For the lean phase. Freeboard and
3031 fast fluidization", *Industrial and Engineering Chemistry Research*, vol. 29, no. 7, pp.
3032 1226-1234.
- 3033 [180] Turnbull, E. and Davidson, J. F. (1984), "Fluidized combustion of char and
3034 volatiles from coal", *American Institute of Chemical Engineers Journal*, vol. 30, no.
3035 6, pp. 881-889.
- 3036 [181] Li, Z. and Cai, N. (2007), "Modeling of multiple cycles for sorption-enhanced
3037 steam methane reforming and sorbent regeneration in fixed bed reactor", *Energy &*
3038 *Fuels*, vol. 21, no. 5, pp. 2909-2918.
- 3039 [182] Kunii, D. and Levenspiel, O. (1997), "Circulating fluidized-bed reactors",
3040 *Chemical Engineering Science*, vol. 52, no. 15, pp. 2471-2482.
- 3041 [183] Kunii, D. and Levenspiel, O. (2000), "The K-L reactor model for circulating
3042 fluidized beds", *Chemical Engineering Science*, vol. 55, no. 20, pp. 4563-4570.
- 3043 [184] Martínez, I., Grasa, G., Murillo, R., Arias, B. and Abanades, J. C. (2012),
3044 "Kinetics of calcination of partially carbonated particles in a Ca-looping system for
3045 CO₂ capture", *Energy and Fuels*, vol. 26, no. 2, pp. 1432-1440.
- 3046 [185] Myöhänen, K. and Hypänen, T. (2011), "A three-dimensional model frame for
3047 modelling combustion and gasification in circulating fluidized bed furnaces",
3048 *International Journal of Chemical Reactor Engineering*, vol. 9.
- 3049 [186] Silcox, G. D., Kramlich, J. C. and Pershing, D. W. (1989), "Mathematical model
3050 for the flash calcination of dispersed CaCO₃ and Ca(OH)₂ particles", *Industrial and*
3051 *Engineering Chemistry Research*, vol. 28, no. 2, pp. 155-160.
- 3052 [187] Barin, I. (ed.) (1989), *Thermochemical data of pure substances*, VCH
3053 Verlagsgesellschaft mbH, Weumheim, Federal Republic of Germany.
- 3054 [188] Atsonios, K., Zeneli, M., Nikolopoulos, A., Nikolopoulos, N., Grammelis, P. and
3055 Kakaras, E. (2015), "Calcium looping process simulation based on an advanced
3056 thermodynamic model combined with CFD analysis", *Fuel*, vol. 153, pp. 371-381.

- 3057 [189] Ylätaalo, J., Ritvanen, J., Arias, B., Tynjälä, T. and Hyppänen, T. (2012), "1-
3058 Dimensional modelling and simulation of the calcium looping process", *International*
3059 *Journal of Greenhouse Gas Control*, vol. 9, pp. 130-135.
- 3060 [190] Fennell, P. S., Pacciani, R., Dennis, J. S., Davidson, J. F. and Hayhurst, A. N.
3061 (2007), "The effects of repeated cycles of calcination and carbonation on a variety
3062 of different limestones, as measured in a hot fluidized bed of sand", *Energy and*
3063 *Fuels*, vol. 21, no. 4, pp. 2072-2081.
- 3064 [191] Senneca, O., Urciuolo, M. and Chirone, R. (2013), "A semidetalled model of
3065 primary fragmentation of coal", *Fuel*, vol. 104, pp. 253-261.
- 3066 [192] Gibbins, J. R. and Crane, R. I. (2004), "Scope for reductions in the cost of CO₂
3067 capture using flue gas scrubbing with amine solvents", *Proceedings of the*
3068 *Institution of Mechanical Engineers, Part A: Journal of Power and Energy*, vol. 218,
3069 no. 4, pp. 231-239.
- 3070 [193] Khalilpour, R. and Abbas, A. (2011), "HEN optimization for efficient retrofitting of
3071 coal-fired power plants with post-combustion carbon capture", *International Journal*
3072 *of Greenhouse Gas Control*, vol. 5, no. 2, pp. 189-199.
- 3073 [194] Kishimoto, S., Hirata, T., Iijima, M., Ohishi, T., Higaki, K. and Mitchell, R.
3074 (2009), "Current status of MHI's CO₂ recovery technology and optimization of CO₂
3075 recovery plant with a PC fired power plant", *Energy Procedia*, vol. 1, no. 1, pp.
3076 1091-1098.
- 3077 [195] Cengel, Y. A. and Boles, M. A. (2007), *Thermodynamics: an engineering*
3078 *approach*, 6th in SI units ed, McGraw-Hill, New York, NY, USA.
- 3079 [196] Grasa, G., Murillo, R., Alonso, M. and Abanades, J. C. (2009), "Application of
3080 the random pore model to the carbonation cyclic reaction", *AIChE Journal*, vol. 55,
3081 no. 5, pp. 1246-1255.
- 3082 [197] Joutsenoja, T., Heino, P., Hernberg, R. and Bonn, B. (1999), "Pyrometric
3083 temperature and size measurements of burning coal particles in a fluidized bed
3084 combustion reactor", *Combustion and Flame*, vol. 118, no. 4, pp. 707-717.
- 3085 [198] Manovic, V., Komatina, M. and Oka, S. (2008), "Modeling the temperature in
3086 coal char particle during fluidized bed combustion", *Fuel*, vol. 87, no. 6, pp. 905-
3087 914.
- 3088 [199] Symonds, R. T., Lu, D. Y., Manovic, V. and Anthony, E. J. (2012), "Pilot-scale
3089 study of CO₂ capture by CaO-based sorbents in the presence of steam and SO₂",
3090 *Industrial and Engineering Chemistry Research*, vol. 51, no. 21, pp. 7177-7184.

- 3091 [200] Lara, Y., Lisbona, P., Martínez, A. and Romeo, L. M. (2014), "A systematic
3092 approach for high temperature looping cycles integration", *Fuel*, vol. 127, pp. 4-12.
- 3093 [201] Lara, Y., Lisbona, P., Martínez, A. and Romeo, L. M. (2013), "Design and
3094 analysis of heat exchanger networks for integrated Ca-looping systems", *Applied*
3095 *Energy*, vol. 111, pp. 690-700.
- 3096 [202] ECN (2012), *ECN Phyllis classification*, available at: <http://bit.ly/1hrh1cu>
3097 (accessed 30/05/2015).
- 3098 [203] Arias, B., Abanades, J. C. and Grasa, G. S. (2011), "An analysis of the effect of
3099 carbonation conditions on CaO deactivation curves", *Chemical Engineering Journal*,
3100 vol. 167, no. 1, pp. 255-261.
- 3101 [204] Martínez, A., Lara, Y., Lisbona, P. and Romeo, L. M. (2013), "Operation of a
3102 cyclonic preheater in the ca-looping for CO₂ capture", *Environmental Science and*
3103 *Technology*, vol. 47, no. 19, pp. 11335-11341.
- 3104 [205] Biliyok, C. and Yeung, H. (2013), "Evaluation of natural gas combined cycle
3105 power plant for post-combustion CO₂ capture integration", *International Journal of*
3106 *Greenhouse Gas Control*, vol. 19, pp. 396-405.
- 3107 [206] Miller, B. G. (2011), *Clean Coal Engineering Technology*, Butterworth-
3108 Heinemann, Boston, USA.
- 3109 [207] IEA (2012), *CO₂ Emissions from Fuel Combustion - Highlights*, 2012 ed,
3110 OECD/IEA, Paris, France.
- 3111 [208] Versteeg, P. and Rubin, E. S. (2011), "A technical and economic assessment of
3112 ammonia-based post-combustion CO₂ capture at coal-fired power plants",
3113 *International Journal of Greenhouse Gas Control*, vol. 5, no. 6, pp. 1596-1605.
- 3114 [209] Black, J. (2013), *Cost and Performance Baseline for Fossil Energy Plants*
3115 *Volume 1: Bituminous Coal and Natural Gas to Electricity*, DOE/2010/1397
3116 Revision 2a, National Energy Technology Laboratory.
- 3117 [210] Romano, M. C. and Lozza, G. G. (2010), "Long-term coal gasification-based
3118 power plants with near-zero emissions. Part A: Zecomix cycle", *International*
3119 *Journal of Greenhouse Gas Control*, vol. 4, no. 3, pp. 459-468.
- 3120 [211] IEA (2012), *Technology Roadmap: High-Efficiency, Low-Emissions Coal-Fired*
3121 *Power Generation*, OECD/IEA, Paris, France.
- 3122 [212] Anantharaman, R., Bolland, O., Booth, N., van Dorst, E., Ekstrom, C., Sanchez
3123 Fernandes, E., Franco, F., Macchi, E., Manzolini, G., Nikolic, D., Pfeffer, A., Prins,

3124 M., Rezvani, S. and Robinson, L. (2011), *CArbon-free Electricity by SEWGS:*
3125 *Advanced materials, Reactor-, and process design. D 4.9 European best practice*
3126 *guidelines for assessment of CO₂ capture technologies*, 213206 FP7 -
3127 ENERGY.2007.5.1.1, Politecnico di Milano – Alstom UK.

3128 [213] Bollard, O., Booth, N., Franco, F., Macchi, E., Manzolini, G., Naqvi, R., Pfeffer,
3129 A., Rezvani, S. and Abu Zara, M. (2009), *Enabling advanced pre-combustion*
3130 *capture techniques and plants. D 1.4.1 Common Framework Definition Document*,
3131 211971 FP7 - ENERGY.2007.5.1.1, Alstom UK.

3132

3133

Fossil fuels are expected to remain essential for the global power generation portfolio. As a result, carbon capture and storage technologies are expected to play a crucial role in greenhouse gas emissions reduction from the power generation sector. Mature technologies, such as amine scrubbing and oxy-combustion that are currently under demonstration at a commercial scale, are projected to reduce the net efficiency of electricity production by up to 12.5% points. For this reason, in order to minimise the efficiency penalty and the associated increase in the cost of electricity, novel CO₂ capture technologies are being developed. Calcium looping processes appears to be a promising technology that could reduce the efficiency penalty to 7% points. Development of this technology has advanced at a rapid rate over the past decade, especially since 2009. This review provides a comprehensive overview of bench- and pilot-plant testing, the available models to represent the process performance, alternative process configurations to reduce energy requirements and approaches for process integration for commercial-scale power generation systems. It is shown that further pilot-plant testing to generate data for process models validation could significantly minimise prediction uncertainty. Also, the requirement for baseline modelling assumptions and further development in sorbent performance are highlighted as key to future development.